8-2013

Geosynchronous Earth Orbit/Low Earth Orbit Space Object Inspection and Debris Disposal: A Preliminary Analysis Using a Carrier Satellite With Deployable Small Satellites

Derick A. Crockett
Utah State University

GEOSYNCHRONOUS EARTH ORBIT/LOW EARTH ORBIT SPACE OBJECT INSPECTION AND DEBRIS DISPOSAL: A PRELIMINARY ANALYSIS USING A CARRIER SATELLITE WITH DEPLOYABLE SMALL SATELLITES

by

Derick Alan Crockett

A thesis submitted in partial fulfillment
of the requirements for the degree

of

MASTER OF SCIENCE

in

Aerospace Engineering

Approved:

Dr. David Geller Major Professor	Dr. R. Rees Fullmer Committee Member
Dr. Stephen A. Whitmore Committee Member	Dr. Mark R. McLellan Vice President for Research and Dean of the School of Graduate Studies

UTAH STATE UNIVERSITY
Logan, Utah

2012

Abstract

Geosynchronous Earth Orbit/Low Earth Orbit Space Object Inspection and Debris Disposal: A Preliminary Analysis Using a Carrier Satellite With Deployable Small Satellites

by

Derick Alan Crockett, Master of Science

Utah State University, 2012

Major Professor: Dr. David Geller
Department: Mechanical and Aerospace Engineering

Detailed observations of geosynchronous satellites from earth are very limited. To better inspect these high altitude satellites, the use of small, refuelable satellites is proposed. The small satellites are stationed on a carrier platform in an orbit near the population of geosynchronous satellites. A carrier platform equipped with deployable, refuelable SmallSats is a viable option to inspect geosynchronous satellites. The propellant requirement to transfer to a targeted geosynchronous satellite, perform a proximity inspection mission, and transfer back to the carrier platform in a nearby orbit is determined. Convex optimization and traditional optimization techniques are explored, determining minimum propellant trajectories. Propellant is measured by the total required change in velocity, Δv. The trajectories were modeled in a relative reference frame using the Clohessy-Wiltshire equations. Mass estimations for the carrier platform and the SmallSat were determined by using the rocket equation. The mass estimates were compared to the mass of a single, non-refuelable satellite performing the same geosynchronous satellite inspection missions. From the minimum Δv trajectories and the mass analysis, it is determined that using refuelable SmallSats and a carrier platform in a nearby orbit can be more efficient than using a single non-refuelable

satellite to perform multiple geosynchronous satellite inspections.

(125 pages)

Public Abstract

Geosynchronous Earth Orbit/Low Earth Orbit Space Object Inspection and Debris Disposal: A Preliminary Analysis Using a Carrier Satellite With Deployable Small Satellites

by

Derick Alan Crockett, Master of Science

Utah State University, 2012

Major Professor: Dr. David Geller
Department: Mechanical and Aerospace Engineering

From communication to weather prediction, to national security, geosynchronous satellites play an important role in our society. Geosynchronous satellites are about 35,786 km (22,236 miles) from the surface of the earth. Getting a satellite to this altitude is very expensive, making geosynchronous satellites highly valued assets. Ground-based observation of these satellites is very limited and provides little insight when failures or anomalies occur. To provide detailed images and information of these critical satellites, highly functioning smaller satellites can be employed. This study explores the potential benefits of using these smaller satellites to perform on-orbit proximity inspections of geosynchronous satellites. The smaller satellites, referred to as inspectors, will be stationed on a larger satellite, called a carrier, in an orbit close to the geosynchronous orbit. The propellant that is required of the inspector to travel to the desired geosynchronous satellite, stay in proximity to perform an inspection, and then travel back to the carrier (to refuel and await its next mission) will be minimized. New and traditional minimization techniques will be used to find minimum propellant solutions. Using the minimum propellant solutions, estimates of the required mass of the inspector and the carrier can be made through the use of well know methods. The total mass estimates of the inspector and carrier system were compared to the mass estimate of a single satellite, without carrier or refueling, performing the same inspection missions. From the analysis and comparison, a carrier with deployable and refuelable small satellites has the potential to reduce total satellite mass.

(125 pages)

Acknowledgments

I am indebted to all those that have helped me accomplish this work and get through graduate school. First I would like to thank my major professor, Dr. David Geller. He has been a great mentor and teacher. He has always been willing to take time and help give guidance and support for this research. Even though he was half way around the world, with a big time difference, he always made himself available for meetings and help over the phone. I couldn't have had a better advisor. I am also grateful for all the help I recieved from fellow graduate student Shane Robinson, who was always willing to help solve the problems I encountered. I also want to thank the guys at SDL, Adam Shelly, Randy Christensen, and Bryan Bingham, for their ideas and feedback. I also need to to thank my wife for her love and support throughout my education. Her constant encouragement helped me everyday. I couldn't have done this on my own. Lastly I would like to give thanks to God for His guidance in my everyday life.

Derick Alan Crockett

Contents

Page

List of Tables

List of Figures

Acronyms

CW	Clohessy-Wiltshire
DoD	United States Department of Defense
ECEF	Earth Centered Earth Fixed
ETS	Engineering Test Satellite
GEO	geosynchronous earth orbit
GNC	guidance navigation and control
IADC	Inter-Agency Space Debris Coordination Committee
LEO	Low Earth Orbit
LVLH	Local Vertical Local Horizontal Coordinate Frame
NASA	National Aeronautics and Space Administration
OE	Orbital Express
ORU	orbital replacement unit
RSO	resident space object
SSR	Satellite Situation Report
TLE	Two Line Element
US	United States
USD	United States dollar

Chapter 1

Introduction

A Geosynchronous Earth Orbit (GEO) is a unique circular orbit about the Earth that has a period equal to one sidereal day. The altitude of GEO is about 35,786 km above the surface of the Earth. When a satellite is placed in GEO, with zero inclination, it will remain above the Earth's equator at the same longitudinal position. Theoretically a GEO satellite (GEO Sat) will appear to be in the same spot in the sky at all times, as observed from any given location on the Earth's surface. This is assuming line of sight to the satellite.

Due to a GEO Sat's ability to remain in the same location in the sky, ground based antennas do not need to track the satellite. This makes GEO a great orbit for communication satellites. GEO Sats also have the ability to see approximately 41% of the Earths surface, assuming at least 5° elevation angle [1]. GEO Sats, because of their unique attributes, are used to provide important services to our society. They enable observation of real-time climate conditions, helping predict important weather patterns. They also provide communication around the world by way of phone, radio and TV. GEO Sats are used to broadcast live events around the world. Some have the ability to assist in search and rescue efforts for ships and airplanes in distress. Other GEO Sats are designed to monitor solar activity [2]. The U.S. Department of Defense has GEO Sats that can detect when missiles are launched. These satellites are valuable for national security and are very costly. Based on a 2010 report to congress an average missile detection GEO Sat costs about $2.5 billion [3]. Not all GEO Sats cost billions of dollars but, their unique orbits, capabilities, cost to develop, launch, and maintain, make them highly valuable space assets.

The United States Strategic Command maintains a current computerized catalog of all Earth-orbiting man-made objects since the launch of Sputnik in 1957. According to their website, www.space-track.org, there are over 700 resident space objects (RSOs) currently in

the GEO region. The GEO region defined here is one that has an apogee and perigee altitude ± 300 km from GEO altitude. These RSOs could be working satellites, dead satellites, spent upper-stage rocket bodies, or other debris.

There could possibility be more debris in the GEO region than is documented. Current RSO tracking technology, using Earth based sensors, limits the size of objects able to be seen at GEO. These Earth based observations provide poorly detailed images of GEO RSOs, limiting the insight on satellites and debris in the GEO belt [4]. Much more detailed images of GEO RSOs and debris can be obtained from sensors placed in GEO or in a near GEO orbit [5].

Not all of the satellites in the GEO region are operational. Government and commercial entities have shown interests in missions that could service these highly valuable GEO Sats [6]. On-orbit GEO Sat servicing technologies of interest include inspection, refueling, repairing, and upgrading. Also of interest is identifying, detecting and removing inoperable or damaged GEO Sats, and other space debris, to the GEO graveyard orbit [5, 7, 8]. The GEO graveyard orbit is a disposal orbit near the GEO belt. U.S. government requires that satellites at the end of their life should maneuver to an orbit with perigee altitude above 36,100 km (approximately 300 km above GEO) [9]. Servicing missions can benefit GEO Sats by extending their mission life, reducing the cost of operation or delaying a replacement.

There have been many documented failures of satellites [10]. Some of these failures in GEO are not fully understood because of the limited insight gained from earth based sensors. Future servicing missions in GEO could not only help determine causes for failures but also be able to fix inoperable satellites. With higher resolution images of GEO RSOs their failures and successes could be better understood. Information from servicing missions can aid in lessons learned for planing and designing future GEO Sats.

One way to perform these GEO RSO servicing missions is to place a single carrier platform with multiple deployable small satellites (SmallSats) in a near GEO orbit. The carrier platform will be referred to as the Carrier, and the deployable SmallSat as the Inspector. The whole system will be referred to as a carrier concept. This carrier concept is similar to

how an aircraft carrier works for the Navy. The Carrier will have the ability to deploy an Inspector for a specific servicing missions to a GEO RSO. Once deployed, the Inspector will transfer to the desired GEO RSO to perform rendezvous or proximity operations per the servicing mission. Once the servicing of the GEO RSO has taken place the Inspector will then return to the Carrier, dock, refuel and await another deployment. The Carrier will act as a service station or base for the Inspectors.

This thesis will investigate the total mission Δv required by an Inspector to depart from a Carrier, in a near GEO orbit, rendezvous with a GEO RSO and return to the Carrier. The analysis will be done using relative motion dynamics from the well known Clohessy-Wiltshire (CW) equations [11]. The analysis will also look at the effect that the orbit of the Carrier has on the total mission Δv. Minimizing the Δv required from various orbits will be performed. There may be certain advantages to different orbits. These advantages and disadvantages will be explored. The required launch mass of the carrier concept to perform numerous GEO inspection missions will also be investigated. A carrier concept is hypothesized to be more mass and fuel efficient than a single satellite for multiple servicing missions.

Chapter 2

Thesis Statement

The thesis of this research is that the minimum propellant solutions to the unconstrained-time double orbital rendezvous problem is convex using the Clohessy-Wiltshire (CW) equations, and can thus be solved using well know convex optimization techniques. It is also the thesis of the research that a carrier platform, with one or more deployable, refuelable small satellites, can perform multiple GEO RSO inspection missions more efficiently, in terms of required mass to orbit, than a single satellite.

Chapter 3

Literature Survey

3.1 Orbital Maneuvering

Satellite's use orbital maneuvers to change its orbit to a desired orbit. Orbital maneuvering requires a change in the orbit's energy. This is accomplished by a change in the orbital velocity, or Δv. This change in velocity is synonymous with propellant used to perform the maneuver. Often optimal orbital maneuvers are those which require minimum amounts of propellant. For orbits that are co-planer, Walter Hohmann first proposed a theory that the minimum Δv to perform an orbital maneuver from one circular orbit to another was to use two tangential burns [12]. When transferring from one circular orbit to another using two tangential burns results in an elliptical transfer orbit. Figure 3.1a shows the interplanetary transfer from Earth to Venus using an elliptical orbit transfer and two tangential burns. Figure 3.1a is Figure 25 from [12], Hohmann's original paper translated into English. The use of an elliptical orbit to transfer between two orbits is rightly called a Hohmann transfer. The Hohmann transfer can also be extended to transfers between elliptical orbits as long as the burns remain to be tangential (a zero flight path angle) see Figure 3.1b taken from [13]. The Hohmann transfer has been proved to provide a minimum Δv transfer between co-planer orbits by Lawden and Palmore [14, 15]. Hohmann transfers are well known and are presented in detail in many textbooks [1, 13, 16, 17, 18, 19, 20, 21, 22, 23]

When a spacecraft is performing orbital rendezvous and proximity operations it is convenient to describe spacecraft's motion relative to the target spacecraft. The Clohessy-Wiltshire (CW) equations or Hill's equations are a set of linearized differential equations that describe the relative motion of a chaser spacecraft with respect to a target spacecraft, in a circular orbit with a linear gravity field [11]. The CW equations are derived from the general equations of motion from Newton's second law. The analytic solution to the CW

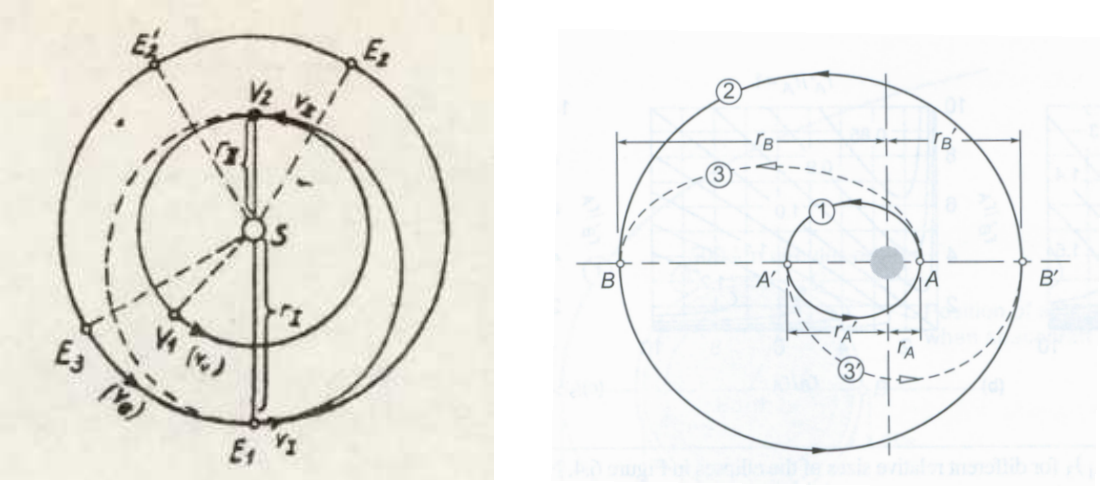

(a) Interplanetary rendezvous.

(b) Transfer between coaxial elliptical orbits.

Figure 3.1: Hohmann transfers.

equations provides a practical way to perform orbital rendezvous and proximity operations analysis. These solutions are well understood and have been used for relative orbital analysis for many years. The derivation of the CW equations, and the analytic solutions are presented in many text books as Hill's equations, Clohessy-Wiltshire equations, or relative equations of motion [13, 20, 21, 22, 23]. Figure 3.2 shows an examples of the relative motion coordinate definition.

The CW equations have been used to find the optimal transfer time for a minimum propellant rendezvous between two spacecraft [24]. If the position and time of the first impulsive Δv are know then a solution for the optimal transfer time that minimizes the the two impulse transfer can be found. This means that there is no initial coast. This approach also uses a transformation of the CW equations that requires the use of the method of successive approximations. However, the result is a convex solution space and terminates at the minimum solution.

The solution of the CW equations assumes the reference orbit is circular. For reference orbits that are elliptical a linearized solution that is a direct generalization of the CW equations is found in [25]. Here the CW equations are extended to the use of an elliptical reference frame. The formulation of this solution uses time as the independent variable. The

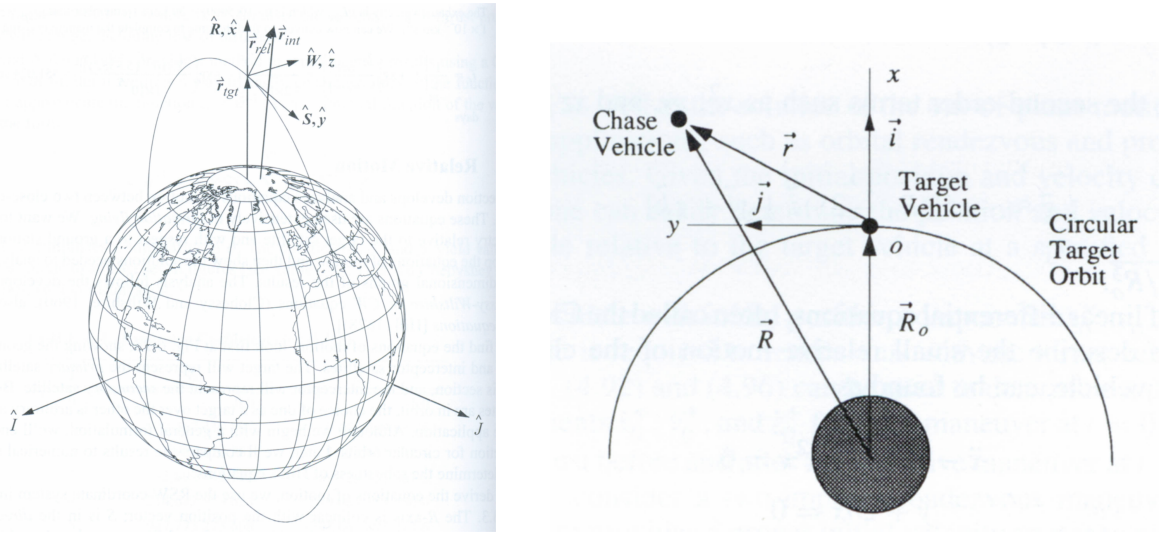

(a) Three dimensional view. (b) Two dimensional view.

Figure 3.2: Relative motion coordinate geometry.

equations for elliptic targeting are also formulated and presented.

The CW equations are also used to develop algorithms for approaching, performing proximity operations, and departing autonomously from a target space object [26]. Here the CW equations are used for glideslope guidance to approach and depart the target. Glideslop is a straight path from the current location to the desired location. This approach is used when propellant minimization is not the most important parameter to optimize about. The proximity operation is a fly-around the target. Algorithms developed from the CW equations for three fly-arounds are presented: natural elliptical in-plane (also know as a football orbit), forced circular in-plane, and forced circular in any plane.

Detailed description and examples of different relative motion maneuvers and the resulting orbits using the CW equations are presented in [27]. Woffinden shows that the CW equations can be used to produce many different resulting relative orbits for the chaser. These different relative orbits or trajectories that the chaser maneuvers into are useful for different types of rendezvous or proximity operations depending upon mission requirements.

3.2 Convex Optimization

The definition of convex optimization in [28] is

A convex optimization problem is one of the form

$$\begin{aligned} &\text{minimize} f_0(x) \\ &\text{subject to} f_i(x) \leq b_i, \qquad i = 1, \ldots, m, \end{aligned}$$

where the functions $f_0, \ldots, f_m$ $\mathbf{R}^n \to \mathbf{R}$ are convex, *i.e.*, satisfy

$$f_i(\alpha x + \beta y) \leq \alpha f_i(x) + \beta f_i(x)$$

for all x, $y \in \mathbf{R}^n$ and all α, $\beta \in \mathbf{R}$ with $\alpha + \beta = 1$, $\alpha \geq 0$, $\beta \geq 0$. Least squares and linear programming problems are both special cases of the general convex optimization problem.

Relatively little work has been done on applying convex optimization on orbital rendezvous maneuvers. There has been some work on applying convex optimization to formation flying of satellites [29].

The solution to a convex optimization problem has no general analytical formula. However there does exist known effective methods for solving problems that are convex. If a problem can be formulated to be convex then it can be solved. Convex optimization techniques can be used similar to how least squares and linear programming are used to find solutions to problems. The challenge is the ability to recognize the problem to be convex, this can be difficult. Once the problem is formulated to be convex solving the problem is straightforward.

Shane Robinson was able to show that the discrete relative dynamics of the CW equations, used to describe orbital rendezvous can be formulated as a convex problem. The orbital rendezvous problem was formulated using classical calculus of variations optimization using a zero terminal error, and penalty function approach presented by Bryson and Ho [30]. An equivalent problem was then described as being a convex. The minimum propellant solutions for rendezvous using the classical approach and the convex approach were then compared.

The convex optimization provided less computational time and converged rapidly to stable solutions. Also the convex approach provided more flexibility in applying constraints [31].

The work of this thesis will use the work that Robinson has done with a single rendezvous scenario and apply it to the case of a minimizing the Δv required for a SmallSat to rendezvous with a GEO RSO and then return and re-rendezvous with a carrier platform. With the problem formulated as convex, CVX will be used to solve the problem. CVX is MATLAB software developed by Stephen Boyd and Michael Grant to solve convex optimization problems [32].

3.3 Propulsion and Mass

A propulsion system is needed to accomplish orbital maneuvering. Propulsion produces thrust, or force; the mechanism for providing acceleration to accomplish required Δv for a maneuver. The type of propulsion system used to achieve the Δv will determine the mass of the propellant needed. This propellant mass will add to the overall mass of the satellite. The well know Tsiolkovsky rocket equation, equation 3.1, will be used to make calculations for propellant mass required to perform the orbital maneuvers. The rocket equation is presented and discussed in many textbooks [1, 19, 33]. Also presented in the textbooks are general and in depth discussions on the propulsion systems.

$$\Delta v = I_{sp} g_0 ln \left(\frac{m_0}{m_f} \right) \tag{3.1}$$

3.4 Unmanned Autonomous On-Orbit Satellite Servicing

Autonomous unmanned on-orbit servicing of satellites could bring financial profit. A study of the economics of servicing missions is given in [34]. The study estimate that every year $3.8 billion USD (2007) worth of GEO satellite investments are retired because of lack of propellant. About 20 GEO Sats run out of propellant each year. If there were a system in place to service and refuel satellites, the satellite's lifetime could be extended. From

1994-2003 insurance companies payed approximately $748 million USD per year for failures in GEO investments. Once satellites are claimed by an insurer they left inoperable or sold for use in a reduced capacity. Having the capability to refuel/service GEO satellites can also significantly increase a commercial company's internal rate of return (financial profit) on their satellite investment. On-orbit servicing can be an economically viable mission.

The Engineering Test Satellite VII (ETS-VII) launched in 1997 demonstrated autonomous rendezvous and docking with the use of space robotics. ETS-VII performed three successful autonomous soft-docking tests. ETS-VII also used a robotic arm to perform a swapping of an orbital replacement unit (ORU) [35]. This demonstration gives validity to the use of robotics to perform unmanned servicing of satellites.

Launched in 2006, Orbital Express (OE) was a successful mission that demonstrated many on-orbit servicing technologies. OE successfully demonstrated for the first time autonomous on-orbit refueling and exchange of ORU with an uncooperative target. OE also used a robotic arm to perform the demonstration [36, 37, 38]. With the successful demonstrations of ETS-VII and OE autonomous on-orbit satellite servicing such as re-fueling and exchanging or upgrading components is possible.

Using a parent satellite and a child satellite to collect and remove dead geosynchronous satellites is discussed in [39]. Proposed in this paper a parent satellite is placed in a geosynchronous orbit and the child satellite departs from the parent satellite to rendezvous with a dead GEO Sat. The child satellite performs orbital maneuvers such as plane change, orbit transfer, phase modulation, approach, target acquisition, de-orbit to graveyard, and return to parent satellite. Hohmann transfers are assumed for orbit transfers and phase modulation. Example of a disposal mission calculates that 160 1,500 kg dead GEO Sats could be removed with a 200 kg child satellite if parent satellite could hold 2000 kg of propellant. The study concludes that using a child and parent satellite can save propellant mass rather than one satellite of similar mass.

3.5 Proposed Work

The proposed thesis will perform a preliminary analysis of using a carrier concept for on-orbit space object servicing. The analysis will be used to determine if a carrier concept is a viable option and more efficient than using a single satellite for inspecting or removing GEO space objects. The CW equations will be used to model the orbital maneuvers. The Carrier will be placed in a near but not GEO synchronous orbit. Propellant optimal solutions to the problem will be found using convex and traditional optimization techniques. The propellant optimal solutions will be used for mass analysis to quantitatively determine effectiveness of using a carrier concept.

Chapter 4

GEO Region

4.1 GEO Population

The United States Strategic Command maintains a catalog database of all satellites launched since the launch of Sputnik in 1957. This database, available from www.space-track.org, contains the Two Line Element (TLE) of each space object that can be tracked. Some objects are too small or too far from Earth to be detected, thus the report does not include all objects orbiting the earth. Because GEO is about 35,786 km from the Earth's surface only space objects larger than 1 meter can currently be detected and tracked by ground based radar and optical sensors.

To determine the number of objects in GEO, the TLE sets of all currently orbiting space objects were downloaded from www.space-track.org. The TLE data was in the form of a .txt document. A MATLAB script was written to read in the TLE .txt file, parse each TLE, gather Keplerian orbital elements from the TLE, and determine if the object was in the defined GEO region. For this study the GEO region was defined as objects having a an altitude between 35,286 - 36,286 km. The altitude was determined from the semi-major axis of the space object's orbit. The semi-major axis was calculated from the knowledge of the mean motion in the TLE of the space object. From [13, 21]

$$n = \frac{2\pi}{T} \tag{4.1}$$

$$T = \frac{2\pi}{\sqrt{\mu}} a^{\frac{3}{2}} \tag{4.2}$$

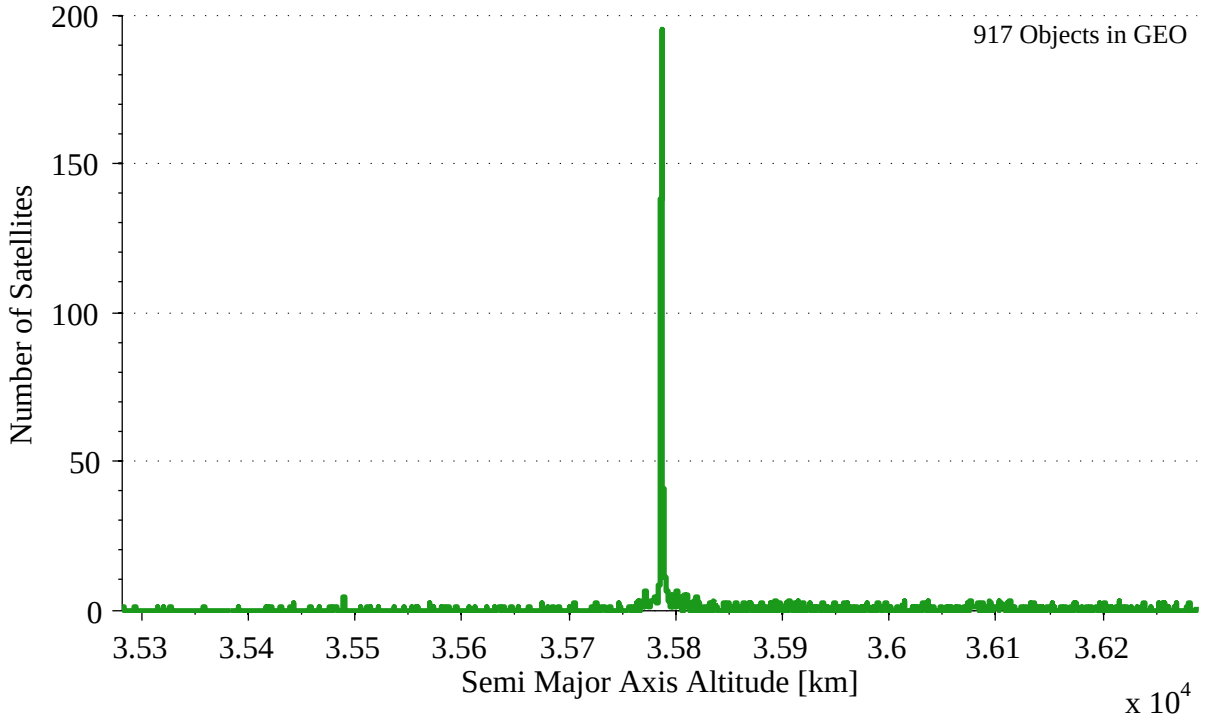

Figure 4.1: Space object dispersion as a function of semi-major axis of orbit for GEO region.

$$a = \left(\frac{\mu}{n^2} \right)^{\frac{1}{3}} \tag{4.3}$$

where n is the mean motion of the space object, T is the period of the space object's orbit, μ is the Gravitational Parameter of the Earth (a known constant), and a is the semi-major axis of the space object's orbit. Given Equations 4.1 and 4.2, Equation 4.3 is found by solving for a in terms of n and μ.

The number of space objects as a function of various Keplerian orbital elements was binned and the results plotted. Figure 4.1 shows the number of space objects that are at a certain semi-major axis altitude. The Figure shows that almost all of the satellites in the defined GEO region are very near the GEO altitude of about 35,786 km. The data in this Figure is binned every 1 km. From the data there are 917 space objects that fall within the defined GEO region.

Figure 4.2 shows the number of space objects in the GEO region with given inclinations.

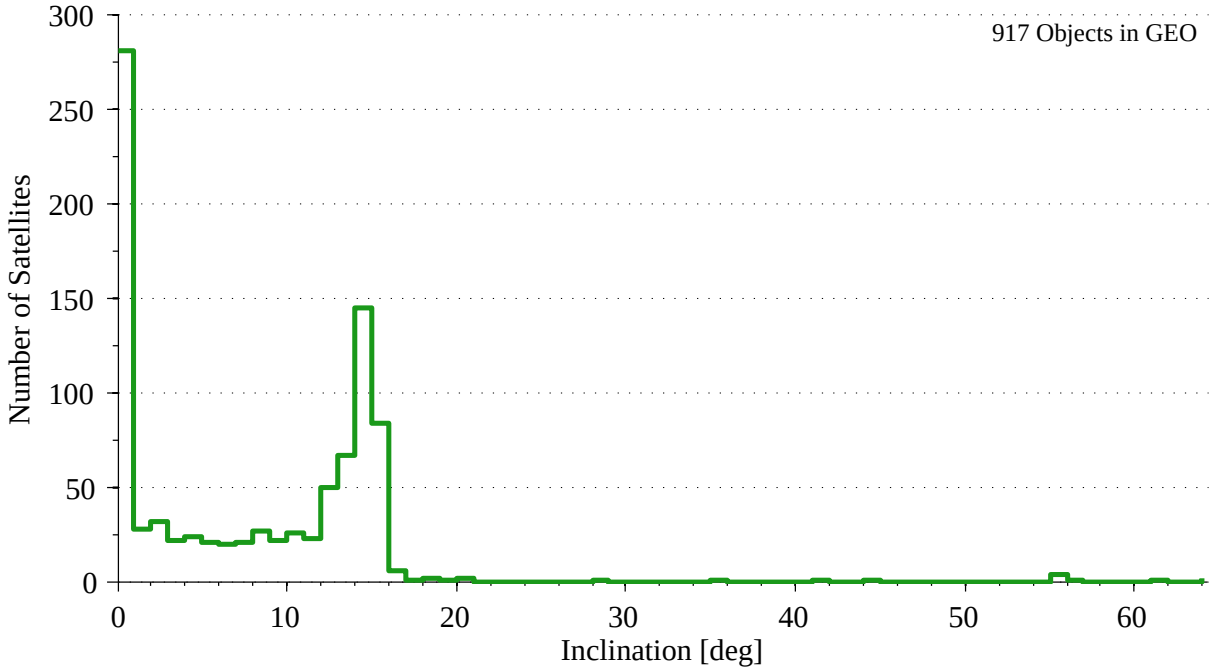

Figure 4.2: Space object dispersion as a function of inclination of orbit for GEO region.

The data is binned every 1° of inclination. There are two prevalent spikes in the data, the largest at 0-1° inclination. This is because most functioning GEO satellites strive to maintain a 0° inclination. The smaller spike in the data occurs at 14-15° inclination.

Figure 4.3 shows the number of space objects as a function of both semi-major axis and inclination. This is a combination of the data in Figures 4.1 and 4.2. Here the data is binned every 1° of inclination and 20km. This Figure shows the spikes represented in both Figures 4.1 and 4.2. Most of the space objects that are very near the GEO altitude also have a 0-1° inclination. This is expected because functioning geosynchronous satellites operate optimally at 0° inclination. Over 250 cataloged objects have inclinations less than 0.1° with semi-major axes between 42,163-42,167 km. It is shown that when the space object is not at the GEO altitude the inclination is greater than 1°. From the data 98% of the space objects in the defined GEO region have an inclination less than 18°.

The data used to produce Figures 4.1-4.3 is from May 2012. From the data it is seen that there are over 900 known space objects in the GEO region defined as 35,286 - 36,286 km altitude. Most of the data shows that the space objects in this region are very near the

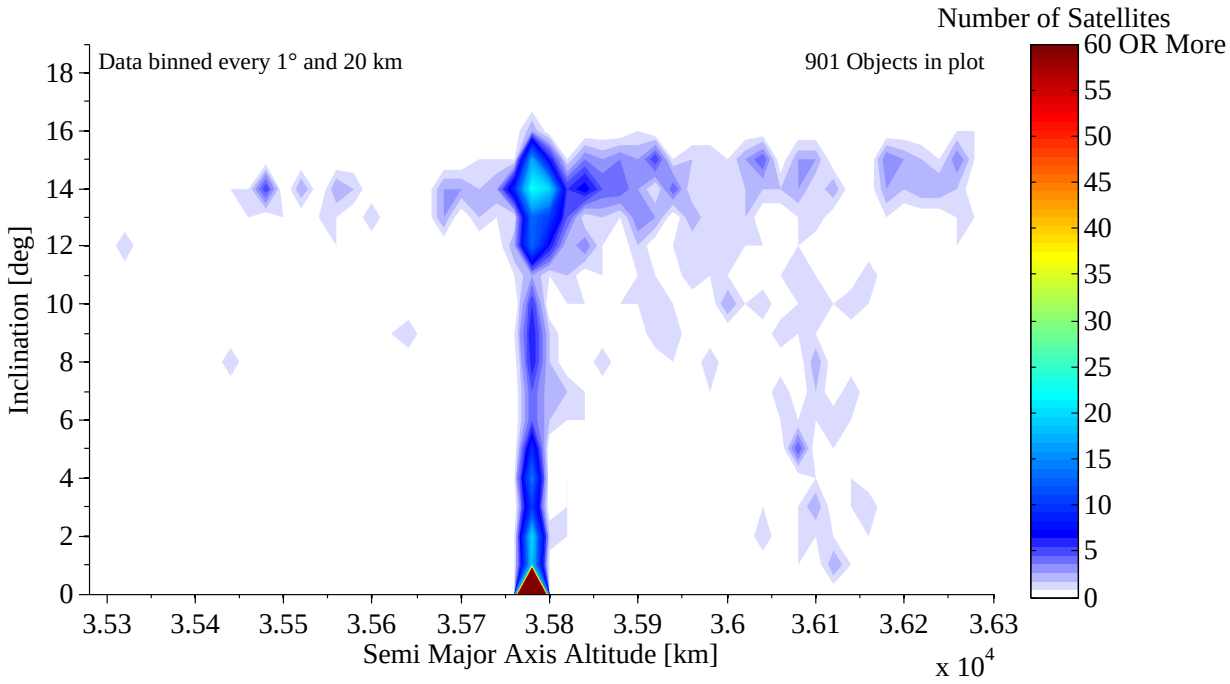

Figure 4.3: Space object dispersion as a function of semi-major axis and inclination of orbit for GEO region.

GEO altitude and have zero inclination.

4.2 GEO Graveyard

Spacecraft that are launched into and operate in GEO are supposed to dispose of themselves from GEO at the end of their lifetime. Because GEO is so far from the surface of the Earth it is too costly, in terms of propellant and mass, to have the spacecraft return to the Earth's atmosphere and burn up. Instead the spacecraft is to reserve enough propellant to raise its perigee beyond GEO to a GEO Graveyard.

In 1997 a U.S. interagency working group led by NASA and the DoD created a set of guidelines for post-mission disposal of spacecraft [40]. These guidelines were set up to help mitigate and control the growing space debris problem. The document is called the U.S. Government Orbital Debris Mitigation Standard Practices. The document is intended to guide the disposal of government launched, operated, or procured spacecraft, launch vehicles, and upper stages. The guidelines are also shared with the aerospace industry in a joint effort to control the growing space debris problem. Per the guidelines, a successful

disposal of a spacecraft in GEO is accomplished when the spacecraft maneuvers to an orbit with perigee altitude above 36,100 km. This is about 300 km above GEO altitude. The region of space that is 300 km above GEO will be referred to as the GEO Graveyard.

The Inter-Agency Space Debris Coordination Committee (IADC), a forum composed of international government space agencies, outlines GEO as a protected region in outer space. A protected region is established to ensure that there are plans in place to mitigate space debris and protect the region for future use and sustainability. The Geosynchronous Region that is protected is defined as the altitude's between 35,586 - 35,986 km (±200 km from GEO), and inclination between -15° and +15° [41, 42]. Figure 4.4 shows this region as Region B. The IADC came up with a way of calculating the distance that a space object should reorbit itself from the GEO protected region, at end of life, that ensures the space object will not interfere with objects still operating in the GEO protected region.

$$\Delta h_{GEO} = 235\,km + \left(1000 \cdot C_R \cdot \frac{A}{m}\right) \tag{4.4}$$

where Δh_{GEO} is the minimum perigee altitude increase from GEO that the spacecraft needs to maneuver too, C_R is the solar radiation pressure coefficient, $\frac{A}{m}$ is the aspect area to dry mass ratio of the space object $\left(\frac{m^2}{kg}\right)$. The 235 km in Equation 4.4 is the sum of the upper altitude of the GEO protected region and the maximum descent of the re-orbited space object due to luni-solar and geopotential perturbations. IADC also states that an eccentricity less than or equal to 0.003 is needed at the end of re-orbit. When a space object re-orbits itself Δh_{GEO} from GEO it will take an extremely long period for the object to re-enter the GEO protected region under natural forces alone. This approach will ensure the preservation of the GEO region for future spacecraft. Figure 4.5 shows the region defined by Δh_{GEO} which the IADC labels Super-GEO. Super-GEO is the same as the GEO graveyard for this thesis.

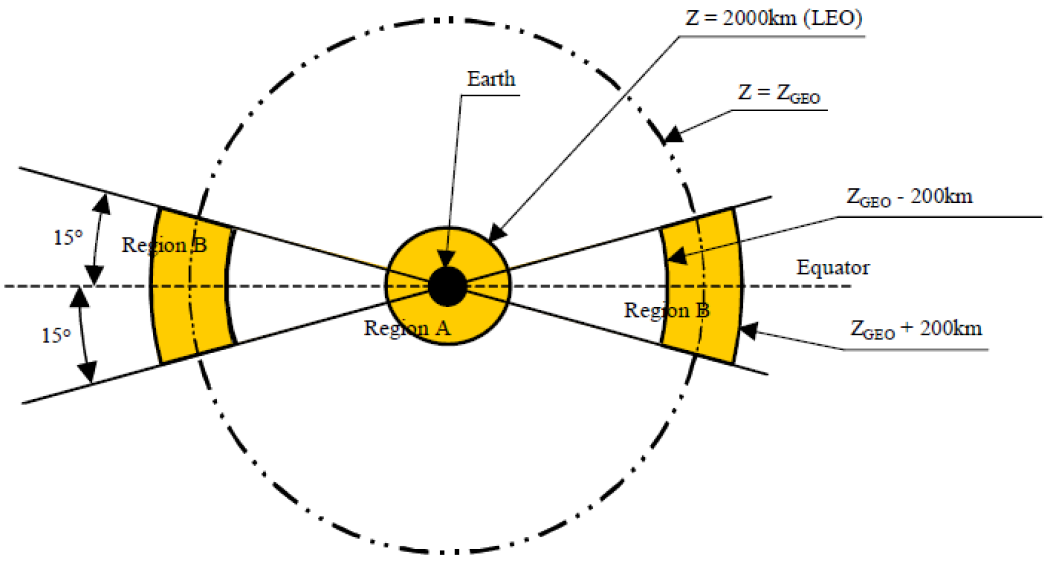

Figure 4.4: Protected regions of outer space defined by the IADC.

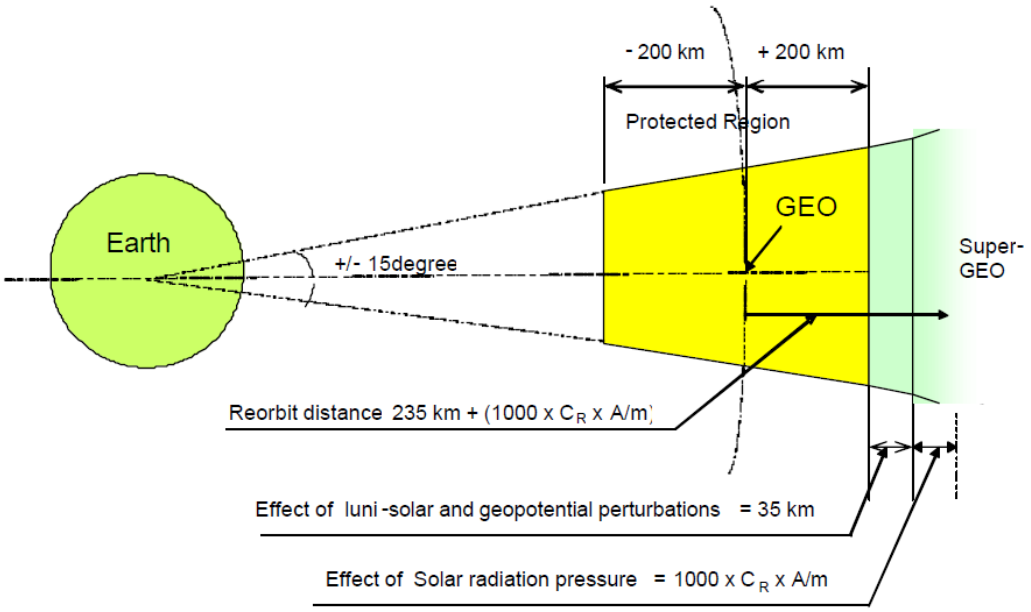

Figure 4.5: GEO protected and reorbit regions defined by the IADC.

Although these guidelines have been established to protect the GEO region, there remains many spacecraft that are not functional in the GEO protected region. As of May 2012 there are 419 operational satellites in GEO [43]. This means that less than half of the population shown in Figures 4.1-4.3 are active, functioning satellites. Even with spacecraft following the guidelines of reserving propellant to reorbit at end of lifetime, unforeseen failures of key spacecraft systems can prevent it from properly disposing of itself to the GEO graveyard region.

Many times satellites remain operable after their propellant is depleted [34]. In the GEO region, without propellant to control orbit drift, satellites naturally drift into inclined orbits, however their semi-major axis remains unchanged. Some satellite operators choose to keep a satellite in an inclined GEO orbit operating at a reduced capacity because of monetary reasons. A satellite with no propellant to correct its orbit inclination perturbations will remain at the GEO altitude drifting in inclination. Remaining in GEO without propellant implies that the satellite will not be able to reorbit itself to the GEO graveyard. Currently there is not a way to dispose of these inoperable drifting GEO Sats.

Chapter 5

Carrier Concept

A proposed solution to perform inspections of space objects in the GEO region is to use a system of multiple satellites. The system will contain one Carrier platform, referred to as the Carrier, and one or more SmallSats deemed Inspectors. The Inspectors are docked to the Carrier and have the capability to depart the Carrier, to perform proximity operations and inspection, and return and re-dock with the Carrier. The Carrier has the capability to release, capture and refuel the Inspectors. This system, composed of one Carrier and one or more Inspectors, will be referred to as the carrier concept.

The Carrier is placed in a near GEO orbit and remains in this near GEO orbit. An Inspector departs the near GEO orbit and performs an inspection on a defined GEO RSO. Once the inspection mission has concluded, the Inspector returns and docks to the Carrier.

The transfer to the GEO RSO is modeled as an orbital rendezvous problem using the CW equations. The equations will be discussed later. The return to the Carrier is also modeled as an orbital rendezvous problem using the CW equations. This poses a two phase rendezvous problem with one time constraint. The time constraint is the specified time that the Inspector is in the proximity of the GEO RSO, where as the transfer times are unconstrained.

5.1 Capabilities

The Carrier vehicle is designed to serve primarily as an active docking and refueling station for the Inspector. It maintains a full set of basic guidance navigation and controls (GNC) functions, a communications link with the ground, a minimal propulsion capability, a short-range inter-satellite communications link with the Inspector, and serves optionally as a high-speed data link to the ground.

The Inspector vehicle is purposed to provide a GEO RSO inspection capability. Each individual inspection mission performed by the Inspector will be referred to as a sortie. The Inspector maintains a full set of basic GNC functions, a communications link with the ground, a propulsion capability, and a short-range inter-satellite communications link with the Carrier. Inertial navigation is nominally achieved by ground tracking and optionally supported by the Carrier inter-satellite communications link. Each Inspector maintains an optical camera for long-range relative optical navigation (1 km - 100 km), inspection imagery, and close-in (< 100 m) 6-dof relative (pose) navigation. An optional artificial illumination device is also maintained. A flash Lidar is also considered for robust, close-in (<100m), 6-dof relative (pose) navigation.

5.2 Carrier Orbit

The Carrier will be placed in a coelliptic orbit with GEO. This will provide minimal propellant plane change maneuvers of the Inspector when transferring between the two orbits. Two types of coelliptic orbits will be examined, circular and elliptical.

5.2.1 Circular

One possible Carrier orbit is a circular orbit that is coplanar with GEO. The radial difference between the Carrier orbit and GEO is ΔH. The ΔH determines the synodic period that the Carrier has with a specific GEO Sat. The synodic period is the frequency that minimum propellant trajectories, via Hohmann transfers, can occur with a specific GEO RSO. To determine the relationship between the synodic period and Δh, the synodic period equation from [13] is used.

$$T_{syn} = \frac{T_{GEO} T_{carrier}}{|T_{GEO} - T_{carrier}|} \tag{5.1}$$

where T_{syn} is the synodic period, T_{GEO} is the period of GEO orbit, $T_{carrier}$ is the period of the Carrier orbit. Assuming that both the Carrier orbit and GEO are perfectly circular

orbits the equations for the orbital periods are

$$T_{GEO} = \frac{2\pi}{\sqrt{\mu}} R_{GEO}^{\frac{3}{2}} \tag{5.2}$$

$$T_{carrier} = \frac{2\pi}{\sqrt{\mu}} (R_{GEO} + \Delta H)^{\frac{3}{2}} \tag{5.3}$$

where R_{GEO} is the radius of GEO, and μ is the gravitational parameter of Earth. Both of these are know values. Substituting in the equations for the orbit period into the equation for the synodic period yields and equation in terms of ΔH.

$$T_{syn} = \frac{2\pi R_{GEO}^{\frac{3}{2}} \left(R_{GEO} + \Delta H\right)^{\frac{3}{2}}}{\sqrt{\mu} \left| R_{GEO}^{\frac{3}{2}} - \left(R_{GEO} + \Delta H\right)^{\frac{3}{2}} \right|} \tag{5.4}$$

As the ΔH grows larger the synodic period is reduced. Figure 5.1 shows a plot of how the synodic period, T_{syn}, is affected by varying the radial distance from GEO, ΔH, for circular orbits.

An advantage of using the circular orbit is that the Carrier orbit will remain outside of the GEO protected region, as described in 4.2, for the entire synodic period. Figure 5.2 shows an example orbit trace of the circular Carrier orbit for one synodic period in an Earth Centered Earth Fixed (ECEF) coordinate system. The ECEF reference frame rotates at the same rate as the rotation of the Earth. The Carrier is placed in a circular orbit 300 km above GEO, the blue curve is its orbit trace. The red dashed curve is the GEO altitude. The red dots are samples of actual GEO RSOs. Int the ECEF reference frame the red dots remain stationary. The black dots show the position of the Carrier as a function of time. For a circular orbit 300 km above GEO the synodic period is about 94 days.

5.2.2 Cycloid (Elliptical)

The Carrier can also be placed in an coelliptic orbit with GEO. This orbit is termed a

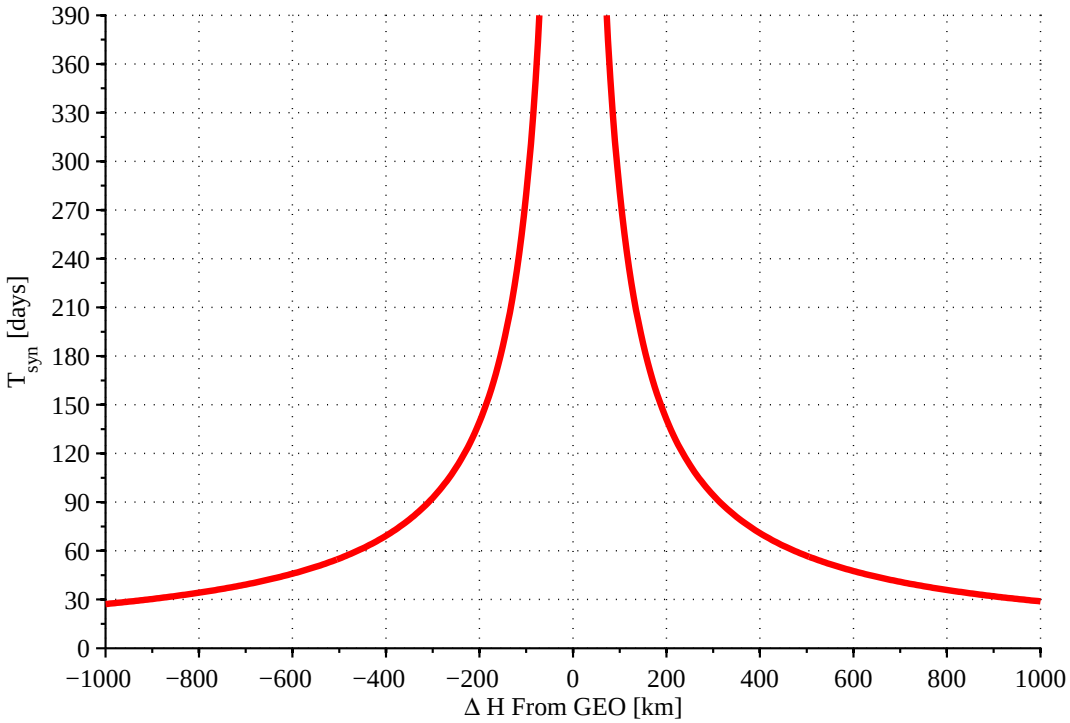

Figure 5.1: Synodic period between Carrier and GEO as a function of ΔH.

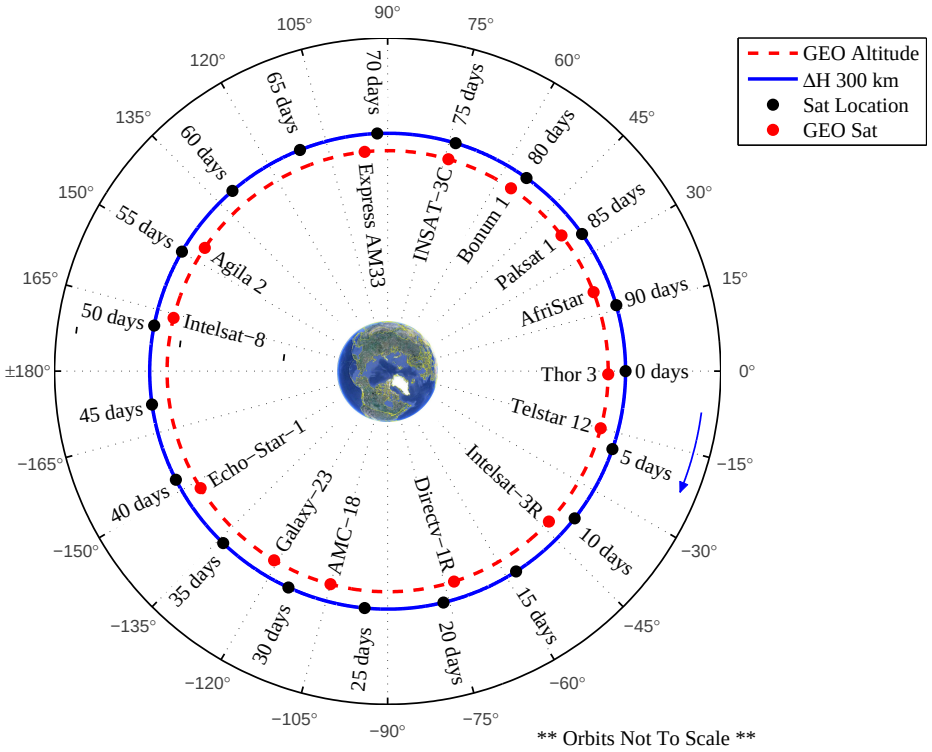

Figure 5.2: Carrier in a circular orbit in an ECEF coordinate system.

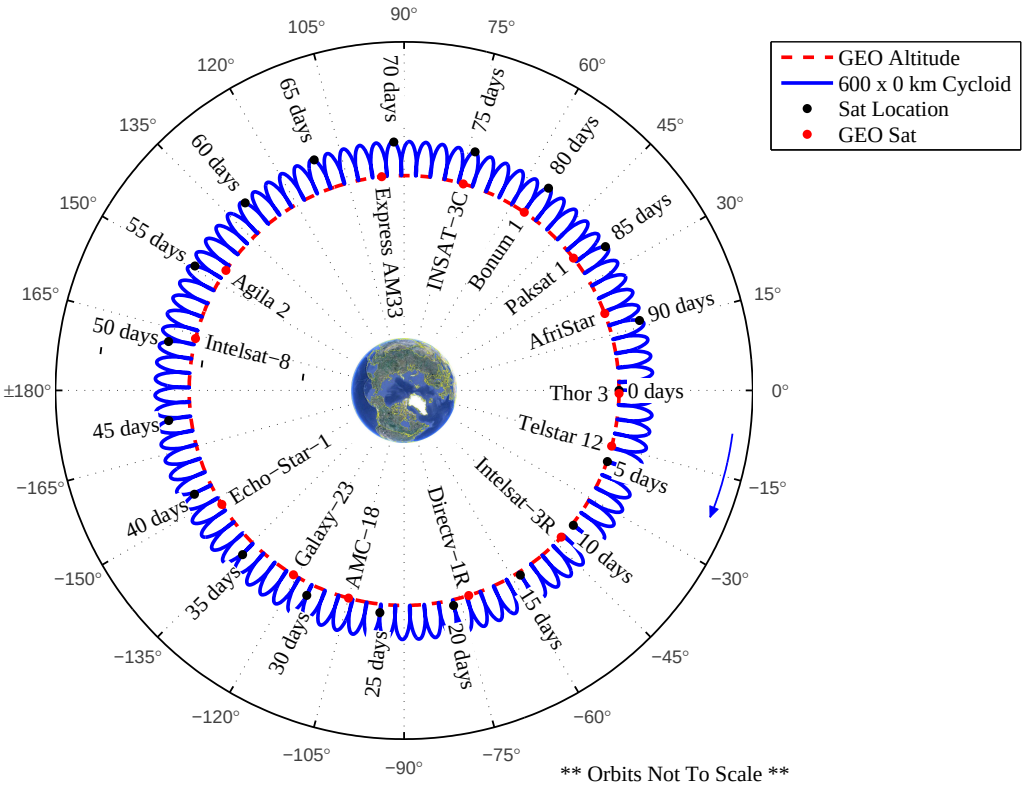

Figure 5.3: Carrier in a cycloid orbit in an ECEF coordinate system.

cycloid orbit because of its orbit trace in the ECEF coordinate system with respect to the GEO orbit. The cycloid orbit has the same synodic period as a circular orbit of equal orbit energy. The equation for the orbit's energy is

$$\xi = -\frac{\mu}{2a} \tag{5.5}$$

where ξ is the specific mechanical energy of the orbit, μ is the gravitational parameter of Earth, and a is the semimajor axis of the orbit [21]. For example a cycloid orbit with perigee at GEO and apogee 600 km above GEO will have the same synodic period as a circular orbit 300 km above GEO. Figure 5.3 shows an example cycloid orbit in the ECEF reference frame. In this plot the red dashed curve is the GEO altitude, the blue curve is the orbit of the Carrier, the black dots represent the Carrier position as a function of time, and the red dots are sample stationary GEO RSOs.

Placing a Carrier in a cycloid orbit has the advantage of bringing the Carrier close to the GEO altitude. This can provide opportunities for the Carrier to observe GEO RSOs from close range. Also it can provide lower propellant requirements for the Inspector when transferring to a targeted GEO RSO. A disadvantage, or possible concern, is that cycloid orbits may enter the GEO protected region as defined in 4.2. If the cycloid orbit of the Carrier is designed to stay out of the GEO protected region, it loses its advantages over the circular orbit.

5.3 Hohmann Transfers

Hohmann transfers provide minimum change in velocity (Δv) transfers between coaxial coelliptic orbits. Minimum Δv transfers implies minimum propellant usage. Hohmann transfer analysis for transfers between the Carrier orbit and GEO will be used as benchmarks. A Hohmann transfer is used to transfer the Inspector from the Carrier orbit to the GEO RSO. For this analysis, the Inspector intersects GEO at the location of the RSO of interest, i.e. no phasing is required once the Inspector is at GEO. A Hohmann transfer is then used to transfer the Inspector back to the Carrier. For the Inspector to utilize two Hohmann transfers to accomplish the inspection mission, it must stay in proximity with the GEO RSO for the synodic period of the Carrier orbit. The time that the Inspector stays in proximity with the GEO RSO will be referred to as stay time or T_{stay}. Figure 5.4 shows the Δv required for the Inspector to complete the two Hohmann transfers for a Carrier in a circular orbit of ΔH from GEO. Figure 5.5 shows Figure 5.1 superimposed on Figure 5.4. For a given Carrier ΔH, there will be a minimum Δv and specified stay time of the Inspector (the synodic period).

To calculate the Hohmann transfer Δv the steps presented in [13, 21, 22] were used. This Hohmann transfer analysis is used as a baseline or guideline for the theoretical minimum Δv. Duel Hohmann transfers cannot be utilized for an inspection sortie if T_{stay} is not the synodic period of the Carrier orbit. For this reason the CW equations will be used to find minimum Δv solutions when T_{stay} is not the synodic period.

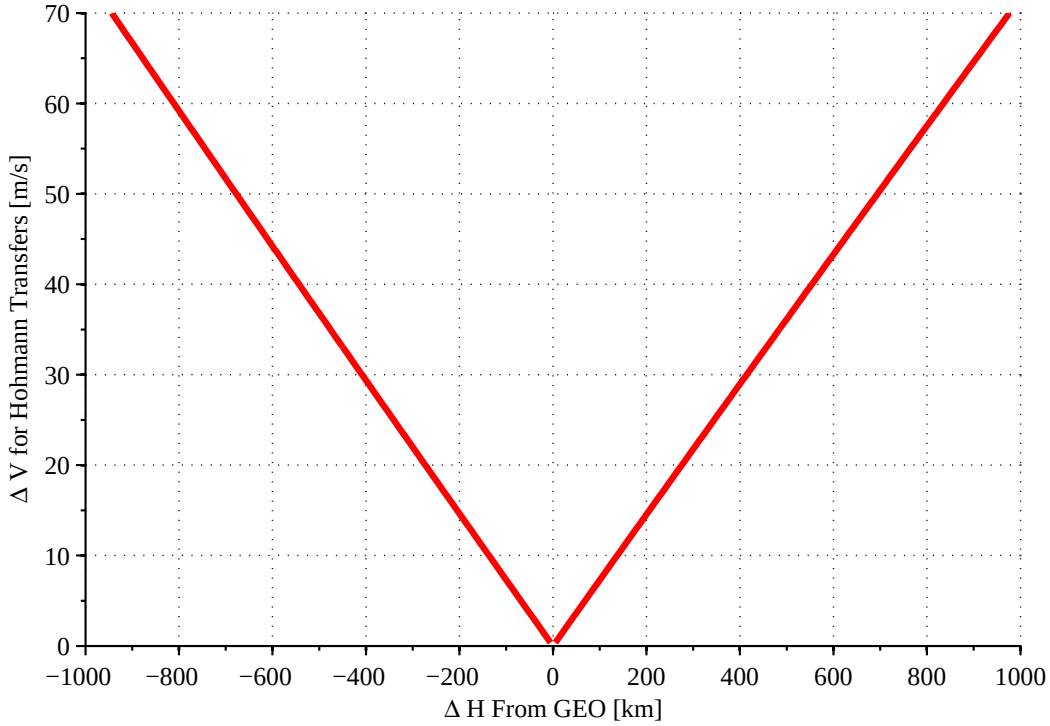

Figure 5.4: Hohmann transfer Δv as a function of ΔH.

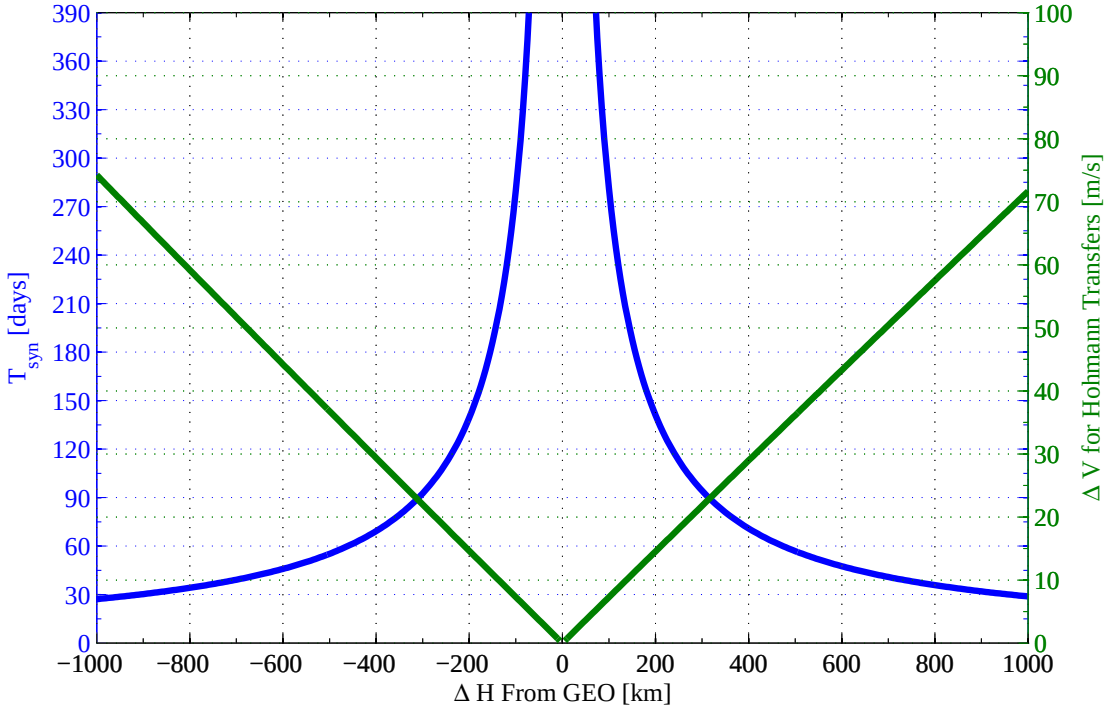

Figure 5.5: Synodic period and Hohmann transfer Δv as a functions of ΔH.

Chapter 6

Optimal Non-Hohmann Maneuvers

For the Inspector to perform orbital transfers from the Carrier to the GEO RSO and back to the Carrier without the stay time being defined by the synodic period, non-Hohmann transfers are needed, and the desired stay time of the Inspector becomes a variable.

In this chapter the CW equations are presented and used to describe the Inspector trajectory from the Carrier to the GEO RSO, and from the GEO RSO back to the Carrier. CW targeting is used to calculate the required Δv for an inspection sortie. Traditional optimization and convex optimization techniques will be applied to determine trajectories that produce minimum Δv.

6.1 Problem Description

A Carrier, equipped with one or more Inspectors, is in a near GEO orbit. The Carrier is in a coelliptic orbit that is a specified radial distance, ΔH, above or below GEO. Both orbits are assumed to be perfectly circular.

$$\left\|\bar{R}_{Carrier}\right\| = \left\|\bar{R}_{GEO}\right\| + \Delta H \tag{6.1}$$

The Inspector transfers from the Carrier to a specific GEO RSO, stays in GEO for a specified time, and then transfers back to the Carrier. The transfer to the GEO RSO will be called transfer 1. The time that it takes the Inspector to transfer from the Carrier to the GEO RSO will be T_1. Once the Inspector has arrived at the GEO RSO it remains there for a specified amount of time, T_{stay}. After the specified stay time, the Inspector transfers back to the Carrier. This will be transfer 2. The time that it takes to transfer back to the Carrier will be T_2. The stay time will be specified, however the two transfer times are unconstrained. This is the unconstrained-time double rendezvous problem.

Each of the two transfers are modeled as a two-burn impulse maneuver. Thus four impulsive burn Δv's are needed to complete the round-trip mission for the Inspector. The instantaneous velocity change, Δv, associated with each impulse burn is calculated using the well known CW or Hills equations. The problem is to find the minimum total change in velocity, Δv_{total} for a specified ΔH and T_{stay}.

6.2 CW Equations

The CW equations are used to describe the relative dynamics of the Carrier and Inspector in the Local Vertical Local Horizontal (LVLH) relative reference frame. For this problem the LVLH frame will initially be referenced from the center of mass of the GEO RSO (see Figure 6.1). The x-axis is in the radial direction or altitude/local vertical, the y-axis is in the near velocity direction or the downrange/local horizontal, and the z-axis is in the direction of the angular momentum or cross-track/out-of-plane. From [44] the CW equations for this LVLH frame are

$$\ddot{x} - 3\Omega^2 x - 2\Omega\dot{y} = 0 \tag{6.2}$$

$$\ddot{y} + 2\Omega\dot{x} = 0 \tag{6.3}$$

$$\ddot{z} + \Omega^2 z = 0 \tag{6.4}$$

$$\Omega = \sqrt{\mu_{\oplus} / \|R\|^3} \tag{6.5}$$

where Ω is the angular rate of the reference orbit, $\mu_{\oplus}$ is the gravitational parameter of the Earth, and R is the radius of the reference orbit from the center of the Earth.

The CW equations are a set of linear differential equations and can be written in the form $\dot{X} = FX$. The state, X, is the relative position and velocity in the LVLH frame.

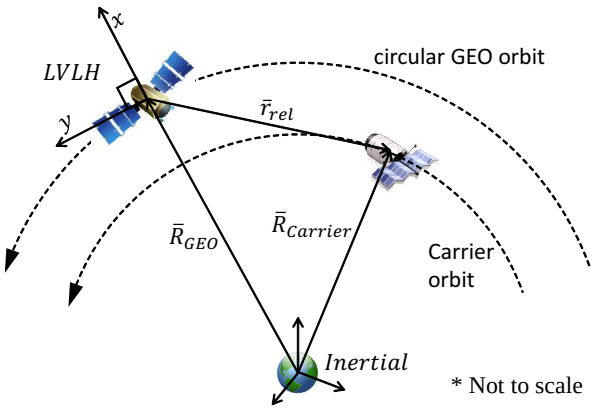

Figure 6.1: Geometry of the LVLH frame.

$$\bar{r}_{rel} = \begin{bmatrix} x \\ y \\ z \end{bmatrix} \qquad \bar{v}_{rel} = \begin{bmatrix} \dot{x} \\ \dot{y} \\ \dot{z} \end{bmatrix} \tag{6.6}$$

$$X = \begin{bmatrix} \bar{r}_{rel} \\ \bar{v}_{rel} \end{bmatrix} \tag{6.7}$$

$$\overbrace{\begin{bmatrix} \dot{x} \\ \dot{y} \\ \dot{z} \\ \ddot{x} \\ \ddot{y} \\ \ddot{z} \end{bmatrix}}^{\dot{X}} = \overbrace{\begin{bmatrix} 0 & 0 & 0 & 1 & 0 & 0 \\ 0 & 0 & 0 & 0 & 1 & 0 \\ 0 & 0 & 0 & 0 & 0 & 1 \\ 3\Omega^2 & 0 & 0 & 0 & 2\Omega & 0 \\ 0 & 0 & 0 & -2\Omega & 0 & 0 \\ 0 & 0 & 0 & 0 & 0 & -\Omega^2 \end{bmatrix}}^{F} \overbrace{\begin{bmatrix} x \\ y \\ z \\ \dot{x} \\ \dot{y} \\ \dot{z} \end{bmatrix}}^{X} \tag{6.8}$$

Because the CW equations are linear constant coefficient differential equations the analytical solutions are know. From [13, 44] the solutions are

$$x(t) = x_0(4 - 3cos\Omega t) + \dot{x}_0 sin\Omega t/\Omega + 2\dot{y}_0(1 - cos\Omega t)/\Omega \tag{6.9}$$

$$y(t) = 6x_0(sin\Omega t - \Omega t) + y_0 + 2\dot{x}_0(cos\Omega t - 1)/\Omega + \dot{y}_0(4sin\Omega t - 3\Omega t)/\Omega \tag{6.10}$$

$$z(t) = z_0 cos\Omega t + \dot{z}_0 sin\Omega t/\Omega \tag{6.11}$$

$$\dot{x}(t) = 3x_0\Omega sin\Omega t + \dot{x}_0 cos\Omega t + 2\dot{y}_0 sin\Omega t \tag{6.12}$$

$$\dot{y}(t) = 6x_0\Omega(cos\Omega t - 1) - 2\dot{x}_0 sin\Omega t + \dot{y}_0(4cos\Omega t - 3) \tag{6.13}$$

$$\dot{z}(t) = -z_0\Omega sin\Omega t + \dot{z}_0 cos\Omega t \tag{6.14}$$

The solutions can also be written in the matrix form of $X(t) = \Phi(\Delta t)X(t_0)$ with $\Delta t = t - t_0$. Where $\Phi(\Delta t)$ is the CW transition matrix.

$$\Phi(\Delta t) = \begin{bmatrix} 4 - 3cos\Omega\Delta t & 0 & 0 & sin\Omega\Delta t/\Omega & 2(1 - cos\Omega\Delta t)/\Omega & 0 \\ 6(sin\Omega\Delta t - \Omega\Delta t) & 1 & 0 & 2(cos\Omega\Delta t - 1)/\Omega & (4sin\Omega\Delta t - 3\Omega\Delta t)/\Omega & 0 \\ 0 & 0 & cos\Omega\Delta t & 0 & 0 & sin\Omega\Delta t/\Omega \\ 3\Omega sin\Omega\Delta t & 0 & 0 & cos\Omega\Delta t & 2sin\Omega\Delta t & 0 \\ 6\Omega(cos\Omega\Delta t - 1) & 0 & 0 & -2sin\Omega\Delta t & 4cos\Omega\Delta t - 3 & 0 \\ 0 & 0 & -\Omega sin\Omega\Delta t & 0 & 0 & cos\Omega\Delta t \end{bmatrix} \tag{6.15}$$

Φ is simply a function of the time difference between the initial state and the final state, and the orbital angular rate. For each impulse maneuver Δt is the transfer time. The orbital rate is the rotation rate of the reference frame. To compute impulse maneuver Δv's, Φ is computed first using $\Delta t = T_1$ for calculating Δv_1 and Δv_2 and $\Delta t = T_2$ for calculating Δv_3 and Δv_4.

For ease of calculations Φ is partitioned into four sub-matrices

$$\Phi = \begin{bmatrix} \Phi_{rr} & \Phi_{rv} \\ \Phi_{vr} & \Phi_{vv} \end{bmatrix} \tag{6.16}$$

Using Φ, the relative position and velocity at any time can be found if the initial relative position and velocity are know [44]

$$\begin{bmatrix} \bar{r}_{rel}(t) \\ \bar{v}_{rel}(t) \end{bmatrix} = \begin{bmatrix} \Phi_{rr} & \Phi_{rv} \\ \Phi_{vr} & \Phi_{vv} \end{bmatrix} \begin{bmatrix} \bar{r}_{rel}(t_0) \\ \bar{v}_{rel}(t_0) \end{bmatrix} \tag{6.17}$$

6.3 Calculating Δv for Impulsive Burn Maneuvers

All calculations for determining the impulsive burn Δv required for each maneuver are made in the LVLH reference frame. For simplicity the subscript "rel" is left off position and velocity vectors.

6.3.1 Transfer 1: Transfer to GEO RSO

Transfer 1 consists of two impulsive maneuvers. The goal is to find the change in velocity, Δv_1 and Δv_2, that will place the Inspector at the GEO RSO.

The initial position of the Inspector referenced from the GEO RSO is

$$\bar{r}_0 = \begin{bmatrix} \Delta H \\ DR_0 \\ 0 \end{bmatrix} \tag{6.18}$$

where DR_0 is the initial downrange position of the Inspector in the LVLH frame. There is no out-of-plane component because the orbits are coplanar. Because the Inspector is initially

in a circular orbit, ΔH is constant, and this implies that Equation 6.12 must equal zero. Because ΔH does not change with time the initial altitude rate, $\dot{x}_0$, also equals zero. The initial downrange velocity can be found by setting Equation 6.12 equal to zero and $\dot{x}_0$ equal to zero and solving for $\dot{y}_0$ [44].

$$\dot{y}_0 = -\frac{3}{2}\Omega_{GEO}\Delta H \tag{6.19}$$

Thus, all of the Inspector initial velocity is in the downrange direction

$$\bar{v}_0 = \begin{bmatrix} 0 \\ -\frac{3}{2}\Omega_{GEO}\Delta H \\ 0 \end{bmatrix} \tag{6.20}$$

For this problem it is desired to rendezvous with the GEO RSO at the end of transfer 1. The desired position at the end of transfer 1 is

$$\bar{r}_d = \begin{bmatrix} 0 \\ 0 \\ 0 \end{bmatrix} \tag{6.21}$$

With the initial position and velocity and the final desired position and velocity known, the CW equations and the associated transition matrix, $\Phi_1 = \Phi\left(\Omega_{GEO}, T_1\right)$, can be used to determine the required changes in velocity. The first change in velocity, Δv_1, is needed to start the transfer to the GEO RSO. The second change in velocity, Δv_2, is needed to end the transfer. Using Equation 6.17,

$$\bar{r}\left(t_0 + T_1\right) = \Phi_{1rr}\bar{r}_0 + \Phi_{1rv}\left[\bar{v}_0 + \Delta v_1\right] \tag{6.22}$$

Setting $\bar{r}\left(t_0 + T_1\right) = \bar{r}_d = \bar{0}$ in Equation 6.22 and solving for Δv_1 yields

$$\Delta v_1 = -\Phi_{1rv}^{-1}\Phi_{1rr}\bar{r}_0 - \bar{v}_0 \tag{6.23}$$

To find Δv_2 Equation 6.17 is used to find the velocity at the end of the transfer (arrival at GEO RSO).

$$\bar{v}\left(t_0 + T_1\right) = \Phi_{1vr}\bar{r}_0 + \Phi_{1vv}\left[\bar{v}_0 + \Delta v_1\right] \tag{6.24}$$

Rearranging Equation 6.23

$$\bar{v}_0 + \Delta v_1 = -\Phi_{1rv}^{-1}\Phi_{1rr}\bar{r}_0 \tag{6.25}$$

And substituting Equation 6.25 into 6.24 produces

$$\bar{v}\left(t_0 + T_1\right) = \Phi_{1vr}\bar{r}_0 - \Phi_{1vv}\Phi_{1rv}^{-1}\Phi_{1rr}\bar{r}_0 \tag{6.26}$$

The change in velocity of the second burn is

$$\Delta v_2 = \bar{v}_d - \bar{v}\left(t_0 + T_1\right) = -\bar{v}\left(t_0 + T_1\right) \tag{6.27}$$

where the final desired velocity, $\bar{v}_d$, is zero. Thus,

$$\Delta v_2 = \Phi_{1vv}\Phi_{1rv}^{-1}\Phi_{1rr}\bar{r}_0 - \Phi_{1vr}\bar{r}_0 \tag{6.28}$$

6.3.2 Transfer 2: Transfer Back to the Carrier

Similar to transfer 1, transfer 2 consists of two impulsive maneuvers. The goal is to find the change in velocity, Δv_3 and Δv_4, that will return the Inspector to the Carrier.

When the Inspector is ready to return to the Carrier, the position of the Carrier must be known. To update the relative state (position and velocity) of the Carrier, the CW equations are used. The initial state of the Carrier is the same as the initial state of the Inspector for

Table 6.1: States of Carrier for Circular Orbit

State	Description
X_{C_0}	Initial conditions of Carrier at beginning of Inspector's transfer 1
X_{C_1}	State of Carrier at the end of Inspector's transfer 1
X_{C_2}	State of Carrier at beginning of Inspector's transfer 2
X_{C_3}	State of Carrier at the end of Inspector's transfer 2

transfer 1.

$$X_{C_0} = \begin{bmatrix} \Delta H \\ DR \\ 0 \\ 0 \\ -\frac{3}{2}\Omega_{GEO}\Delta H \\ 0 \end{bmatrix} \tag{6.29}$$

The state of the Carrier at the time the Inspector arrives at the GEO RSO is state one, X_{C_1}. The state of the Carrier when the Inspector is ready to depart from the GEO RSO is state two, X_{C_2}. The state of the Carrier when the Inspector returns and with it is state three, X_{C_3}. Figure 6.2 shows a diagram of these states and Table 6.1 has an overview of the states.

The equations for the state updates are

$$X_{C_1} = \Phi\left(T_1\right) X_{C_0} \tag{6.30}$$

$$X_{C_2} = \Phi\left(T_{stay}\right) X_{C_1} = \Phi\left(T_{stay}\right) \Phi\left(T_1\right) X_{C_0} \tag{6.31}$$

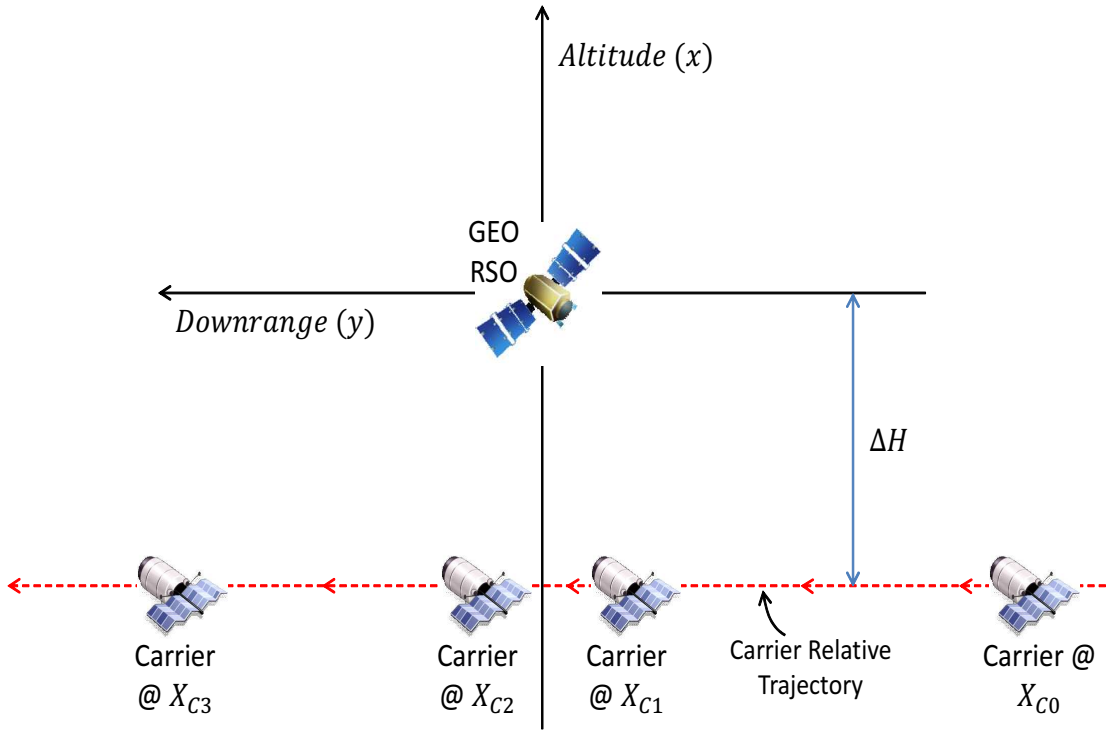

Figure 6.2: The four different states of the Carrier during the mission. The LVLH coordinate frame is centered at the GEO RSO.

$$X_{C_3} = \Phi\left(T_2\right) X_{C_2} = \Phi\left(T_2\right) \Phi\left(T_{stay}\right) \Phi\left(T_1\right) X_{C_0} \tag{6.32}$$

where the transition matrices used for updating the Carrier state use the angular rate of the GEO RSO.

Depending on how long the total mission time is, $T_{mission} = T_1 + T_{stay} + T_2$, the downrange of the Carrier at a given state may need to be adjusted. The maximum (or minimum) downrange, DR_{max}, is equal to half of the GEO orbit's circumference. This is because the maximum angle between the GEO RSO and the Carrier from an inertial frame is 180°. See Figure 6.3.

$$DR_{max} = \pi \left\| \bar{R}_{GEO} \right\| \tag{6.33}$$

Each time the Carrier state is updated the Carrier downrange, DR_C, must fall between the maximum and minimum allowed downrange.

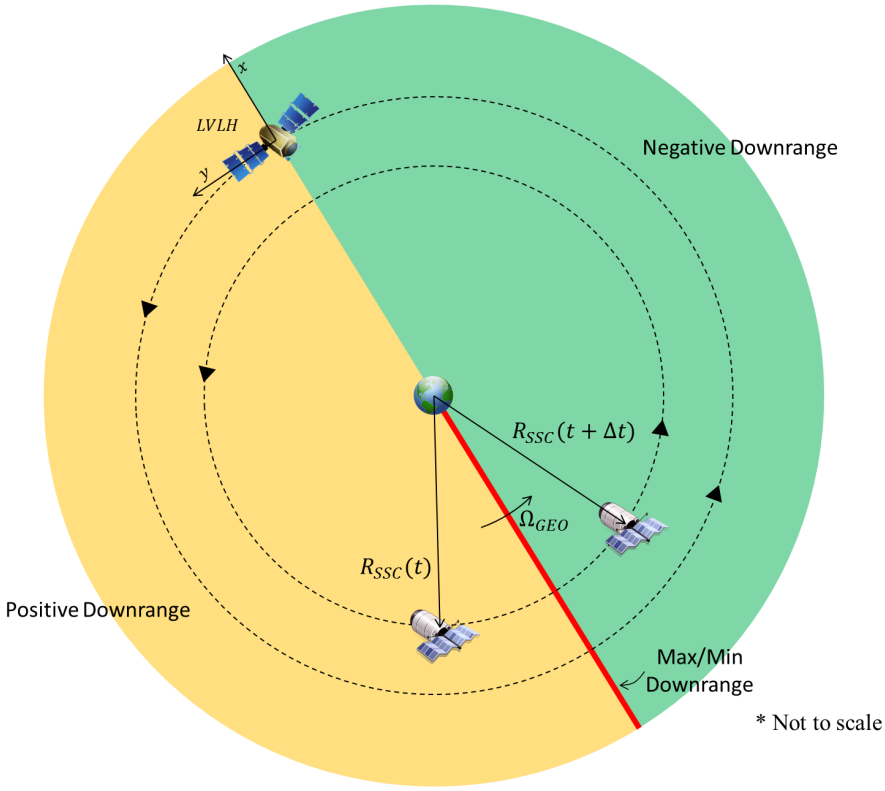

Figure 6.3: Description of the maximum downrange for a coelliptic orbit in the LVLH frame. The two shaded regions rotate with the LVLH frame.

$$-DR_{max} \leq DR_C \leq DR_{max} \tag{6.34}$$

If the downrange of the Carrier is not within the check then the appropriate adjustment must be made.

$$DR_C^* = DR_C - n \cdot DR_{max} \tag{6.35}$$

where DR_C^* is the updated downrange of the Inspector Carrier and n is

$$n = fix\left(\frac{DR_C}{DR_{max}}\right) + sign\left(DR_C\right) \tag{6.36}$$

where *fix* rounds towards zero and *sign* is either positive one or negative one depending on if DR_C is positive or negative.

Transfer 1 is assumed to have placed the Inspector exactly at the GEO RSO with zero relative velocity. The sub-subscript 2 corresponds to transfer 2. The initial relative position and velocity of the Inspector for transfer 2 is

$$\bar{r}_{0_2} = \begin{bmatrix} 0 \\ 0 \\ 0 \end{bmatrix} \qquad \bar{v}_{0_2} = \begin{bmatrix} 0 \\ 0 \\ 0 \end{bmatrix} \tag{6.37}$$

The Carrier's position and velocity at state three, X_{C_3}, (Equation 6.32 and Figure 6.2) is the desired position, $\bar{r}_{d_2}$, and velocity, $\bar{v}_{d_2}$, at the end of transfer 2.

$$X_{C_3} = \begin{bmatrix} \bar{r}_{C_3} \\ \bar{v}_{C_3} \end{bmatrix} \tag{6.38}$$

$$\bar{r}_{C_3} = \bar{r}_{d_2} \qquad \bar{v}_{C_3} = \bar{v}_{d_2} \tag{6.39}$$

$$\bar{r}_{d_2} = \bar{r}_{C_3} \qquad \bar{v}_{d_2} = \bar{v}_{C_3} \tag{6.40}$$

Now using the same approach that was used to find Δv_1 and Δv_2, Δv_3 and Δv_4 can be solved for. For this approach the transition matrix is $\Phi_2 = \Phi\left(\Omega_{GEO}, T_2\right)$. From Equation 6.17

$$\bar{r}_{d_2} = \Phi_{2rr}\bar{r}_{0_2} + \Phi_{2rv}\left[\bar{v}_{0_2} + \Delta v_3\right] \tag{6.41}$$

$$\Delta v_3 = \Phi_{2rv}^{-1}\bar{r}_{d_2} \tag{6.42}$$

Again using Equation 6.17 for the final velocity

$$\bar{v}_f = \Phi_{2vr}\bar{r}_{0_2} + \Phi_{2vv}\left[\bar{v}_{0_2} + \Delta v_3\right] \tag{6.43}$$

where $\bar{v}_f$ is the velocity when the Inspector reaches the desired final position (Carrier). This is at time $t = t_0 + T_1 + T_{stay} + T_2$.

$$\bar{v}_f = \Phi_{2vv}\Delta v_3 = \Phi_{2vv}\Phi_{2rv}^{-1}\bar{r}_{d_2} \tag{6.44}$$

The fourth burn is the difference between the desired velocity and the final velocity at the end of transfer 2.

$$\Delta v_4 = \bar{v}_d - \bar{v}_f = \bar{v}_d - \Phi_{2vv}\Phi_{2rv}^{-1}\bar{r}_{d_2} \tag{6.45}$$

6.3.3 Total Δv For the Mission

The total change in velocity required of the Inspector to transfer to GEO and then transfer back to the Carrier is the sum of the four impulse Δv's. Although the calculations were made in the relative frame using relative positions and velocities the Δv's are the absolute change in velocity.

$$\Delta v_{total} = \|\Delta v_1\| + \|\Delta v_2\| + \|\Delta v_3\| + \|\Delta v_4\| \tag{6.46}$$

6.3.4 Modifications for Cycloid Orbit

The above steps can also be used to solve for the Δv_{total} required of the Inspector to perform a round trip inspection mission from a Carrier in a cycloid orbit. The only change that needs to take place is to set the initial conditions of the Inspector and the Carrier such that they are for a cycloid orbit instead of a circular orbit.

In the LVLH reference frame the cycloid orbit appears to hop in the downrange direction. The maximum (or minimum) altitude of the hop, ΔH_{max}, can be defined and is set by the apogee (or the perigee) altitude of the cycloid orbit. The downrange distance that the hop

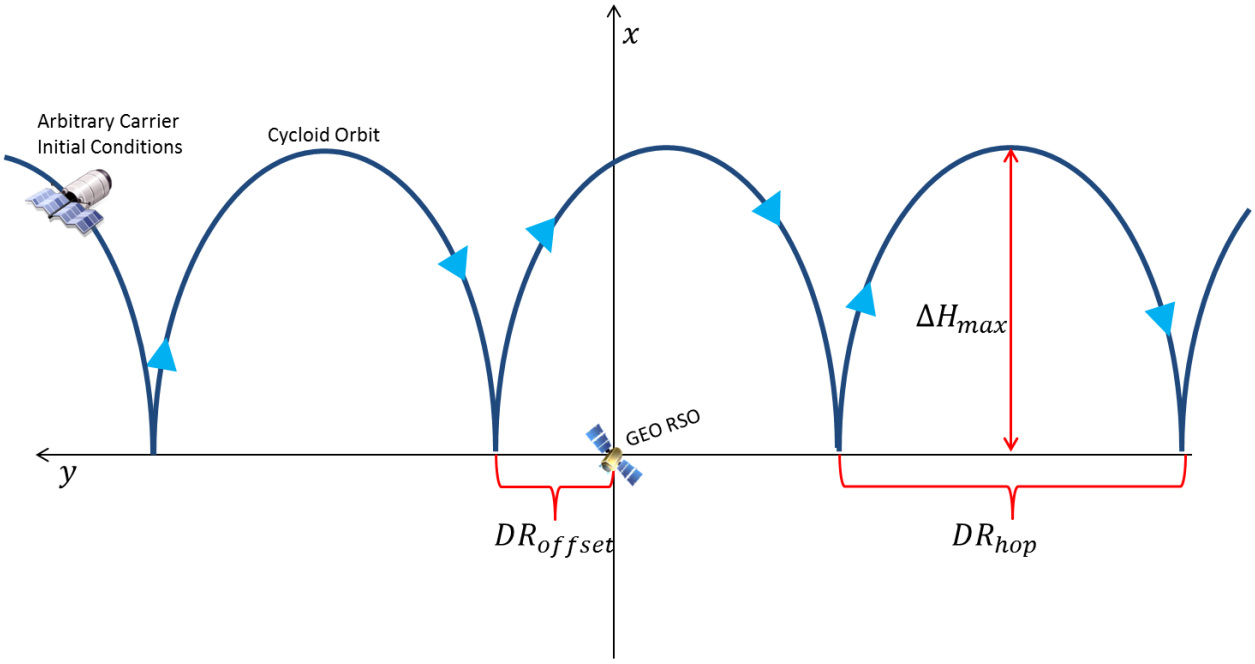

Figure 6.4: Cycloid orbit in LVLH reference frame.

of the cycloid orbit will cover in one orbit period, DR_{hop}, is then defined from the solutions to the CW equations (Equations 6.9-6.14).

$$DR_{hop} = \frac{3\pi}{2}\Delta H_{max} \tag{6.47}$$

The hop, due to natural relative motion, will come to GEO altitude at a specified distance from the GEO RSO. This specified downrange distance from the target is called the downrange offset, DR_{offset}. This offset can be set by the phasing of the hop relative to the GEO RSO. The percent of downrange offset relative to the downrange hop is defined as:

$$\%DR_{offset} = \frac{DR_{offset}}{DR_{hop}} \times 100 \tag{6.48}$$

The geometry of the hop trajectory is laid out in Figure 6.4.

6.4 Numerical Optimization: Searching Method via MATLAB

For a Carrier in a circular orbit, the total change in velocity formulated above, Equation

6.46, is a scalar function of the difference in altitude from GEO, the initial downrange position of the Carrier, the transfer time for transfer 1, the time of stay at GEO, and the transfer time of transfer 2. All calculations are dependent upon these five inputs, assuming that the gravitational parameter of the Earth ($\mu_{\oplus}$), and the magnitude of the radius to GEO (R_{GEO}), are constants.

$$\Delta v_{total} = function(\Delta H, DR_0, T_1, T_{stay}, T_2) \tag{6.49}$$

The MATLAB optimization toolbox contains a function called *fmincon*, that can then be used to find the DR_0, T_1 and T_2 that produce a minimum Δv_{total} for constant ΔH and T_{stay}. The MATLAB help files state, "*fmincon* attempts to find a constrained minimum of a scalar function of several variables starting at an initial estimate. This is generally referred to as constrained nonlinear optimization or nonlinear programming." The constraints are used to ensure that T_1 and T_2 are positive and that the downrange falls within the range specified in Equation 6.34. The transfer time and downrange associated with a Hohmann Transfer is used as an initial guess.

The Hohmann transfer time is computed as follows [13],

$$T_H = \pi \sqrt{\frac{(R_{GEO} + \Delta H/2)}{\mu_{\oplus}}} \tag{6.50}$$

where the subscript H stands for Hohmann. The initial downrange is based off of the arc length between the Carrier and GEO at departure

$$\theta_H = \pi - \Omega_{GEO} T_H \tag{6.51}$$

$$DR_H = -R_{GEO} \theta_H \tag{6.52}$$

Making substitutions the downrange is a function of ΔH

$$DR_H = -\pi R_{GEO}\left(1 - \sqrt{\frac{(R_{GEO} + \Delta H/2)}{\mu_\oplus}}\right) \tag{6.53}$$

A MATLAB function script had to be written that is in the form of Equation 6.49 and uses the methods presented in Section 6.3 to calculate Δv_{total}. The *fmincon* function allows some of the inputs to be constant. Holding ΔH and T_{stay} constant, MATLAB was then used to find the values of DR_0, T_1, and T_2 that produce the minimum Δv_{total}. The minimum values of Δv_{total}, for all ΔH and T_{stay}, is accomplished by looping through a range of values for T_{stay} and a range of values for ΔH. The algorithm that *fmincon* uses must be set to the "interior-point" method as opposed to its default algorithm.

To build confidence in using the *fmincon* function a degree of freedom was taken away from the problem. Taking away the initial downrange as a degree of freedom, and making this a fixed value, a code was written in MATLAB that would loop through initial downrange with a specified ΔH and T_{stay}. Δv_{total} was then calculated at each iteration. Plotting Δv_{total} as a function of initial downrange shows the initial downrange that produce minimum Δv_{total}. These results matched the outputs produced by using *fmincon* to optimize all three inputs. This gave confidence in using *fmincon*.

When the Carrier is in a cycloid orbit, Equation 6.46 remains a scalar function of scalar inputs that can be optimized using the *fmincon* MATLAB function, however, the inputs to the scalar equation are slightly different. The new variables of the equation are the initial position and velocity of the Carrier, X_{C_0}, and the time of the first burn, $T_{go} > 0$, with T_1, T_2, and T_{stay} still being used.

$$\Delta v_{total} = function(X_{C_0}, T_{go}, T_1, T_{stay}, T_2) \tag{6.54}$$

Now using *fmincon* the variables to solve for are T_{go}, T_1, and T_2, with X_{C_0} and T_{stay} being held constant. X_{C_0} is the initial condition that satisfies the solution to the CW equations and produces the cycloid orbit. A simple example of an initial condition that satisfies this is

to start the Carrier downrange at the GEO altitude. The initial downrange of the Carrier, DR_{C_0}, depends on whether the cycloid orbit is above GEO or below GEO. For the case of the cycloid above GEO, DR_{C_0} is placed in the positive downrange so that the Carrier hops along GEO and passes over the GEO RSO.

$$DR_{C_0} = DR_{offset} + N\left(DR_{hop}\right) \tag{6.55}$$

where N is a positive integer. Then

$$X_{C_0} = \begin{bmatrix} 0 \\ DR_{C_0} \\ 0 \\ 0 \\ \frac{\Omega}{4}\Delta H_{max} \\ 0 \end{bmatrix} \tag{6.56}$$

is an example of initial Carrier conditions that produce a cycloid orbit in the LVLH reference frame. Subsequent states of the Carrier are shown in Table 6.2.

The state update equations are now

$$X_{C_1} = \Phi\left(T_{go}\right) X_{C_0} \tag{6.57}$$

$$X_{C_2} = \Phi\left(T_1\right) X_{C_1} \tag{6.58}$$

$$X_{C_3} = \Phi\left(T_{stay}\right) X_{C_2} \tag{6.59}$$

$$X_{C_4} = \Phi\left(T_2\right) X_{C_3} \tag{6.60}$$

Table 6.2: States of Carrier for Cycloid Orbit

State	Description
X_{C_0}	Initial conditions that provide a cycloid orbit
X_{C_1}	State of Carrier at the beginning of Inspector's transfer 1
X_{C_2}	State of Carrier at end of Inspector's transfer 1
X_{C_3}	State of Carrier at the beginning of Inspector's transfer 2
X_{C_4}	State of Carrier at the end of Inspector's transfer 2

A MATLAB script was written that looped through values of T_{stay} and DR_{offset} for specific values of ΔH_{max} and used *fmincon* with the method set to interior-point to find values of T_{go}, T_1, and T_2 that produced a minimum Δv_{total}. For different values of ΔH_{max} the was used. This provides a conservative approach. When the Carrier is in the cycloid orbit the DR_{offset} will be different for each GEO RSO. For this reason the worst case Δv_{total}, from all the possible DR_{offset} is used as the Δv_{total} for a given ΔH_{max} and T_{stay} that define the Inspector mission. The results are presented below in Section 6.4.1.

6.4.1 Circular Obit Results

Figure 6.5 shows the minimum Δv_{total} results from applying *fmincon* as describe above in Equation 6.46 for a Carrier in a circular orbit. The altitude of the circular Carrier orbit was looped from -500 km below to 500 km above GEO. The time that the Inspector is in proximity with the GEO RSO, T_{stay}, was varied from 0 to 24 hours.

Figure 6.6 shows where the Inspector must depart the Carrier and where it will return to the Carrier for minimum Δv_{total} inspection sorties that where solved for using *fmincon*. The line colors show different Inspector stay times, T_{stay}. Due to the symmetry of the problem, the plot can also be reflected about the zero relative downrange axis. For a given relative altitude of the Carrier orbit, ΔH (the y-axis), the Inspector must depart the Carrier at the specified relative downrange (x-axis), indicated by the lines with negative slope (nearly on top

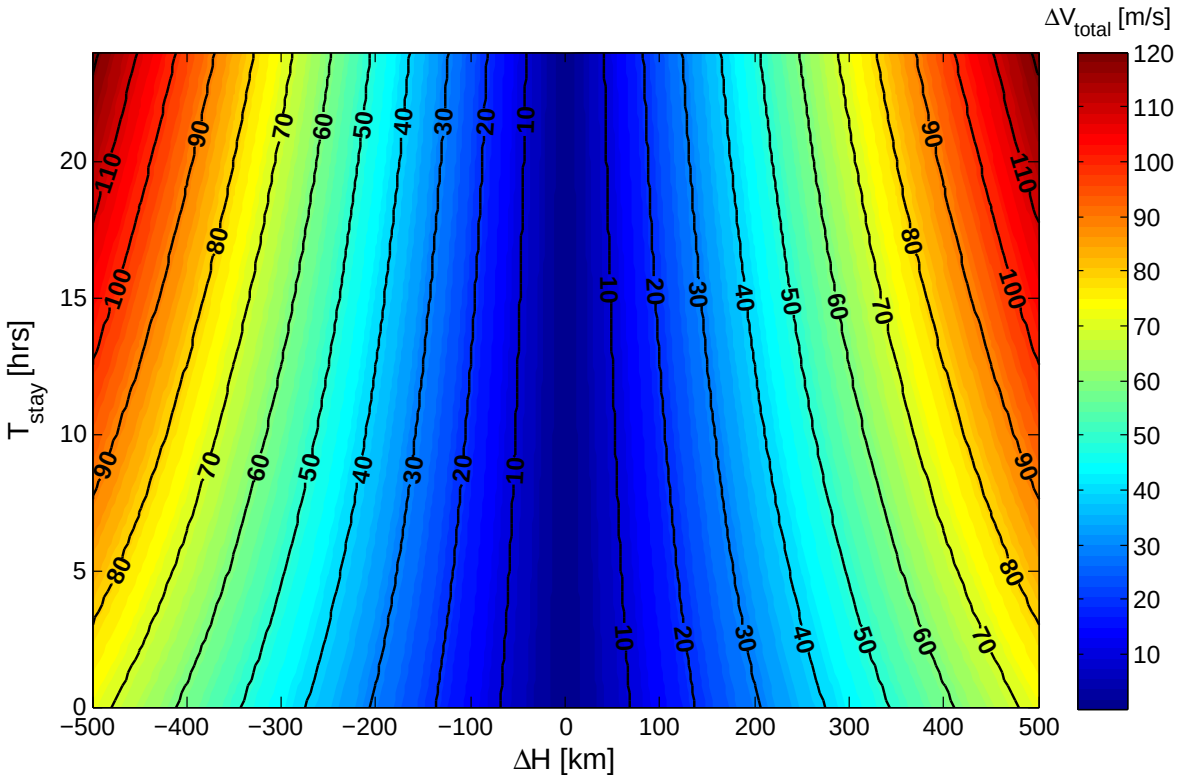

Figure 6.5: Required Δv for an inspection mission from a Carrier in a circular orbit.

of each other), to achieve a minimum Δv_{total} inspection sortie. This initial transfer is found to be very near Hohmann. The relative downrange of the Carrier when the Inspector returns to it is described by the lines with positive slope that are spread out. The relative downrange values can be switched, that is the relative downrange for the return could be the departure downrange and the associated departure downrange would be the return downrange.

Figure 6.7 shows an example trajectory of an inspection sortie from a Carrier in a 300 km circular orbit in a relative reference frame. For this example case the requirements are that the Inspector stay in proximity of the GEO RSO for 24 hours (T_{stay}), and the Carrier is in a 300 km circular orbit. The blue dashed line is the Carrier orbit. The green curve is the transfer to the GEO RSO from the Carrier. The red curve is the transfer from the GEO RSO back to the Carrier after a 24 hour stay time in GEO. The white squares are the locations of the Carrier when the Inspector departs, t_{go}, arrives at the GEO RSO, t_1, departs GEO RSO, t_2, and returns to the Carrier, t_3. The black dot is the desired GEO RSO.

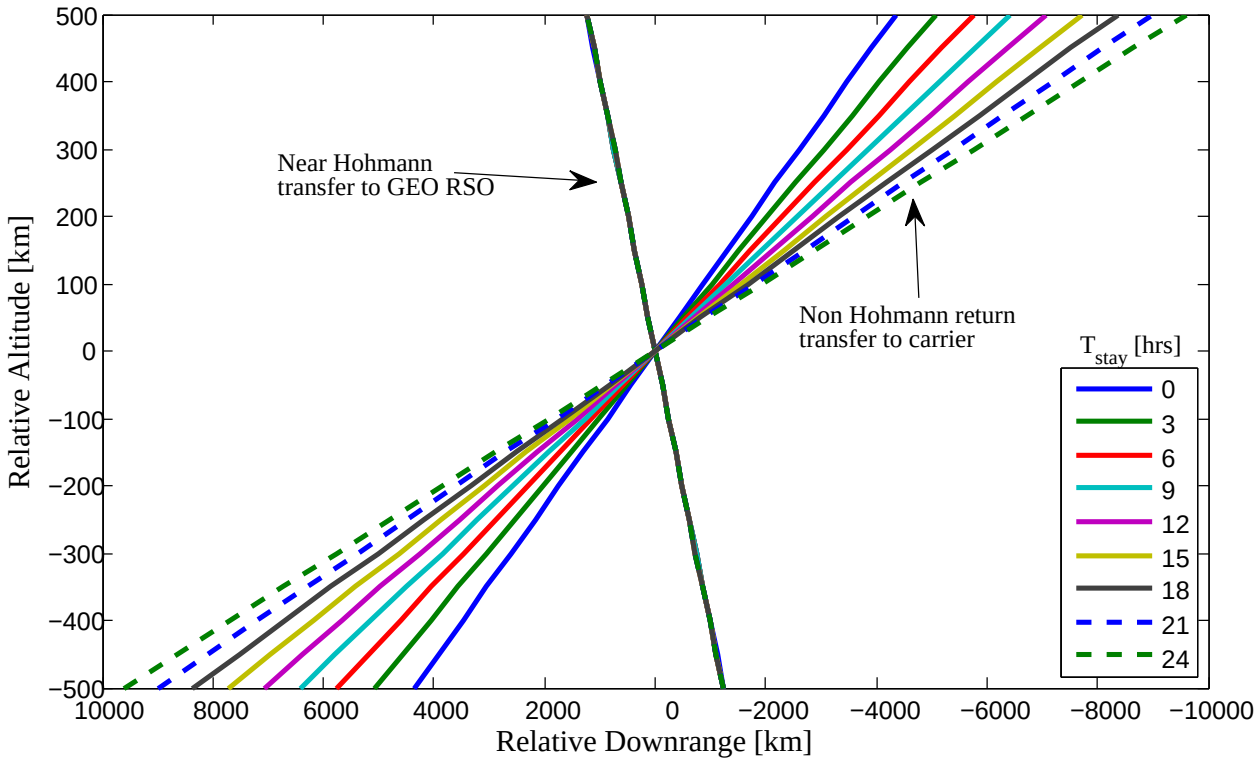

Figure 6.6: Downrange targeting lines as a function of T_{stay}.

The downrange of the Inspector at its initial position, green triangle, and final position, red triangle, correspond with the $T_{stay} = 24$ hours curve at an altitude of 300 km in Figure 6.6. The Δv_{total} required of the Inspector can be found from Figure 6.5 with $T_{stay} = 24$ hours and $\Delta H = 300$ km.

6.4.2 Cycloid Orbit Results

For cycloid orbits the equations described in Section 6.3.4 and *fmincon* were used to find the minimum Δv_{total} solutions for inspection sorties from a Carrier in a cycloid orbit. Figure 6.8 shows the minimum Δv_{total} for inspection sorties from a cycloid orbit with apogee/perigee 600 km above/below GEO and the associated perigee/apogee at GEO (i.e. ΔH_{max} is 600 km above or below GEO as shown in Figure 6.4).The Δv_{total} results in Figure 6.8 are symmetric about the 0% downrange offset. The 0% downrange offset is associated with the Carrier cycloid orbit coming to GEO altitude precisely at the GEO RSO location.

Figure 6.9 shows an example of an inspection sortie from a Carrier in a 600x0 km cycloid

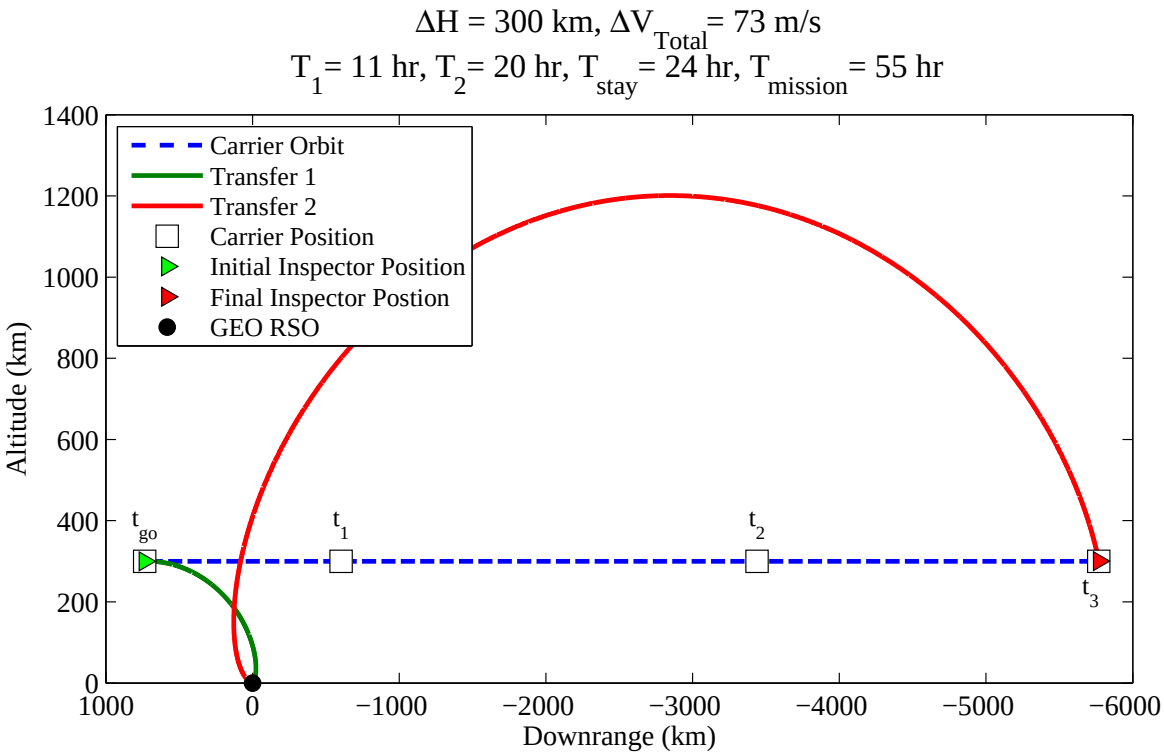

Figure 6.7: Example trajectory of an Inspector departing from a Carrier in a circular orbit in an LVLH reference frame.

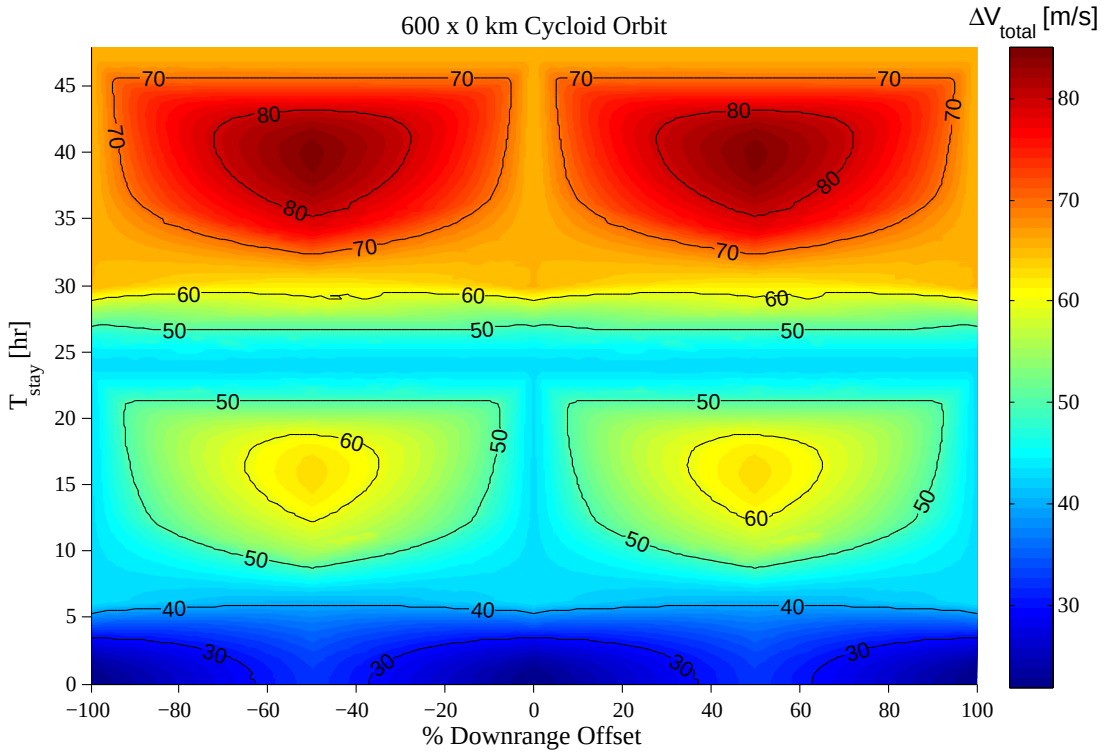

Figure 6.8: Required Δv for an inspection mission from a Carrier in a 600 x 0 km cycloid orbit.

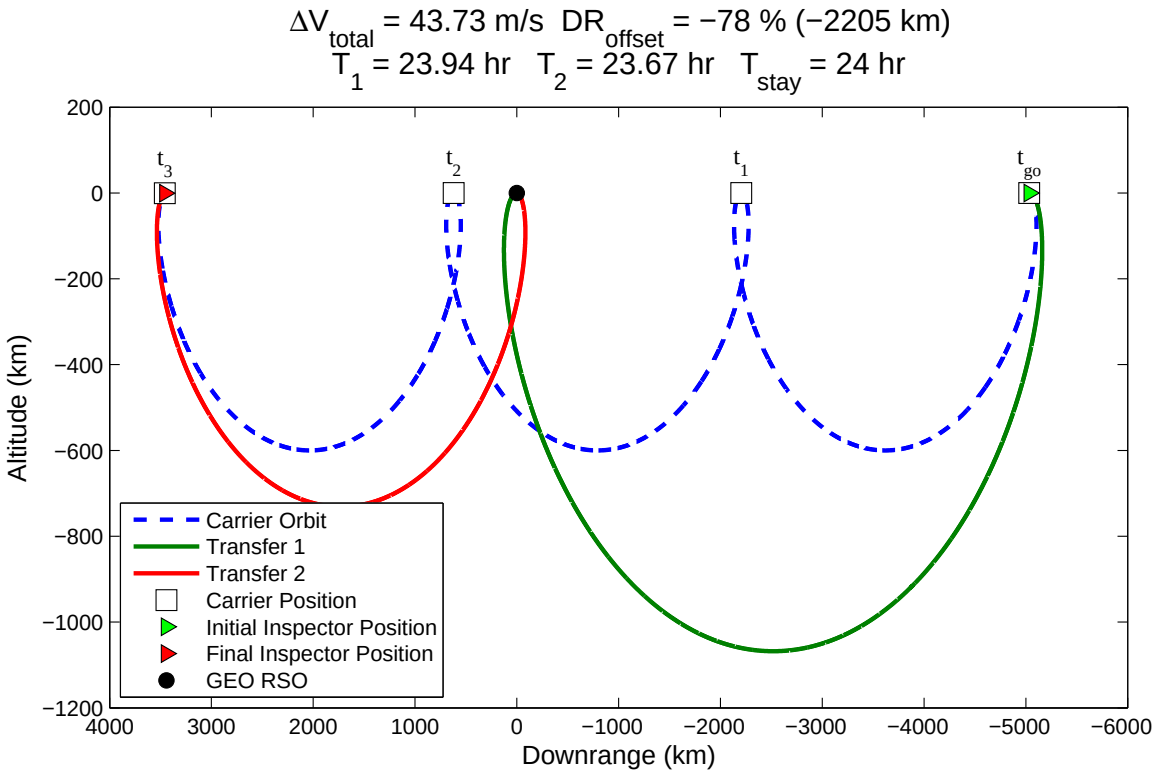

Figure 6.9: Example trajectory of an Inspector departing from a Carrier in a 600x0 km cycloid orbit, in an LVLH reference frame.

orbit. The blue curve is the Carrier orbit trace in the LVLH reference frame. The green curve is the Inspector's transfer from the Carrier to the GEO RSO. The red curve is the Inspector's transfer from the GEO RSO back to the Carrier. The position of the Carrier is shown by the white squares at t_{go}, t_1, t_2, and t_3. Figure 6.9 shows the trajectories that produce a worst case Δv_{total} for a fixed T_{stay} time of 24 hours. This worst case minimum Δv_{total} occurs at the -78% downrange offset. Lower minimum Δv_{total} occur at other percent downrange offset values but are not used because the percent downrange offset will vary for each GEO RSO, thus the worst case minimum for a given stay time is chosen as an example. Figure 6.8 shows how the minimum Δv_{total} changes for various percent downrange offset values. This cycloid orbit has the same synodic period and same orbit energy as the 300 km ΔH circular orbit shown in Figure 6.7.

Figure 6.10 shows the required Δv_{total} of the Inspector to complete an inspection sortie from a Carrier in a 300x0 km cycloid orbit as a function of the Inspector's stay time, T_{stay},

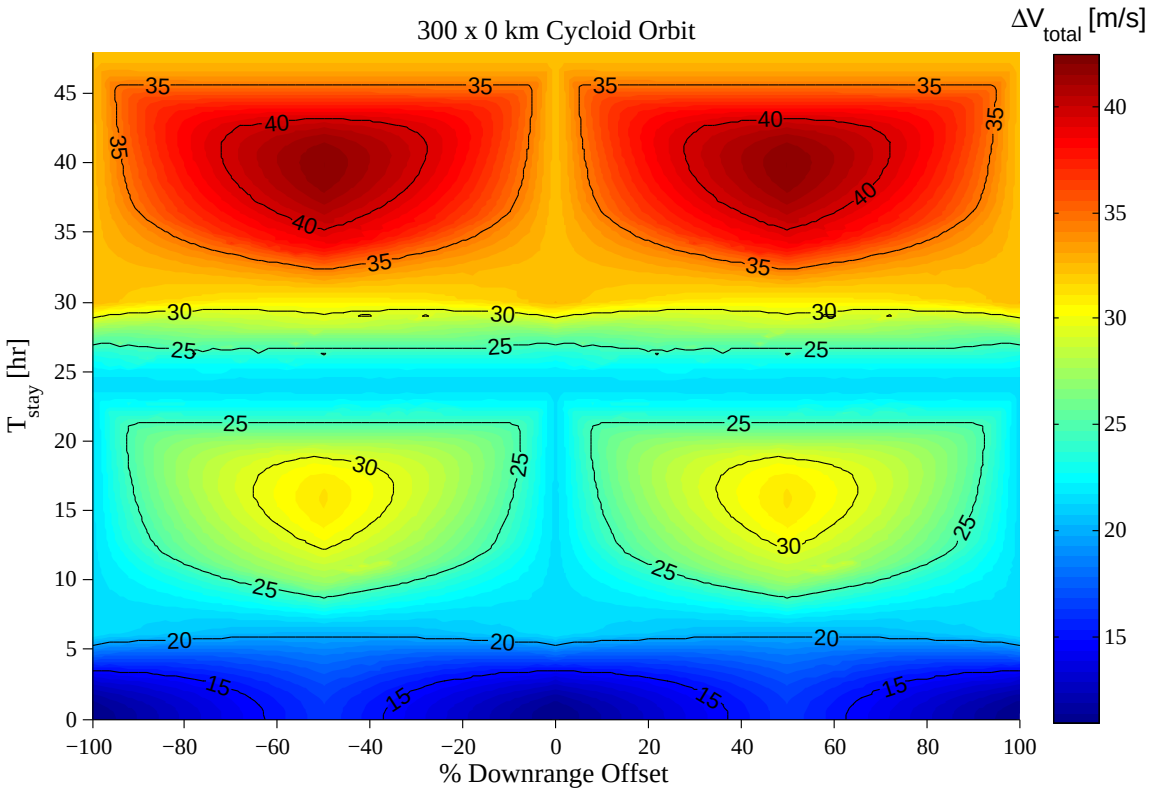

Figure 6.10: Required Δv for an inspection mission from a Carrier in a 300 x 0 km cycloid orbit.

and the percent downrange offset of the Carrier orbit with the GEO RSO. The 300x0 km cycloid orbit has the same synodic period as a 150 km ΔH circular Carrier orbit.

Figure 6.11 shows and example trajectory of the Inspector from the 300x0 km cycloid orbit with a specified stay time of 24 hours. The curves and markers are the same as in Figure 6.9, and the overall trend and shape of the trajectories are very similar. Again this is the worst case scenario for a 24 hour stay time, i.e. the percent downrange offset that produces a maximum optimal Δv_{total}.

6.4.3 Compare Circular and Cycloid Results

Figure 6.12 shows the worst case minimum Δv_{total} scenario, required of an Inspector to complete an inspection sortie, as a function of stay time at the GEO RSO, for a Carrier placed in a circular orbit compared to a cycloid orbit. Because their exists a wide range of downrange offsets for the cycloid orbit the worst case minimum Δv_{total} scenario for a specified

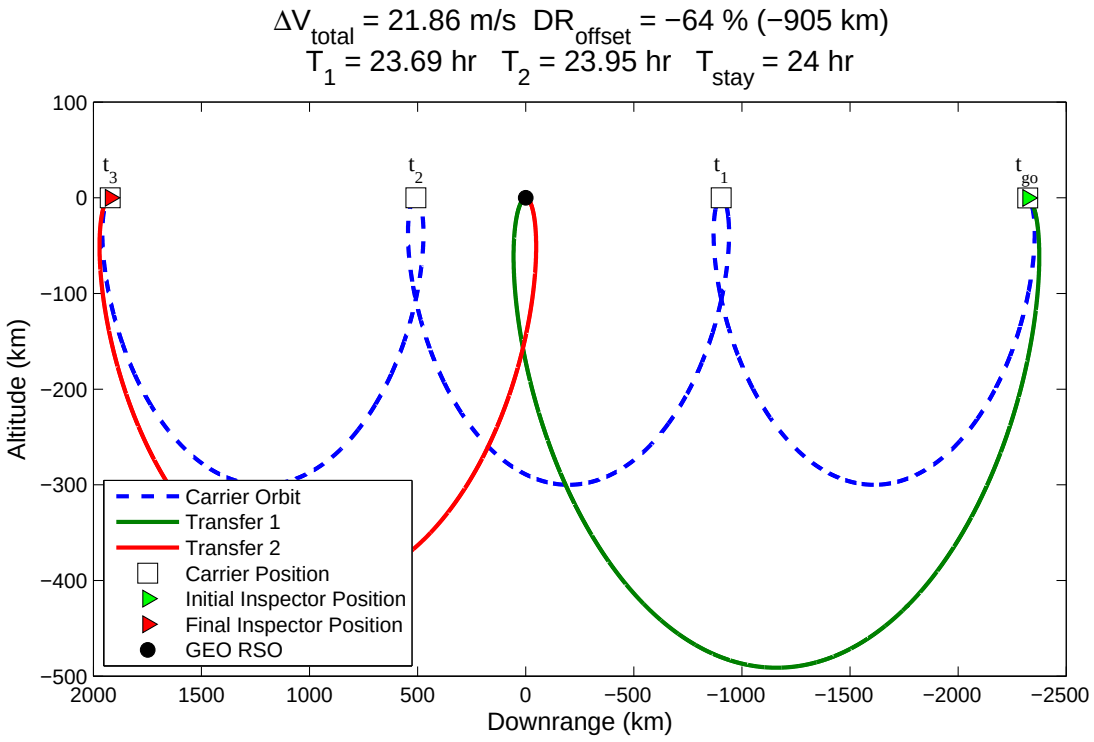

Figure 6.11: Example trajectory of an Inspector departing from a Carrier in a 300x0 km cycloid orbit, in an LVLH reference frame.

stay time is used. When the Carrier is placed in a circular obit the required Δv_{total} increases linearly as stay time increases. For the case of the Carrier in the cycloid orbit roughly 24 hour cycles of stay time provide worst case minimum Δv_{total} advantages. When considering only Δv_{total}, cycloid orbits provide the better orbit for completing GEO inspection missions via a carrier concept. However, it is to note that the cycloid orbit does enter in and out of the GEO protected region. Bringing the Carrier in close proximity to GEO RSOs has its theoretical advantages, but also poses practical risk.

6.5 Convex Optimization

Convex optimization techniques are applied to the unconstrained-time double rendezvous problem. The goal is to minimize Equation 6.46. The CW equations must first be put into a convex problem formulation. Once the equations are formulated, MATLAB will be used along with CVX [32], a software program that runs in MATLAB used for solving convex problems.

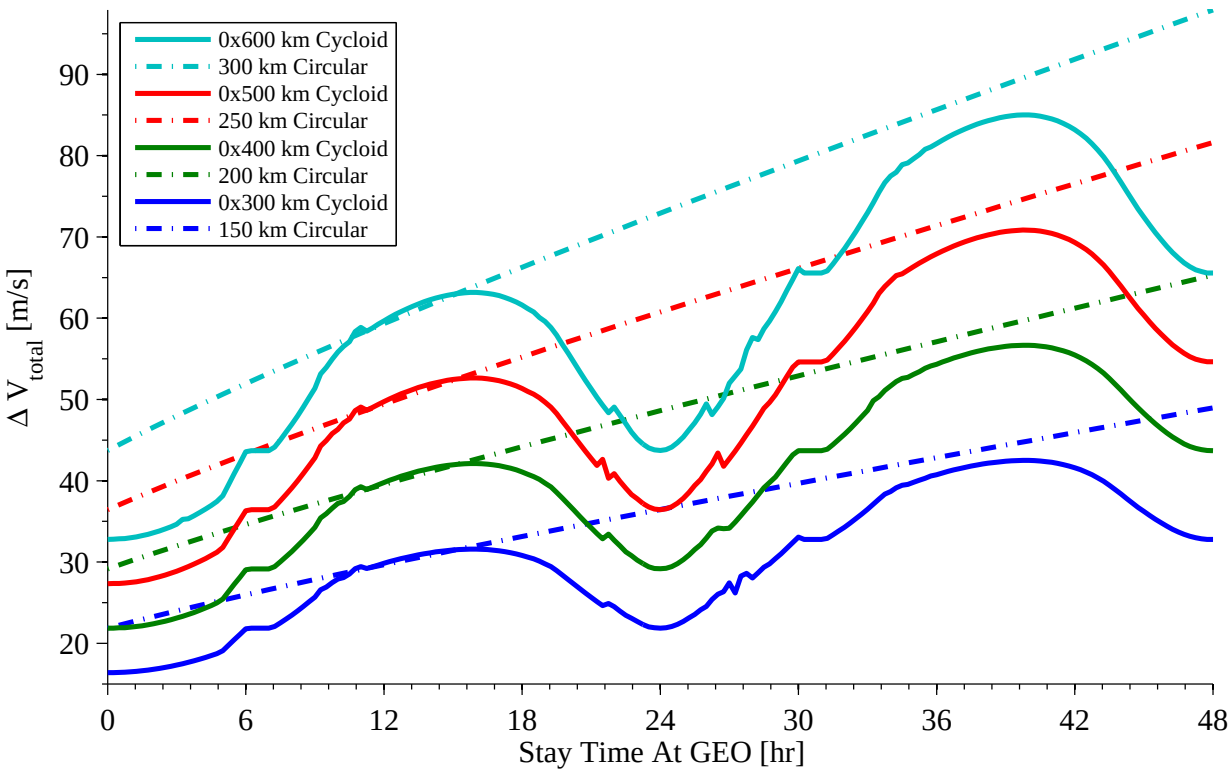

Figure 6.12: Inspection mission Δv comparison of Carrier circular and cycloid orbit.

The definition of convex as described by [28] is

A convex optimization problem is one of the form

$$\begin{aligned} &\text{minimize} f_0(x) \\ &\text{subject to} f_i(x) \leq b_i, \qquad i = 1, \ldots, m, \end{aligned}$$

where the functions $f_0, \ldots, f_m$ $\mathbf{R}^n \to \mathbf{R}$ are convex, *i.e.*, satisfy

$$f_i(\alpha x + \beta y) \leq \alpha f_i(x) + \beta f_i(x)$$

for all x, $y \in \mathbf{R}^n$ and all α, $\beta \in \mathbf{R}$ with $\alpha + \beta = 1$, $\alpha \geq 0$, $\beta \geq 0$. Least squares and linear programming problems are both special cases of the general convex optimization problem.

Convex optimization has been applied to a single rendezvous problem using the CW equations by Robinson [31]. Robinson was able to cleverly transform the CW equations into a convex form. A summary of Robinson's formulation follows in Section 6.5.1.

6.5.1 Formulating the CW Equations for Convex Optimization

The following is a formulation of how the CW equations can be used to set up a convex problem that can be solved using CVX. This formulation is a summary of [31].

The CW equations can be written as

$$f_x = \ddot{x} + 2\omega\dot{z} \tag{6.61}$$

$$f_y = \ddot{y} + \omega^2 y \tag{6.62}$$

$$f_z = \ddot{z} - 3\omega^2 z - 2\omega\dot{x} \tag{6.63}$$

where x is in the near velocity or downrange direction , y is in the orbit angular momentum or cross track direction, and z is in the local vertical or altitude direction. f_x, f_y, and f_z are a sum of all the forces applied to the vehicle along an axis. For the case of natural motion f_x, f_y, and f_z would be set to zero.

The CW equations can be written as a linear system $\dot{\mathbf{x}} = F\mathbf{x} + G\mathbf{u}$

$$\overbrace{\begin{bmatrix}\dot{x}\\ \dot{y}\\ \dot{z}\\ \ddot{x}\\ \ddot{y}\\ \ddot{z}\end{bmatrix}}^{\dot{\mathbf{x}}} = \overbrace{\begin{bmatrix}0 & 0 & 0 & 1 & 0 & 0\\ 0 & 0 & 0 & 0 & 1 & 0\\ 0 & 0 & 0 & 0 & 0 & 1\\ 0 & 0 & 0 & 0 & 0 & -2\omega\\ 0 & -\omega^2 & 0 & 0 & 0 & 0\\ 0 & 0 & 3\omega^2 & 2\omega & 0 & 0\end{bmatrix}}^{F} \overbrace{\begin{bmatrix}x\\ y\\ z\\ \dot{x}\\ \dot{y}\\ \dot{z}\end{bmatrix}}^{\mathbf{x}} + \overbrace{\begin{bmatrix}0 & 0 & 0\\ 0 & 0 & 0\\ 0 & 0 & 0\\ 1 & 0 & 0\\ 0 & 1 & 0\\ 0 & 0 & 1\end{bmatrix}}^{G} \overbrace{\begin{bmatrix}f_x\\ f_y\\ f_z\end{bmatrix}}^{\mathbf{u}} \tag{6.64}$$

This has a general solution of

$$\mathbf{x}(t) = \Phi(t, t_0)\,\mathbf{x}(t_0) + \int_{t_0}^{t} \Phi(t, \tau)\, G\mathbf{u}(\tau)\, d\tau \tag{6.65}$$

where Φ is the state transition matrix of the linear system. Because F is a constant matrix there exists an analytical expression for Φ.

$$\Phi(t, t_0) = e^{F\Delta t} = \begin{bmatrix} 1 & 0 & 6(s-\omega\Delta t) & \frac{4s}{\omega} - 3\Delta t & 0 & \frac{2}{\omega}(c-1)\\ 0 & c & 0 & 0 & \frac{s}{\omega} & 0\\ 0 & 0 & 4-3c & \frac{2}{\omega}(1-c) & 0 & \frac{s}{\omega}\\ 0 & 0 & 6\omega(c-1) & 4c-3 & 0 & -2s\\ 0 & -\omega s & 0 & 0 & c & 0\\ 0 & 0 & 3\omega s & 2s & 0 & c \end{bmatrix} \tag{6.66}$$

where $\Delta t = t - t_0$, $c = \cos(\omega \Delta t)$, and $s = \sin(\omega \Delta t)$. Φ is only dependent upon the difference, Δt and not absolute times.

Assuming that the control can be represented as a polynomial in time

$$\mathbf{u}(t) = \sum_{k=0}^{n} t^k \mathbf{u}_k \tag{6.67}$$

$\mathbf{u}(t)$ is a linear combination of the parameters $\mathbf{u}_k$. Thus $\mathbf{u}(t)$ is convex in $\mathbf{u}_k$. Substituting Equation 6.67 into 6.65 produces the following result

$$\mathbf{x}(t) = \Phi(t, t_0)\,\mathbf{x}(t_0) + \sum_{k=0}^{n} \underbrace{\int_{t_0}^{t} \Phi(t, \tau)\, G \tau^k d\tau}_{\Psi_k} \mathbf{u}_k \tag{6.68}$$

Integrating the last 3 columns of Φ will yield $\Psi(t, t_0)$

$$\Psi(t, t_0) = \int_{t_0}^{t} \Phi(t, \tau)\, G d\tau = \begin{bmatrix} \frac{1}{\omega^2}\left[4(1-c) - \frac{3}{2}\omega^2 \Delta t^2\right] & 0 & \frac{2}{\omega^2}(s - \omega \Delta t) \\ 0 & \frac{1}{\omega^2}(1-c) & 0 \\ \frac{2}{\omega^2}(\omega \Delta t - s) & 0 & \frac{1}{\omega^2}(1-c) \\ \frac{1}{\omega}(4s - 3\omega \Delta t) & 0 & \frac{2}{\omega}(c-1) \\ 0 & \frac{s}{\omega} & 0 \\ \frac{2}{\omega}(1-c) & 0 & \frac{s}{\omega} \end{bmatrix} \tag{6.69}$$

Applying Equation 6.68 recursively with fixed time steps

$$\mathbf{x}_n = \Phi(\Delta t)^n\, \mathbf{x}(t_0) + \sum_{k=0}^{n-1} \Phi(\Delta t)^{n-1-k}\, \Psi(\Delta t)\, \mathbf{u}_k \tag{6.70}$$

This can be rewritten as

$$\mathbf{x}_n = \begin{bmatrix} \Phi^{n-1}\Psi & \Phi^{n-2}\Psi & \dots & \Psi \end{bmatrix} \begin{bmatrix} \mathbf{u}_0 \\ \mathbf{u}_1 \\ \vdots \\ \mathbf{u}_{n-1} \end{bmatrix} + \Phi^n \mathbf{x}_0 \tag{6.71}$$

Equation 6.71 provides only the value of the state at one particular time. An alternate formulation of the discrete system can be used to find an affine relation between all of the states and controls of the system.

$$\begin{bmatrix} -\Phi & I & & & \\ & -\Phi & I & & \\ & & \ddots & \ddots & \\ & & & -\Phi & I \end{bmatrix} \begin{bmatrix} \mathbf{x}_0 \\ \mathbf{x}_1 \\ \vdots \\ \mathbf{x}_n \\ \mathbf{x}_{targ} \end{bmatrix} = \begin{bmatrix} \Psi & & & \\ & \Psi & & \\ & & \ddots & \\ & & & \Psi \end{bmatrix} \begin{bmatrix} \mathbf{u}_0 \\ \mathbf{u}_1 \\ \vdots \\ \mathbf{u}_n \end{bmatrix} \tag{6.72}$$

Where $\mathbf{x}_{targ}$ is the desired final state of the vehicle at the final time. Rewriting Equation 6.72 to account for the boundary conditions

$$\begin{bmatrix} 0 \\ \vdots \\ 0 \\ 1 \end{bmatrix} \mathbf{x}_{targ} - \begin{bmatrix} \Phi \\ 0 \\ \vdots \\ 0 \end{bmatrix} \mathbf{x}_0 = \begin{bmatrix} -\Phi & I & & & & \Psi & & \\ & -\Phi & I & & & & \Psi & \\ & & \ddots & \ddots & & & & \ddots \\ & & & -\Phi & I & & & \Psi \end{bmatrix} \begin{bmatrix} \mathbf{x}_1 \\ \mathbf{x}_2 \\ \vdots \\ \mathbf{x}_n \\ \mathbf{u}_0 \\ \mathbf{u}_1 \\ \vdots \\ \mathbf{u}_n \end{bmatrix} \tag{6.73}$$

The concatenation of the unknown states and controls forms an affine set. The affine equality constraint is advantageous because it will allow for the solution to be found using convex optimization.

6.5.2 Application of Robinson's Formulation

Here, an example rendezvous with a GEO RSO will be investigated using the formulation from Section 6.5.1. The target is a GEO RSO. The satellite performing the rendezvous maneuver with the target is called the chaser. The chaser is initialized 300 km below and 800 km behind the target in an LVLH reference frame. The chaser will have 10 hours to complete the transfer, t_f.

This problem will be solved 5 different times, once with a classical approach to provide a baseline, and 4 times using convex optimization while applying different minimization criteria and constraints.

Part A: Classical Approach

Part A will use a zero terminal error controller to find the optimal control. This control theory is outlined on pages 158-163 [30]. This control problem is written as

$$\begin{aligned} \text{minimize} \quad & \int_{t_0}^{t} \mathbf{u}^T \mathbf{u} dt \\ \text{subject to} \quad & \dot{\mathbf{x}} = F\mathbf{x} + G\mathbf{u} \\ & \mathbf{x}(t_0) = \mathbf{x}_0 \\ & \mathbf{x}(t_f) = \mathbf{x}_{targ} \end{aligned}$$

Part B: Convex Approach - Similar to Classical

Part B will use the discrete dynamics of Equation 6.73 to formulate the problem as a convex optimization problem. The minimization function for this problem will equivalent to that of the zero terminal error method described in Part A.

Equation 6.73 can be written in the form $\mathbf{Ax} = \mathbf{b}$

$$\overbrace{\begin{bmatrix} -\Phi & I & & & \Psi & & \\ & -\Phi & I & & & \Psi & \\ & & \ddots & \ddots & & & \ddots \\ & & & -\Phi & I & & \Psi \end{bmatrix}}^{\mathbf{A}} \overbrace{\begin{bmatrix} \mathbf{x}_1 \\ \mathbf{x}_2 \\ \vdots \\ \mathbf{x}_n \\ \mathbf{x}_{targ} \\ \mathbf{u}_0 \\ \mathbf{u}_1 \\ \vdots \\ \mathbf{u}_n \end{bmatrix}}^{\mathbf{x}} = \overbrace{\begin{bmatrix} \Phi\mathbf{x}_0 \\ 0 \\ \vdots \\ 0 \\ \mathbf{x}_{targ} \end{bmatrix}}^{\mathbf{b}} \tag{6.74}$$

where $\mathbf{x}_{targ}$, $\mathbf{x}_0$, and, t_f, are given values. The number of discrete steps, N, will determine the time step, Δt, and thus Φ and Ψ are known. Because Φ is a 6x6 matrix, Ψ is a 6x3 matrix, $\mathbf{x}_i$ is a 6x1 vector, and $\mathbf{u}_i$ is a 3x1 vector, $\mathbf{A}$ is a $6\,(N+1)$ x$6N+3\,(N+1)$ matrix, $\mathbf{x}$ is a $6N+3\,(N+1)$ x1 vector, and $\mathbf{b}$ is a $6\,(N+1)$ x1 vector.

The optimal control problem for Part B is written as

$$\begin{aligned} \text{minimize} \quad & \sum_{k=0}^{n-1} \mathbf{u}_k^T \mathbf{u}_k \\ \text{subject to} \quad & \mathbf{A}\mathbf{x} = \mathbf{b} \end{aligned}$$

When calling CVX in MATLAB it can be coded as follows

```
cvx_begin
    variable X(6*N+3*(N+1))
```

```
    minimize( Sum_uTu )
    subject to
        A * X == b;
cvx_end
```

where Sum_uTu is a string that contains the expression of the sum of each individual control vector multiplied by its transpose. Note that the first control vector starts at the 6N+1 index of $\mathbf{x}$; $\mathbf{x}\,(6N+1:6N+3) = \mathbf{u}_0$. The MATLAB string will look like

$$\text{Sum\_uTu} = \mathbf{x}\,(6N+1:6N+3)'*\mathbf{x}\,(6N+1:6N+3)+...+\mathbf{x}\,(end-2:end)'*\mathbf{x}\,(end-2:end)$$

Also note that using absolute numbers referencing discrete sections of $\mathbf{x}$ are used when coding, rather than typing N and *end*, CVX may run with less problems.

Part C: Convex Approach - Minimize Sum of Norms

Part C is also a convex optimization problem and is set up similar to Part B except the summation of the norms of the thrust or the ΔV is minimized directly. This is written as

$$\begin{aligned} \text{minimize} \quad & \sum_{k=0}^{n-1} \|\mathbf{u}_k\| \\ \text{subject to} \quad & \mathbf{Ax} = \mathbf{b} \end{aligned}$$

Part D: Convex Approach - Similar to Classical with Constraint

Part D is the same as Part B except that an added constraint is applied to limit the maximum allowable discrete thrust level. The maximum thrust acceleration at any time, u_{max}, is 0.01 m/s/s. This problem is written as

$$\begin{aligned} \text{minimize} \quad & \sum_{k=0}^{n-1} \mathbf{u}_k^T \mathbf{u}_k \\ \text{subject to} \quad & \mathbf{Ax} = \mathbf{b} \\ & \max_k \|\mathbf{u}_k\| \leq u_{max} \end{aligned}$$

To put this maximum thrust constraint in CVX a separate MATLAB script was written that contained all the constraints. CVX then called this file and all the constraints that it contained. Each individual thrust had to be constrained so there would be N+1 constraints needed to constrain the thrust. In MATLAB this would be written as

```
cvx_begin
    variable X(6*N+3*(N+1))
    minimize( Sum_uTu )
    subject to
        A * X == b;
        ThrustLimt
cvx_end
```

where ThrustLimit is a separate MATLAB script that contains each individual thrust constraint.

Part E: Convex Approach - Minimize Sum of Norms with Constraint

Part E is the same optimization as Part C but has the added constraint of limiting the maximum allowable thrust. The same maximum thrust is applied as in Part D. This problem is written as

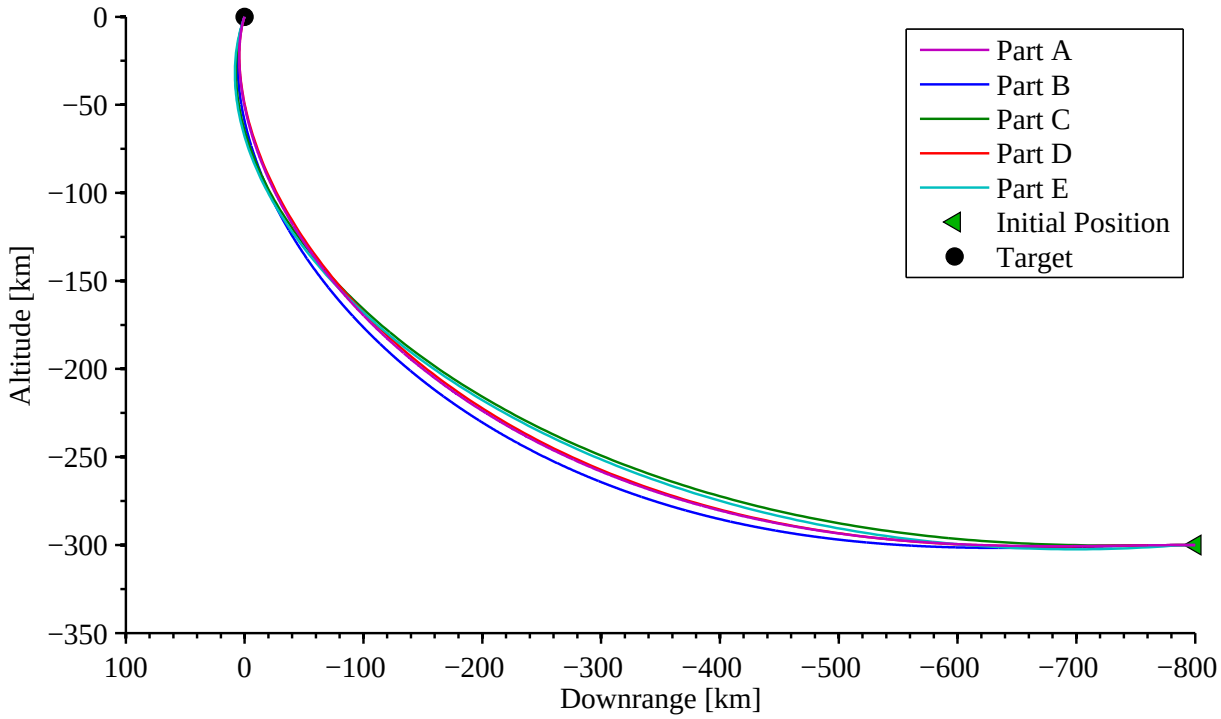

Figure 6.13: Comparison of the trajectory of the rendezvous problem.

$$\begin{aligned} \text{minimize} \quad & \sum_{k=0}^{n-1} \|\mathbf{u}_k\| \\ \text{subject to} \quad & \mathbf{A}\mathbf{x} = \mathbf{b} \\ & \max_k \|\mathbf{u}_k\| \leq u_{max} \end{aligned}$$

Results of GEO Application Problem

Figure 6.13 Shows the comparison of the resulting rendezvous trajectory for the 5 different parts. Each part produces nearly the same trajectory.

Figure 6.14 shows the comparison of downrange control solutions that each part produces for a minimum propellant transfer. Part C and E, convex methods, produce very near impulsive thrust solutions.

Figure 6.15 shows the comparison of altitude control solutions that each part produces for a minimum propellant transfer. Again Part C and E, convex methods, produce very near

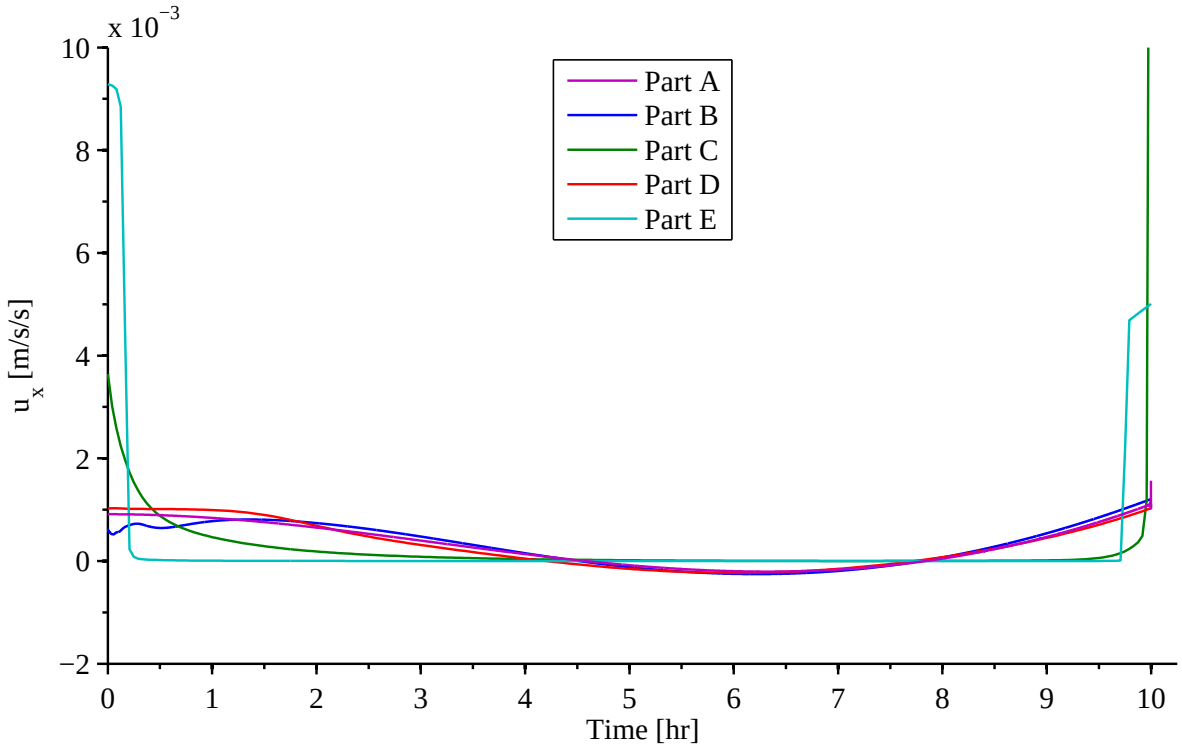

Figure 6.14: Comparison of downrange control.

impulsive thrust solutions.

It was expected that results for Part B would match those of Part A because both were minimizing the same function. This could be due to the fact that the step size used to solve Part B was larger than that used in the method to solve for in Part A. In decreasing the step size in Part B memory issues arose using CVX. When CVX was solving Part B and Part D no sensible solution was found, but still produced results. Results of Part B and D are most likely sub-optimal.

Whether CVX was able to solve Part C and E depended on the step size used. Trial and error were used to find a small step size that would work. Table 6.3 shows the step sizes used and the solution that was obtained.

For this example case CVX was able to find minimum Δv_{total} that differed from the conventional calculus of variations approach (Part A).

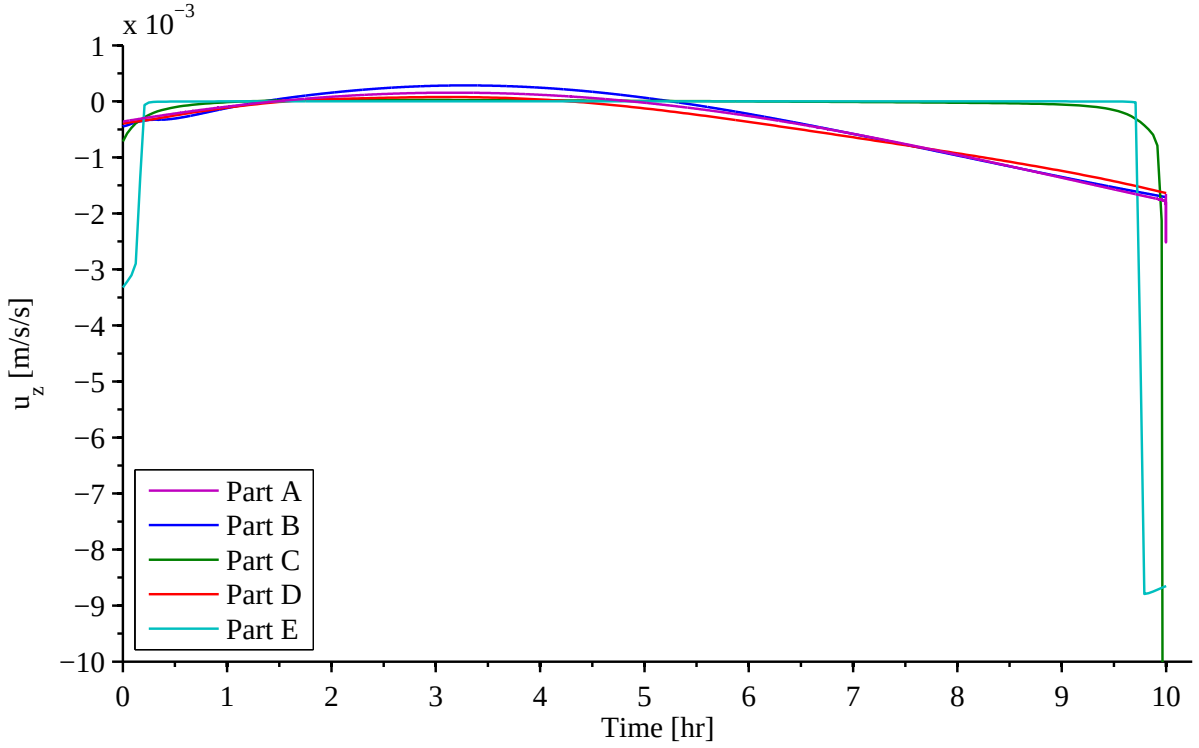

Figure 6.15: Comparison of altitude control.

Table 6.3: Summary of Using CVX for Application of Convex Formulation

Part	Minimizing Function	Thrust Constraint	Δt $(seconds)$	ΔV_{total} $\left(\frac{m}{s}\right)$
A	$\int_{t_0}^{t} \mathbf{u}^T \mathbf{u} dt$	None	(variable)	25.1
B	$\sum_{k=0}^{n-1} \mathbf{u}_k^T \mathbf{u}_k$	None	10	26.1
C	$\sum_{k=0}^{n-1} \|\mathbf{u}_k\|$	None	150	16.5
D	$\sum_{k=0}^{n-1} \mathbf{u}_k^T \mathbf{u}_k$	yes	150	25.6
E	$\sum_{k=0}^{n-1} \|\mathbf{u}_k\|$	yes	150	16.3

Note: When CVX failed to solve the problem some control was found that would fit the results but may not be optimal.

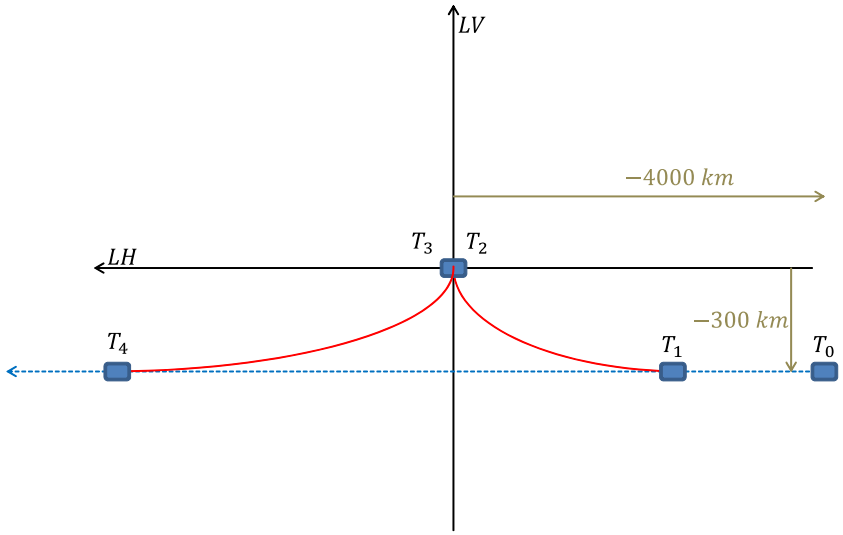

Figure 6.16: Overview of the Inspector rendezvous and return from a coelliptic.

6.5.3 Applying Convex Optimization to the Carrier Concept

It is desired to find the minimum Δv_{total} that is required of an Inspector to maneuver to a GEO RSO (modeled as a rendezvous), stay in the proximity of the GEO RSO for a specified time, and then re-rendezvous with the Carrier. For this approach there are two rendezvous that need to take place. The required transfer time that the Inspector takes for each rendezvous is not specified and can vary for the optimal minimum Δv solution. The only time constraint is the desired stay time the Inspector is in the proximity of the GEO RSO. With no time constraints on the transfers this problem greatly differs from the problem outlined in Section 6.5.2 where the time of transfer is known.

Using 4 impulse burns an Inspector will depart from a Carrier, rendezvous with a GEO RSO, stay at GEO for a specified time, and then return to the Carrier. The Carrier is in a coelliptic orbit 300 km below GEO. The problem is constrained by specifying the stay time at GEO (difference between times T_3 and T_2) and the total mission time to rendezvous and return. The total mission time is the time between the first burn at time T_1 and the last burn at time T_4. The free variables of the problem are T_1 and T_2, when the first and second burns occur, respectively. The performance measurement is the total ΔV required to perform the mission (all 4 burns). The Inspector/Carrier will have an initial position (at T_0) of 300 km below and 4000 km behind the GEO RSO. Figure 6.16 shows the set up of the problem.

Burn 1 occurs at T_1, burn 2 at T_2, burn 3 at T_3, and burn 4 at T_4. The first transfer time is the difference between T_2 and T_1. Stay time at GEO is the difference between T_3 and T_2, and the second transfer time is the difference between T_4 and T_3.

Example inspection missions can be checked to see if the Δv_{total} solution space is convex. To perform this check, T_{stay} and $T_{mission}$ are specified. To determine the solution space T_1 and T_2 are varied while T_3 and T_4 are determined from the inputs and variables. Figure 6.17 shows an example of the Δv_{total} solution space when the Carrier is placed in a circular orbit 300 km below GEO with a stay time, T_{stay}, of 24 hours and a total mission time, $T_{mission}$, of 55 hours. T_1 is looped from 0 to 33 hours, while T_2 is varied between 5 and 20 hours after T_1. The difference between T_1 and T_2 is the first transfer duration.

Some of the Δv_{total} contours of the plot do not have the convex curvature and do not meet the criteria of being convex as described . The 110 m/s contour is not convex.

Stay time was varied from 0 - 48 hours and total mission times were also varied, the results were similar, resulting in non-convex solution spaces.

Another check was performed to determine if the problem is convex in a specific dimension of the problem. This was accomplished by having T_1, T_2, T_3, and T_4 as the free variables. This makes the problem four dimensional. To perform the check, random points from the four dimensional space were selected, for example point A and point B. For each point there are 4 random values for T_1, T_2, T_3, and T_4. Also a constraint on the random numbers need be placed so that $T_1 < T_2 < T_3 < T_4$. This insures that the problem is realistic (no negative transfer times etc). Once this is done the objective function can be evaluated at point A and point B. The output of the objective function is ΔV_{total}. If the problem is convex the average of the Δv_{total} at A and B will be greater than the Δv_{total} at the average of points A and B. This is described in Figure 6.18.

A code was written that chooses these random points to determine if the problem is convex. If there is one case where it is not meet the definition of convexity in Figure 6.18, the problem is not convex. For this problem the function, $f(X)$, determines the Δv_{total} for

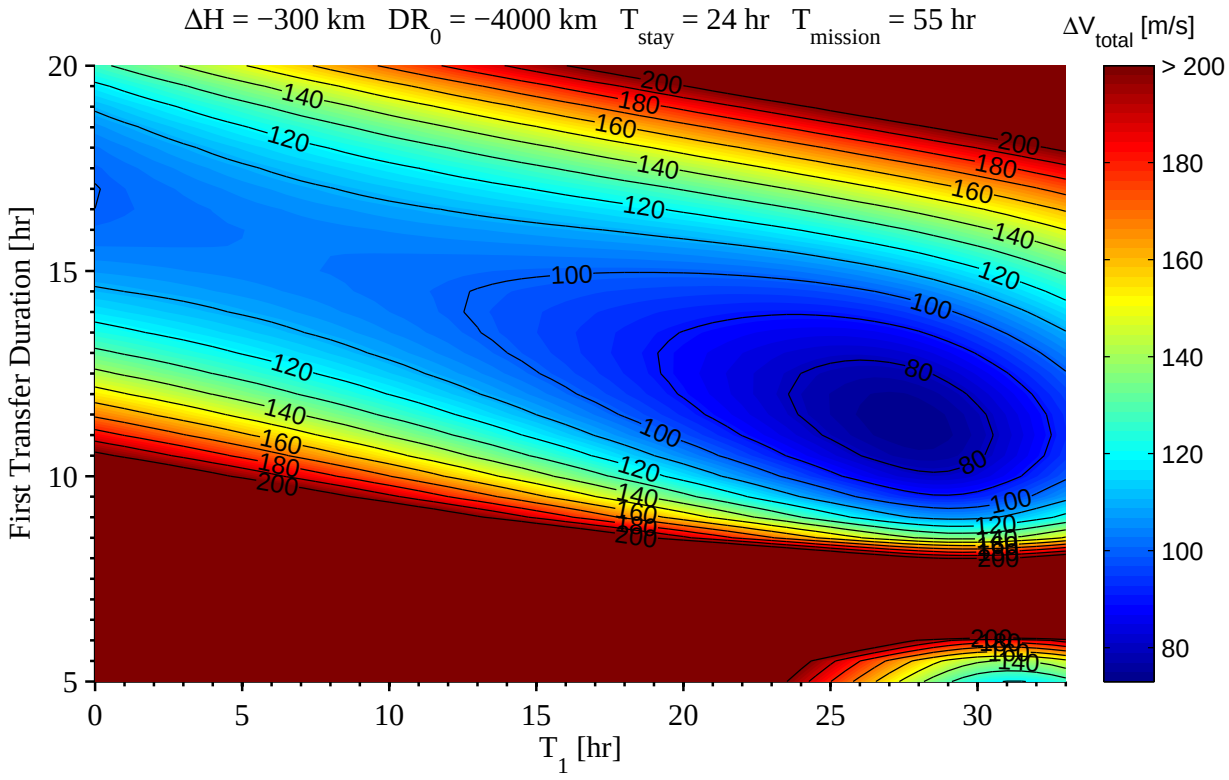

Figure 6.17: ΔV_{total} non convex results.

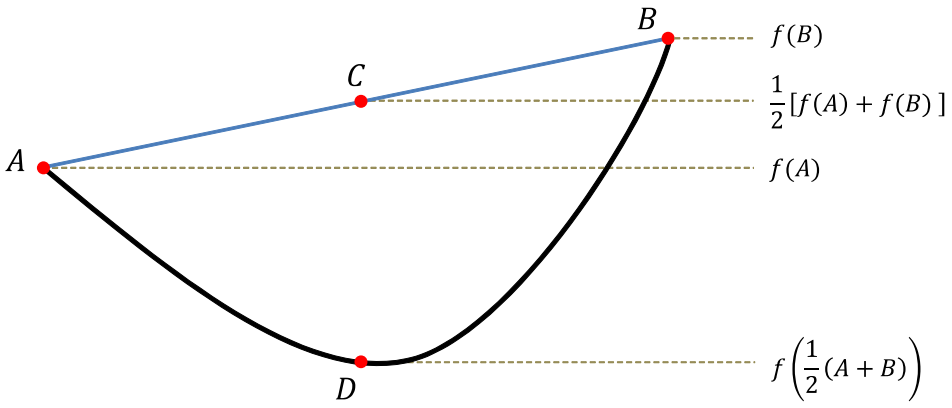

Figure 6.18: Graphical representation of convex definition in one dimension.

the inspection mission, where X is the inputs to the problem.

$$\Delta v_{total} = f\left(T_1, T_2, T_3, T_4\right) \tag{6.75}$$

The randomly chosen inputs to the problem are T_1, T_2, T_3, and T_4. The limits on these randomly chosen inputs are

$$0 < T_1 < 33.86 \qquad 1 < T_2 - T_1 < 24 \qquad 0 < T_3 - T_2 < 48 \qquad 1 < T_4 - T_3 < 24$$

where all times in these ranges are in hours. The upper limit on T_1 was chosen from the time it would take the Carrier to be directly under GEO given the initial conditions of the problem. This constrained the problem so that the Inspector would have to leave before it passed directly under the GEO RSO.

The CW equations were used to propagate the state of the Carrier for determining the Δv for the rendezvous of the inspection mission.

The code was then ran and Δv_{total} was determined for two different cases, point A and point B. The inputs for point D were determined from the definition of a convex problem. Each input for point D, D_i, is determined from each input of point A, A_i, and point B, B_i.

$$D_i = \frac{1}{2}\left[A_i + B_i\right] \tag{6.76}$$

The inputs for point D are then put into the function to determine the Δv_{total}.

$$\left[\Delta v_{total}\right]_{pointD} = f\left(\frac{1}{2}\left(A + B\right)\right) = f\left(D\right) \tag{6.77}$$

To determine if the problem is convex the function evaluated at point D must be less than $\frac{1}{2}$ the function evaluated at point A and point B.

$$\text{For problem to be convex: } f\left(D\right) < \frac{1}{2}\left[f\left(A\right) + f\left(B\right)\right] \tag{6.78}$$

Table 6.4: Non-Convex Example

	Random Inputs				$f(X)$	Determined from Inputs		
Point	T_1 (hr)	T_2 (hr)	T_3 (hr)	T_4 (hr)	Δv_{total} (m/s)	T_{trans1} (hr)	T_{stay} (hr)	T_{trans2} (hr)
A	32.9	48.9	68.1	79.5	209.7	15.9	19.2	11.4
B	14.6	34.6	36.6	40.7	131.4	20.0	2.0	4.1
C	-	-	-	-	170.5	-	-	-
D	23.8	41.7	52.4	60.1	215.9	18.0	10.6	7.8

Note: Δv_{total} at Point C is not the value of the function at that point, it is the average of the function at points A and B. Because the Δv_{total} at point C is less than point D the problem is not convex.

Less than 100 data samples were needed to find one set of inputs that showed the problem to be non-convex. Most often it took less than 20 samples. This check was ran many times and with different ΔH for the Carrier circular orbit. No case was found to be convex.

After performing many random input checks, the inspection mission problem laid out in Section 6.1 no case was found to be convex. One example of randomly chosen inputs that show the problem being non convex are shown in Table 6.4. A one dimensional plot of Δv_{total} as a function of T_1 for this random input convex test is shown in Figure 6.19. When comparing Figure 6.19 to the definition of convexity from Figure 6.18, point D is not less than point C, thus this is an example showing the solution space to be non-convex. Figure 6.19 is only one dimensional in T_1, however any of the other random inputs could also be used to make this plot, showing the non-convex example.

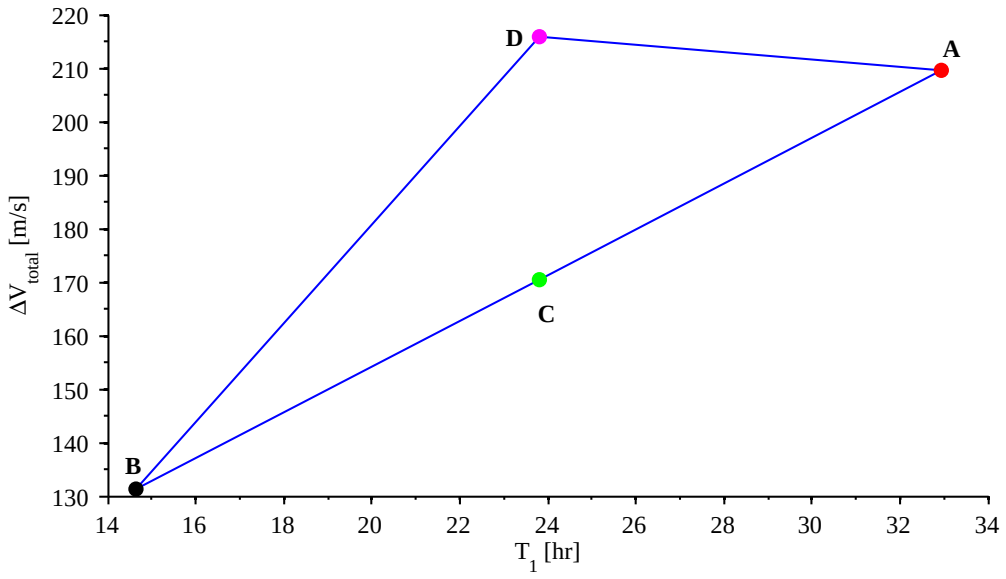

Figure 6.19: Non-convex example from random input test.

6.5.4 Convex Conclusion

Many cases of the inspection problem described in Section 6.1 without any time constraints were tested for convexity. No cases were found to be convex. It was determined that optimal minimum propellant solutions to the unconstrained-time double rendezvous problem can not be found using CVX and convex optimization.

Chapter 7

Mass Analysis for GEO Inspection and Debris Removal

The minimum Δv_{total} that was determined in Chapter 6 will be used along with the rocket equation in this chapter to determine mass estimates of the carrier concept. Mass estimates for inspection sorties along with debris removal sorties will be discussed. The carrier concept mass estimates will then be compared to a single Carrier-less satellite performing the same sorties.

7.1 Inspection Mission Mass Calculation

This section outlines the equations used to perform the mass analysis of an inspection mission. The mass analysis will be done for a carrier concept with one or more Inspectors and for a single Carrier-less satellite that would perform inspection missions. The results will be used to determine if the carrier concept is more mass efficient to perform the inspection missions.

7.1.1 Carrier Concept

The total mass of the Inspector is M_I.

$$M_I = M_{capI} + M_{strI} + M_p \tag{7.1}$$

where M_{capI} is the capable mass of the Inspector. This is the mass of all the subsystems of the Inspector except for the structure. Possible subsystems to be included in M_{capI} may be the payload, propulsion, guidance navigation and control, communications, command and data handling, thermal, and power. M_{strI} is the mass of the structure that supports the capable mass and the required propellant mass, M_p. The required propellant mass is the mass required to perform one GEO servicing mission. M_p is calculated using the rocket

equation, with the final mass of the Inspector being the total dry mass, $M_{capI} + M_{strI}$.

$$M_p = [M_{capI} + M_{strI}] \left[e^{\left(\frac{\Delta v}{I_{sp} g_0}\right)} - 1 \right] \tag{7.2}$$

where Δv is the required change in velocity to accomplish the GEO inspection mission calculated in Chapter 6, I_{sp} is the specific impulse of the thrusters, and g_0 is the acceleration of gravity at sea level.

The typical structural mass, M_{strI}, ranges from 8% to 12% of the spacecraft's loaded mass, or total mass, M_I [19]. The mass fraction of the structural mass to the satellite mass is called the structural fraction, SF, and will range from 0 - 1.

$$SF = \frac{M_{strI}}{M_I} \tag{7.3}$$

Substituting in Equation 7.1 for M_I and solving for M_{strI} produces an equation for the structural mass in terms of the structural fraction, the capable mass and the mass of the propellant.

$$M_{strI} = \left[\frac{SF}{1 - SF} \right] [M_{capI} + M_p] \tag{7.4}$$

Because the structural mass depends on the propellant mass and the propellant mass depends on the structural mass, Equation 7.2 needs to be resolved. For simplicity new variables called the structural fraction ratio R_{SF}, and Euler exponential number EE are introduced

$$R_{SF} = \frac{SF}{1 - SF} \tag{7.5}$$

$$EE = e^{\left(\frac{\Delta v}{I_{sp} g_0}\right)} \tag{7.6}$$

Substituting Equation 7.4 into Equation 7.2 and solving for M_p.

$$M_p = \left[M_{capI} - R_{SF}\left(M_{capI} + M_p\right)\right]\left[EE - 1\right] \tag{7.7}$$

$$M_p = M_{capI}\left[\frac{\left(1 + R_{SF}\right)\left(EE - 1\right)}{1 - R_{SF}\left(EE - 1\right)}\right] \tag{7.8}$$

To help simplify the equations a new variable is introduced, the structural delta-v number, SDN

$$SDN = \left[\frac{\left(1 + R_{SF}\right)\left(EE - 1\right)}{1 - R_{SF}\left(EE - 1\right)}\right] \tag{7.9}$$

$$M_p = M_{capI} SDN \tag{7.10}$$

Equation 7.8 is a function of M_{capI}, SF, Δv, and I_{sp}. This now makes Equation 7.4 and 7.1, the mass of the structure and the total loaded mass of the Inspector, respectively, a function of M_{capI}, SF, Δv, and I_{sp}.

$$M_{strI} = M_{capI} R_{SF}\left(1 + SDN\right) \tag{7.11}$$

$$M_I = M_{capI}\left(1 + SDN\right)\left(1 + R_{SF}\right) \tag{7.12}$$

The total propellant mass needed for the carrier concept, M_{prop}, will now be the number of inspection missions, N_{ins}, minus the number of Inspectors, N_I, times the propellant mass for one mission, M_p. The number of Inspectors has to be subtracted from the number of missions because they are modeled as already being loaded with propellant for one GEO inspection mission.

$$M_{prop} = M_p\left[N_{ins} - N_I\right] \tag{7.13}$$

The total mass of the Carrier is

$$M_{car} = M_{capCAR} + M_{strCAR} + M_{prop} \tag{7.14}$$

where M_{capCAR} is the capable mass for the Carrier, and M_{strCAR} is the structural mass of the Carrier. The structural mass of the Carrier is calculated the same as for the structural mass of the Inspector.

$$M_{strCAR} = R_{SF}\left[M_{capCAR} + M_{prop}\right] \tag{7.15}$$

Substituting Equation 7.15 into 7.14

$$M_{car} = \left[M_{capCAR} + M_{prop}\right]\left[1 + R_{SF}\right] \tag{7.16}$$

Substituting Equation 7.8 into 7.13 into 7.16 gives the equation for the mass of the Carrier that depends on N_{ins}, N_I, M_{capCAR}, M_{capI}, SF, Δv, and I_{sp}.

$$M_{car} = \left[M_{capCAR} + M_{capI} SDN\left(N_{ins} - N_I\right)\right]\left[1 + R_{SF}\right] \tag{7.17}$$

For the total mass of the carrier concept, M_{CC}

$$M_{CC} = M_{car} + N_I M_I \tag{7.18}$$

$$M_{CC} = \left[M_{capCAR} + M_{capI}\left(N_{ins} SDN + N_I\right)\right]\left[1 + R_{SF}\right] \tag{7.19}$$

Equation 7.19 is a function of the inputs N_{ins}, N_I, M_{capCAR}, M_{capI}, SF, Δv, and I_{sp}. Putting equation in terms of the capable mass fraction, MF_{cap}

$$MF_{cap} = \frac{M_{capI}}{M_{CC}} \tag{7.20}$$

$$MF_{cap} = \frac{1 - \frac{M_{capCAR}}{M_{CC}}(1 + R_{SF})}{(1 + R_{SF})(N_{ins}SDN + N_I)} \tag{7.21}$$

7.1.2 Single Carrier-Less Satellite

The total mass of the single satellite system is

$$M_{ss} = M_{cap} + M_{str} + M_{prop} \tag{7.22}$$

The structural mass of the system is calculated similar to the way the Inspector structural mass was calculated in Equation 7.11,

$$M_{str} = R_{SF}\left[M_{cap} + M_{prop}\right] \tag{7.23}$$

recalling that $R_{SF} = \dfrac{SF}{1 - SF}$, with SF being the structural mass fraction.

Using the rocket equation to calculate the propellant mass, M_{prop}

$$M_{prop} = \left[M_{cap} + M_{str}\right]\left[e^{\left(\frac{N_{ins}\Delta v}{I_{sp}g_0}\right)} - 1\right] \tag{7.24}$$

For simplicity the Euler exponent for the single satellite system is called EE_s. Note that this is different from EE in that the number of inspection missions, N_{ins} is in the numerator of the exponent.

$$EE_s = e^{\left(\frac{N_{ins}\Delta v}{I_{sp}g_0}\right)} \tag{7.25}$$

Substituting Equation 7.23 into 7.24 and solving for M_{prop}

$$M_{prop} = \left[M_{cap} + R_{SF}\left(M_{cap} + M_{prop}\right)\right]\left[EE_s - 1\right] \tag{7.26}$$

$$M_{prop} = M_{cap}\left[\frac{(1+R_{SF})(EE_s-1)}{1-R_{SF}(EE_s-1)}\right] \tag{7.27}$$

For simplicity again a new term the structural delta-v number for the single satellite system, SDN_s, is introduced

$$SDN_s = \frac{(1+R_{SF})(EE_s-1)}{1-R_{SF}(EE_s-1)} \tag{7.28}$$

The structural mass of the satellite is now

$$M_{str} = R_{SF}M_{cap}(SDN_s+1) \tag{7.29}$$

and the total loaded single Carrier-less satellite mass is

$$M_{ss} = M_{cap}(1+SDN_s)(1+R_{SF}) \tag{7.30}$$

Equation 7.30 is a function of N_{ins}, M_{cap}, SF, Δv, and I_{sp}.

For the capable mass fraction of the single Carrier-less satellite system, MF_{cap}

$$MF_{cap} = \frac{M_{cap}}{M_{ss}} \tag{7.31}$$

$$MF_{cap} = \frac{1}{(1+SDN_s)(1+R_{SF})} \tag{7.32}$$

7.1.3 GEO Inspection

To determine if the Carrier is a more efficient way to carry out GEO inspection missions, the total single Carrier-less satellite mass and the total carrier concept mass required to conduct a certain number of inspections, N_{ins} is compared. In either case, the initial required on-orbit mass is referred to as total system mass. The objective is to use the delta-v infor-

mation for the individual inspection missions previous presented in Chapter 6 to determine the total initial single Carrier-less satellite mass and the total initial carrier concept mass required to conduct N inspection sorties.

For multiple inspections, the equations previously presented in Sections 7.1.1 and 7.1.2 are used, along with these assumptions: 100 kg Inspector and single Carrier-less satellite capable mass (M_{capI}), 12% structural mass fraction (SF), a 10% delta-v penalty for trajectory corrections, a maximum 0.1 degree inclination change (additional Δv), and 10 m/s for proximity operations. A 90 day responsiveness requirement is enforced by requiring the single Carrier-less satellite to return to a 300 km orbit above GEO after each inspection sortie and by requiring the Inspector to return to its Carrier in a similar orbit. An engine Isp of 220 s is assumed.

Figure 7.1 shows the required totally system mass as a function of the number of required inspection sorties. The black curve shows the launch mass required for a single Carrier-less satellite to complete N inspection sorties. The colored curves show the total system mass required for the carrier concept with 1 Inspector (N_I). The different colors show the sensitivity to time in GEO, and the line styles show the sensitivity to Carrier's capable mass.

Table 7.1 shows the breakdown of the masses for the carrier concept and for the single Carrier-less satellite when performing specified amounts of inspection sorties with the same inputs as described above. This table shows the estimates of the satellites propellant, dry, and wet mass for the case of the Inspector capable mass, M_{capI}, of 100 kg, with a Carrier capable mass, M_{capCAR}, of 100 kg. Here the satellite wet mass is the dry mass of the satellite plus the propellant mass.

$$M_{wet} = M_{dry} + M_{propellant} \tag{7.33}$$

The dry mass is the capable mass plus the required structural mass. Because the Inspector returns to the Carrier to refuel after each inspection sortie, its mass will remain the same no matter the amount of inspection sorties performed by the carrier concept. In contrast the Carrier-less single satellite mass will greatly increase as the number of inspection sorties is

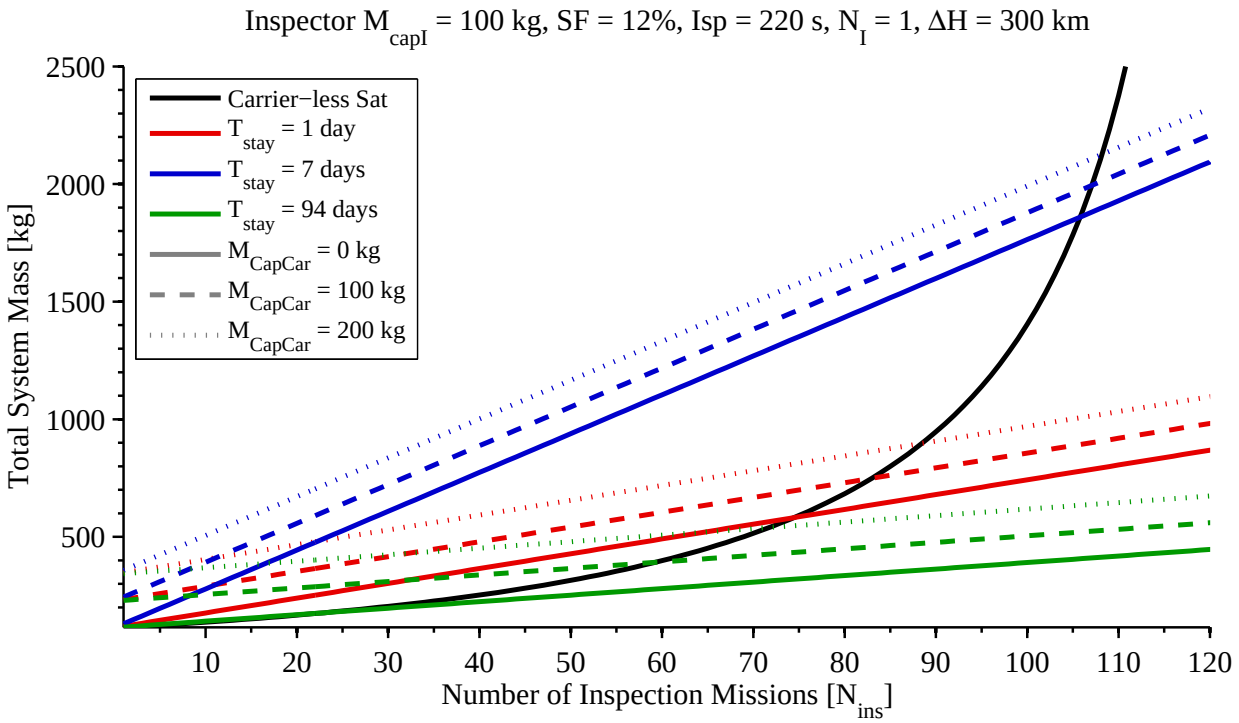

Figure 7.1: Total mass comparison of carrier concept and single satellite for GEO inspection missions.

required (last 3 rows).

It can be seen in Figure 7.1 that when the inspection sortie is desired to be for a short stay time in GEO, i.e. one day or one week, the carrier concept is only more mass efficient for large numbers of sorties (more than 75). If however the stay time at GEO is longer, e.g. the 94 day synodic period of the Carrier orbit (see Figure 5.5), then the Carrier is much more mass efficient when performing more than 23 sorties.

Changing the capable mass of the Inspector and single Carrier-less satellite capable mass (M_{capI}) to 30 kg and leaving the other inputs the same produce the results shown in Figure 7.2. The total system masses are much lower, but the overall trends are nearly the same. Table 7.2 shows the mass breakdown required when the capable mass of the Inspector is 30 kg.

7.2 Debris Removal Mass Calculation

If the satellite is required to move the GEO RSO out of the GEO protected region then

Table 7.1: Mass Breakdown of GEO Inspection Sorties: Inspector Capable Mass 100 kg

		Inspector Sat: M_{capI} = 100 kg			Carrier Sat: M_{capCAR} = 100 kg			Total System Mass (kg)
		Propellant Mass (kg)	Dry Mass (kg)	Wet Mass (kg)	Propellant Mass (kg)	Dry Mass (kg)	Wet Mass (kg)	
Carrier Concept: T_{stay} 1 day	10 Sorties	6	114	120	50	120	170	290
	50 Sorties	6	114	120	271	151	422	542
	100 Sorties	6	114	120	548	188	736	856
Carrier Concept: T_{stay} 7 days	10 Sorties	15	116	130	131	131	262	392
	50 Sorties	15	116	130	712	211	922	1,052
	100 Sorties	15	116	130	1,438	310	1,747	1,878
Carrier Concept: T_{stay} 94 days	10 Sorties	2	114	116	22	117	139	255
	50 Sorties	2	114	116	120	130	249	366
	100 Sorties	2	114	116	241	147	388	504
Carrier-Less Sat	10 Sorties	21	16	137				137
	50 Sorties	177	38	315				315
	100 Sorties	1,135	168	1,404				1,404

Table 7.2: Mass Breakdown of GEO Inspection Sorties: Inspector Capable Mass 30 kg

		Inspector Sat: M_{capI} = 30 kg			Carrier Sat: M_{capCAR} = 100 kg			Total System Mass (kg)
		Propellant Mass (kg)	Dry Mass (kg)	Wet Mass (kg)	Propellant Mass (kg)	Dry Mass (kg)	Wet Mass (kg)	
Carrier Concept: T_{stay} 1 day	10 Sorties	2	34	36	15	116	131	167
	50 Sorties	2	34	36	81	125	206	242
	100 Sorties	2	34	36	164	136	300	336
Carrier Concept: T_{stay} 7 days	10 Sorties	4	35	39	39	119	158	197
	50 Sorties	4	35	39	213	143	356	395
	100 Sorties	4	35	39	431	172	604	643
Carrier Concept: T_{stay} 94 days	10 Sorties	1	34	35	7	115	121	156
	50 Sorties	1	34	35	36	119	154	189
	100 Sorties	1	34	35	72	124	196	231
Carrier-Less Sat	10 Sorties	6	35	41				41
	50 Sorties	53	41	95				95
	100 Sorties	341	81	421				421

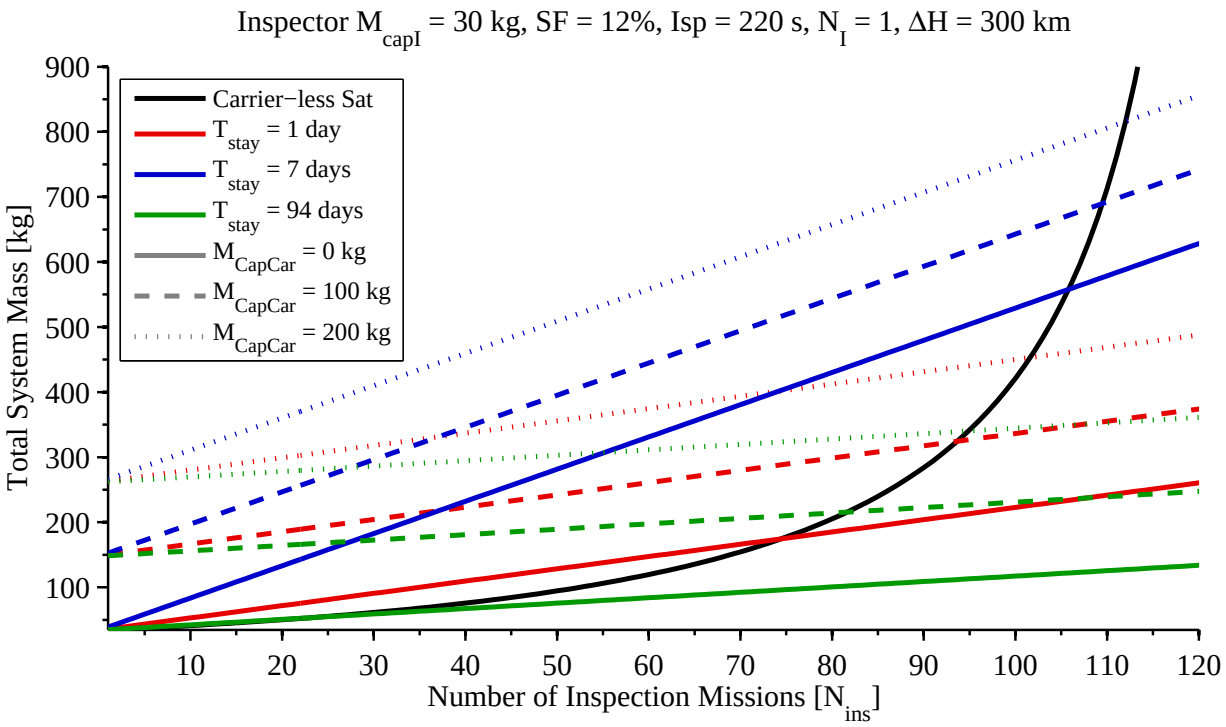

Figure 7.2: Total mass comparison of carrier concept and single satellite for GEO inspection missions.

a debris removal mission will be needed. This section will go through the steps to calculate the propellant mass and total mass of the carrier concept and single satellite concept for a debris removal mission.

7.2.1 Required Propellant Mass to Move Space Debris

For this analysis the propellant mass, M_p, required to perform a debris removal mission is divided into two parts. The first part is the propellant mass required to rendezvous with the debris, M_{p1}. The second part is the propellant mass required to tow the debris to a disposal or graveyard orbit (see Section 4.2), M_{p2}.

$$M_p = M_{p1} + M_{p2} \tag{7.34}$$

Using the rocket equation, the equations for M_{p1} and M_{p2} are

$$M_{p1} = M_{f1}\left(e^{\left(\frac{\Delta v_1}{I_{sp}g_0}\right)} - 1\right) \tag{7.35}$$

$$M_{p2} = M_{f2}\left(e^{\left(\frac{\Delta v_2}{I_{sp}g_0}\right)} - 1\right) \tag{7.36}$$

where Δv_1 and Δv_2 are the required changes in velocity to transfer to the debris and tow the debris to the graveyard orbit, respectively. M_{f1} is the mass of the Inspector after the initial rendezvous with the debris. M_{f2} is the mass of the Inspector and the debris system after towing the debris to the graveyard orbit. For simplicity the Euler Exponential, EE is defined for the first transfer as, EE_1, and as, EE_2, for the second

$$EE_1 = e^{\left(\frac{\Delta v_1}{I_{sp}g_0}\right)} \tag{7.37}$$

$$EE_2 = e^{\left(\frac{\Delta v_2}{I_{sp}g_0}\right)} \tag{7.38}$$

M_{f1} consists of the capable mass of the satellite, M_{cap}, the structural mass, M_{str}, and the remaining propellant mass M_{p2}.

$$M_{f1} = M_{cap} + M_{str} + M_{p2} \tag{7.39}$$

M_{f2} is composed of the capable mass, M_{cap}, the structural mass, M_{str}, and the mass of the disposed debris, M_d.

$$M_{f2} = M_{cap} + M_{str} + M_d \tag{7.40}$$

Substituting Equation 7.40 into 7.36 and recalling that the mass of the structure is a percentage, SF, of the total mass of the spacecraft, M_{total}

$$M_{str} = R_{SF}\left(M_{cap} + M_p\right) \tag{7.41}$$

$$R_{SF} = \frac{SF}{1 - SF} \tag{7.42}$$

$$SF = \frac{M_{str}}{M_{total}} \tag{7.43}$$

$$M_{p2} = \left[M_{cap} + R_{SF}\left(M_{cap} + M_p\right) + M_d\right]\left[EE_2 - 1\right] \tag{7.44}$$

Taking Equation 7.44 and 7.41, and substituting them into Equation 7.39

$$M_{f1} = M_{cap} + R_{SF}\left(M_{cap} + M_p\right) + \left[M_{cap} + R_{SF}\left(M_{cap} + M_p\right) + M_d\right]\left[EE_2 - 1\right] \tag{7.45}$$

Using Equation 7.45 in Equation 7.35

$$M_{p1} = \left[M_{cap} + R_{SF}\left(M_{cap} + M_p\right) + \left[M_{cap} + R_{SF}\left(M_{cap} + M_p\right) + M_d\right]\left[EE_2 - 1\right]\right]\left[EE_1 - 1\right] \tag{7.46}$$

Taking Equation 7.46 and 7.44 and substituting them into Equation 7.34 produces

$$\begin{aligned} M_p = &\left[M_{cap} + R_{SF}\left(M_{cap} + M_p\right) + \left[M_{cap} + R_{SF}\left(M_{cap} + M_p\right) + M_d\right]\left[EE_2 - 1\right]\right]\left[EE_1 - 1\right] \\ &+ \left[M_{cap} + R_{SF}\left(M_{cap} + M_p\right) + M_d\right]\left[EE_2 - 1\right] \end{aligned} \tag{7.47}$$

Solving Equation 7.47 for M_p will produce an equation that is dependent upon the inputs M_{cap}, M_d, Δv_1, Δv_2, SF, and I_{sp}.

$$M_p = \frac{M_{cap}\left(1 - EE_1EE_2\right)}{EE_1EE_2 - 1} - \frac{EE_1\left(EE_2M_{cap} - M_d + EE_2M_d\right)}{R_{SF}\left(EE_1EE_2 - 1\right) - 1} \tag{7.48}$$

7.2.2 Total Mass of carrier concept

To find the total mass of the carrier concept, M_{CC}, for a desired number of GEO debris removal missions, N_{dr}, Equation 7.48 is used to find the propellant required for one debris removal mission using a deployable satellite. The input for M_{cap} is the capable mass of the Inspector.

Using Equation 7.48 to calculate the propellant mass for one debris removal mission using an Inspector, M_{cap} is the capable mass of the Inspector, M_{capI}. Knowing M_p and M_{cap} the structural mass of the Inspector, M_{strI}, and the total mass of the Inspector, M_I, can be calculated. For the debris removal

$$M_{strI} = R_{SF}\left(M_{capI} + M_p\right) \tag{7.49}$$

$$M_I = M_{capI} + M_{strI} + M_p \tag{7.50}$$

The mass of propellant that the Carrier must carry, M_{prop}, to refuel the Inspectors, is calculated from the number of debris removal missions, N_{dr}, number of Inspectors, N_I, and propellant for one mission, M_p.

$$M_{prop} = \left(N_{dr} - N_I\right) M_p \tag{7.51}$$

It is assumed that $N_{dr} > N_{ss}$. If $N_{dr} < N_{ss}$ then there is no need for a Carrier. Using M_{prop} and the capable mass of the Carrier, M_{capCAR}, the structural mass of the Carrier, M_{strCAR} is

$$M_{strCAR} = R_{SF}\left(M_{capCAR} + M_{prop}\right) \tag{7.52}$$

The mass of the Carrier,M_{car}, not including M_I is

$$M_{car} = M_{capCAR} + M_{strCAR} + M_{prop} \tag{7.53}$$

The total mass of the carrier concept to perform debris removal is

$$M_{CC} = M_{car} + N_I M_I \tag{7.54}$$

7.2.3 Total Mass of Single Satellite

The total mass of the single satellite comparison is not as straight forward as the calculation of the total mass of the carrier concept. Equation 7.48 cannot be used if there is going to be more than one debris removal. The Δv inputs cannot simply be multiplied by the number of desired debris removal missions, N_{dr}. Unlike the carrier concept, the required propellant mass, M_p, for a debris removal mission is not constant. This assumes that each debris mass, M_d, is equal. Because the mass of the satellite changes as it burns propellant, M_p will continually decrease. The problem is formulated from the final mass after n debris missions, M_f and worked backwards. The final mass is the capable mass M_{cap}, and the structural mass, M_{str}. The structural mass depends upon the initial total mass of the single satellite, M_{ss}.

$$M_f = M_{cap} + M_{str} = M_{cap} + SF\left(M_{ss}\right) \tag{7.55}$$

The rocket equation that is used here is in the form

$$m_0 = m_f e^{\left(\frac{\Delta v}{I_{sp} g_0}\right)} \tag{7.56}$$

where m_0 is the mass before the burn of Δv, and m_f is the mass after the burn of Δv.

The mass of the satellite after it has attached itself to the n^{th} and final debris, before the transfer to the graveyard orbit, M_n^+ is

$$M_n^+ = (M_f + M_d)\, EE_2 \tag{7.57}$$

The mass of the debris, M_d, is added to the final mass because it is towed to the graveyard orbit before being released. $(M_f + M_d)$ is *effectively* the final mass of this burn.

The mass of the satellite when it starts the transfer to rendezvous with the n^{th} and final debris, M_n^- is

$$\begin{aligned} M_n^- &= \left(M_n^+ - M_d\right) EE_1 \\ &= \left((M_f + M_d)\, EE_2 - M_d\right) EE_1 \end{aligned} \tag{7.58}$$

Repeating this step for the $n-1$ debris

$$\begin{aligned} M_{n-1}^+ &= \left(M_n^- + M_d\right) EE_2 \\ &= \left(\left((M_f + M_d)\, EE_2 - M_d\right) EE_1 + M_d\right) EE_2 \end{aligned} \tag{7.59}$$

$$\begin{aligned} M_{n-1}^- &= \left(M_{n-1}^+ - M_d\right) EE_1 \\ &= \left(\left(\left((M_f + M_d)\, EE_2 - M_d\right) EE_1 + M_d\right) EE_2 - M_d\right) EE_1 \end{aligned} \tag{7.60}$$

The equation repeats itself for each subsequent M^- as

$$\left((\cdots + M_d)\, EE_2 - M_d\right) EE_1$$

This is continued until the mass of the satellite before the transfer to the first debris is reached.

$$\begin{aligned} &M_1^- = \\ &\left((\cdots\left(\left(\left((M_f + M_d)\, EE_2 - M_d\right) EE_1 + M_d\right) EE_2 - M_d\right) EE_1 + \cdots + M_d\right) EE_2 - M_d\right) EE_1 \end{aligned} \tag{7.61}$$

Algorithm 1 Check Equation 7.62

```
M  = Mss;           % Set mass to calculated launch mass
Mf = (Mcap + Mstr); % Final mass based off of calculated launch mass

for N = 1:Ndr                       % Loop through each debris removal
    M = M * exp(-dv1/Isp/g0);       % mass after transfer to debris
    M = (M+Md) * exp(-dv2/Isp/g0); % mass after taking debris to graveyard
    M = M-Md;                       % mass after releasing debris in graveyard
end

error = M - Mf;     % error beteen masses (should be zero)
```

Setting this equal to the initial total mass, M_{ss} and substituting in Equation 7.55

$$\begin{aligned} M_{ss} = \quad & ((\cdots((((M_{cap} + SF\,(M_{ss}) + M_d)\,EE_2 - M_d)\,EE_1 + M_d)\,EE_2 - M_d)\,EE_1 + \cdots \\ & + M_d)\,EE_2 - M_d)\,EE_1 \end{aligned} \tag{7.62}$$

This equation can now be solved for M_{ss}, and is a function of the inputs M_{cap}, SF, M_d, Δv_1, Δv_2, and I_{sp}.

A generic representation of this summation series could not be found. MATLAB was used to construct the equation, with required inputs, and solve the equation for a specified N_{dr}.

Once M_{ss} is solved for given the inputs, the structural mass and the propellant mass are easily calculated

$$M_{str} = SF\,(M_{ss}) \tag{7.63}$$

$$M_{prop} = M_{ss} - M_{cap} - M_{str} \tag{7.64}$$

Algorithm 1 is used to check that these equations are correct. The calculated launch mass, M_{ss}, is used to initialize a rocket equation that iterates to the desired number of debris removal missions, N_{dr}. The final mass produced from the iterative approach is then compared to the calculated final mass.

A few different examples cases were set up for a single satellite to perform debris removal missions. Algorithm 1 was used to find the error between the final mass calculated using Equation 7.62 and an iterative approach. The difference between the two final masses came out to be zero to machine precision, thus validating Equation 7.62. A similar check was performed with the equations for the carrier concept. The error in the masses also came out to be zero to machine precision.

7.2.4 GEO Debris Removal

To compute the total mass for the multiple debris disposal sorties, the equations presented above in Sections 7.2.1-7.2.3 are used. The total system mass is computed using the following assumptions: 100 kg Inspector capable mass, 12% structural mass, 10% delta-v penalty for trajectory corrections, a maximum 0.1 degree inclination change, and 10 m/s for proximity operations. A 90 day responsiveness requirement is enforced by requiring the single Carrier-less satellite to return to a 300 km orbit above GEO after each debris disposal sortie and by requiring the Inspector to return to its Carrier in a similar orbit. An engine Isp of 220 s is assumed. A 94 day GEO stay-time, the synodic period of a 300 km orbit above GEO, is assumed for the Inspector. Figure 7.3 shows the required total system mass as a function of the number of required debris disposal sorties. The black curves show the total system mass required for a single Carrier-less satellite to complete a number of debris disposal sorties, N_{dr}. The colored curves show the total system mass required for a carrier concept (i.e., Inspector mass plus Carrier mass). The different colors show the sensitivity to Carrier capable mass, and the different line styles show the sensitivity to GEO RSO debris mass.

Table 7.3 shows the total system mass estimation comparison of the carrier concept to the single Carrier-less satellite. The table shows the breakdown of the satellites propellant, dry, and wet masses. The table also shows mass estimates that correspond with Figure 7.3, using the same inputs as described above. As with the inspection sorties the mass of the Inspector with a Carrier does not change as the number of debris removal sorties changes.

Table 7.3: Mass Breakdown of GEO Debris Removal Sorties: Inspector Capable Mass 100 kg

			Inspector Sat: M_{capI} = 100 kg			Carrier Sat: M_{capCAR} = 100 kg			Total System Mass (kg)
			Propellant Mass (kg)	Dry Mass (kg)	Wet Mass (kg)	Propellant Mass (kg)	Dry Mass (kg)	Wet Mass (kg)	
Debris Mass 1000 kg	Carrier Concept	10 Sorties	16	116	132	146	134	279	411
		20 Sorties	16	116	132	308	156	463	595
		30 Sorties	16	116	132	469	178	647	779
	Carrier-Less Sat	10 Sorties	189	139	329				329
		20 Sorties	459	176	635				635
		30 Sorties	858	231	1,088				1,088
Debris Mass 3000 kg	Carrier Concept	10 Sorties	23	117	140	205	142	347	486
		20 Sorties	23	117	140	433	173	606	745
		30 Sorties	23	117	140	661	204	865	1,004
	Carrier-Less Sat	10 Sorties	266	150	416				416
		20 Sorties	646	202	848				848
		30 Sorties	1,208	278	1,486				1,486
Debris Mass 5000 kg	Carrier Concept	10 Sorties	29	118	147	265	150	414	561
		20 Sorties	29	118	147	558	190	748	895
		30 Sorties	29	118	147	852	230	1,082	1,229
	Carrier-Less Sat	10 Sorties	344	160	504				504
		20 Sorties	834	227	1,061				1,061
		30 Sorties	1,558	326	1,884				1,884

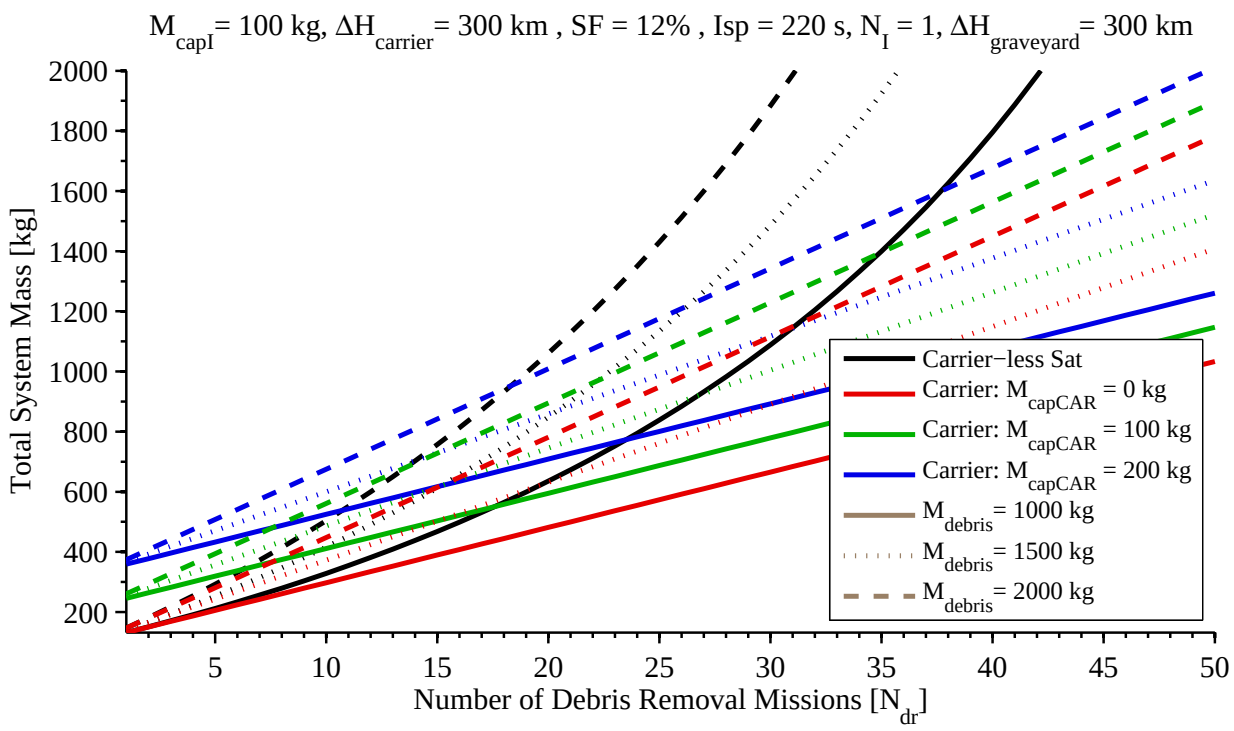

Figure 7.3: Total system mass of the carrier concept and single Carrier-less satellite for debris removal missions.

Figure 7.3 shows that the carrier concept is more mass efficient when more than 19 debris removal sorties take place. Also as the mass of the debris is increased the carrier concept becomes more mass efficient with even less debris removal sorties.

Figure 7.4 shows the results when the capable mass of the Inspector and single Carrier-less satellite is lowered to 30 kg and all other assumptions remain the same. The total system mass is lower than when M_{capI} is 100 kg but the same trends occur at the same number of debris removal sorties. Table 7.4 shows the breakdown of satellite mass estimates when the capable mass of the Inspector is changed to 30 kg. This table corresponds to Figure 7.4.

7.3 Mass Conclusion

The above results show that for a limited number of missions, e.g. < 10, a single Carrier-less satellite has a clear launch mass advantage of over the carrier concept. In this regime, the benefit of using a reusable/refuelable Carrier-based Inspector is not strong enough to overcome the penalty associated with the Carrier mass. The primary reason for this is the

Table 7.4: Mass Breakdown of GEO Debris Removal Sorties: Inspector Capable Mass 30 kg

			Inspector Sat: M_{capI} = 30 kg			Carrier Sat: M_{capCAR} = 100 kg			Total System Mass (kg)
			Propellant Mass (kg)	Dry Mass (kg)	Wet Mass (kg)	Propellant Mass (kg)	Dry Mass (kg)	Wet Mass (kg)	
Debris Mass 1000 kg	Carrier Concept	10 Sorties	14	36	50	127	131	258	308
		20 Sorties	14	36	50	268	150	418	468
		30 Sorties	14	36	50	409	169	578	628
	Carrier-Less Sat	10 Sorties	165	57	221				221
		20 Sorties	400	89	488				488
		30 Sorties	747	136	883				883
Debris Mass 3000 kg	Carrier Concept	10 Sorties	41	40	80	365	163	528	608
		20 Sorties	41	40	80	770	219	988	1,068
		30 Sorties	41	40	80	1,175	274	1,448	1,529
	Carrier-Less Sat	10 Sorties	474	99	572				572
		20 Sorties	1,149	191	1,340				1,340
		30 Sorties	2,147	327	2,474				2,474
Debris Mass 5000 kg	Carrier Concept	10 Sorties	67	43	110	602	196	798	908
		20 Sorties	67	43	110	1,271	287	1,558	1,668
		30 Sorties	67	43	110	1,940	378	2,319	2,429
	Carrier-Less Sat	10 Sorties	782	141	923				923
		20 Sorties	1,898	293	2,191				2,191
		30 Sorties	3,547	518	4,064				4,064

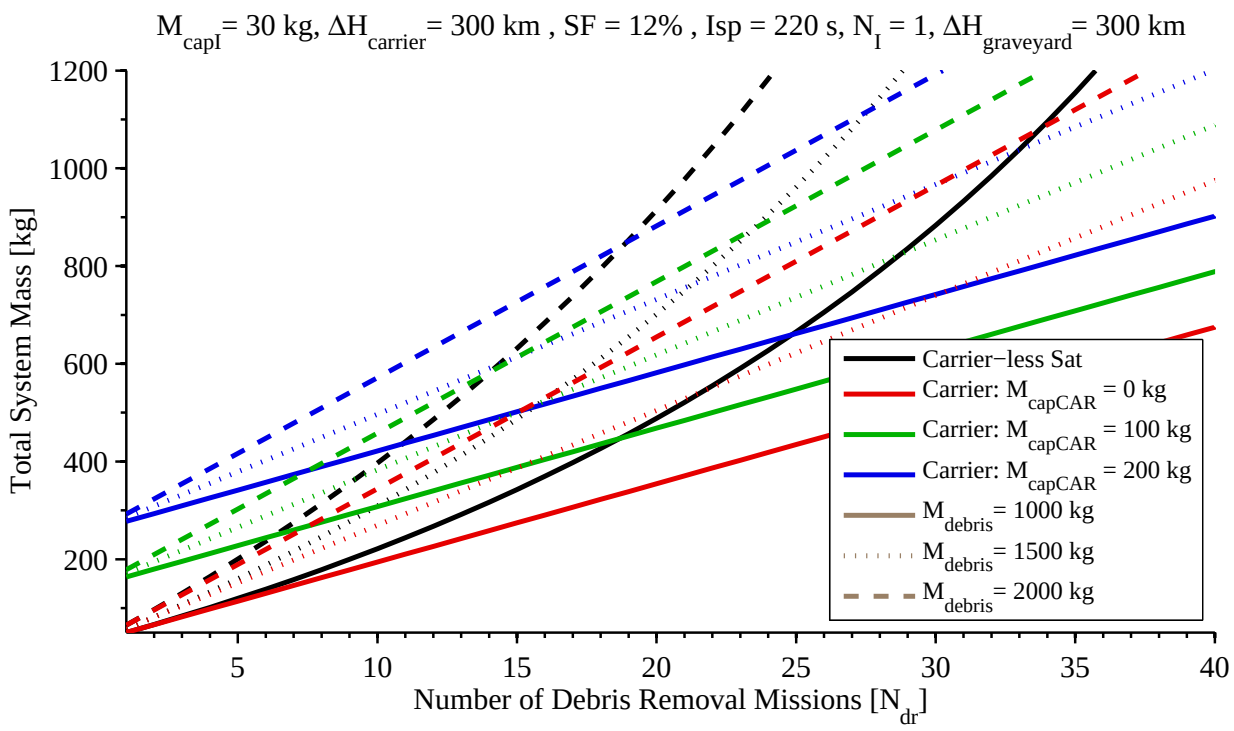

Figure 7.4: Total system mass of the carrier concept and single Carrier-less satellite for debris removal missions.

relatively small delta-v required for each individual sortie. The compounding effect of small delta-v's for multiple sorties on a single Carrier-less satellite mass (via the rocket equation) is nearly linear in this regime and does not offset the additional mass required for a Carrier. However, for hundreds of sorties the compounding effect of many small delta-v's on the single Carrier-less satellite mass becomes exponential and eventually exceeds the required mass for the carrier concept. While hundreds of inspection or debris removal sorties may not be required in the foreseeable future, the Carrier appears to have a clear mass advantage over the single Carrier-less satellite in this regime.

This conclusion, however, may not be universal. An alternative strategy is to consider the deployment of multiple Carrier-less satellites, each capable of conducting multiple sorties without a Carrier or refueling. In this case, the overall launch mass required to conduct hundreds of missions may in fact be less than a carrier concept. That said, if a fleet of Carrier-less satellites can be optimized such that each satellite is capable of conducting multiple sorties, a carrier concept can also be optimized such that each Carrier-based Inspector is

capable of conducting multiple sorties before returning to the Carrier. The solution to this minimal launch mass problem is determined only when a detailed set of mission requirements is specified. Once these requirements are known, an optimal GEO carrier concept can be designed and compared to an optimal fleet of single Carrier-less satellites. And while there may theoretically be a mass advantage to in-space refueling, the additional mass required for a Carrier-based refueling concept – the Carrier mass, docking equipment and propellant transfer/replacement devices – must be properly assessed and traded against the additional capable mass that will be required for multiple Carrier-less satellites.

Chapter 8

Preliminary Analysis for LEO Inspection and Debris Removal

Using the same mass analysis as in Chapter 7, the results of a Low Earth Orbit (LEO) carrier concept is presented. The Δv's required to maneuver a satellite near a GEO orbit as described in Chapter 6 are relatively low. As the required Δv's for inspection and debris removal sorties increases the mass benefits of the carrier concept also increase. The Δv for the Inspector to perform maneuvers in LEO dramatically increases from that of GEO maneuvering.

The population of LEO RSOs is also much different from the population in GEO. LEO RSOs span a wide range of altitudes, inclinations, eccentricities, and ascending nodes. Figures 8.1-8.4 show RSO population trends in LEO from the same database described in Section 4.1. For the purpose of this research, LEO is defined as any orbit that has an altitude less than 2,000 km above the surface of the Earth.

8.1 LEO carrier concept

The LEO carrier concept consists of one or more Inspector attached to a Carrier in a LEO orbit. When an Inspector is deployed, it transfers to a LEO RSO of interest, conducts an inspection or propulsively transfers the LEO debris to a lower orbit that meets the orbital lifetime requirement of < 3 years. The Inspector then returns to the Carrier, docks, and prepares (e.g. refueling) for another sortie.

To accommodate inspection or debris disposal of LEO RSOs an inclination/altitude band with high density of population is chosen. Using Figures 8.1-8.4 as a guide, the LEO region chosen will be RSOs with orbit inclination between 73.5 and 74.5 degrees. A zoomed in view of this inclination band that contains over 2,100 RSOs is shown in Figure 8.5.

The Carrier is initially deployed to a circular orbit at the center of the band, i.e., a 74

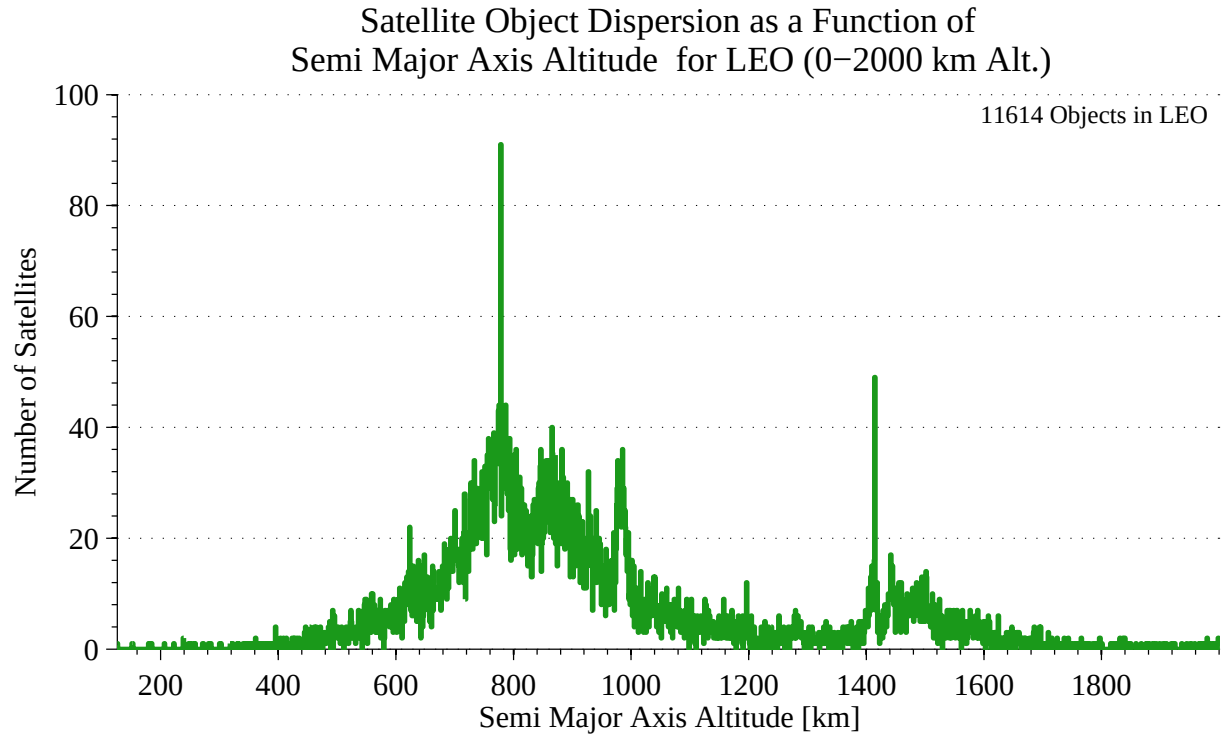

Figure 8.1: Space object dispersion as a function of semi-major axis of orbit for LEO region.

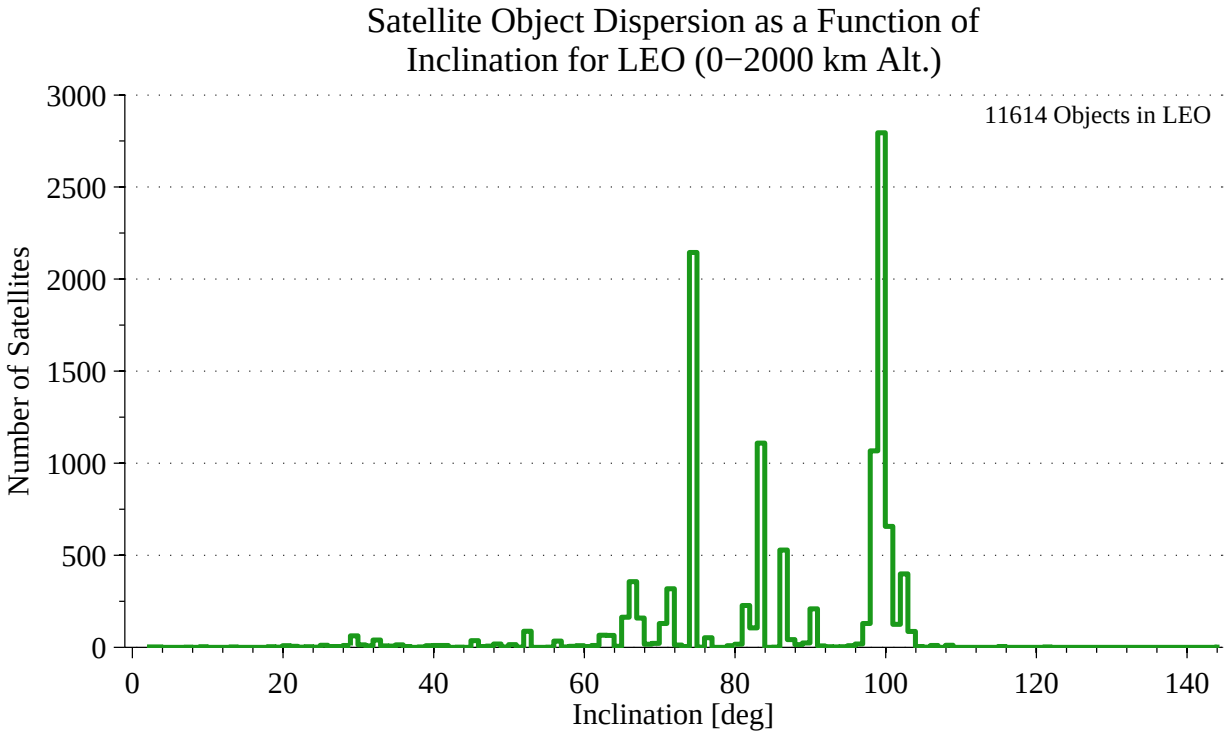

Figure 8.2: Space object dispersion as a function of inclination of orbit for LEO region.

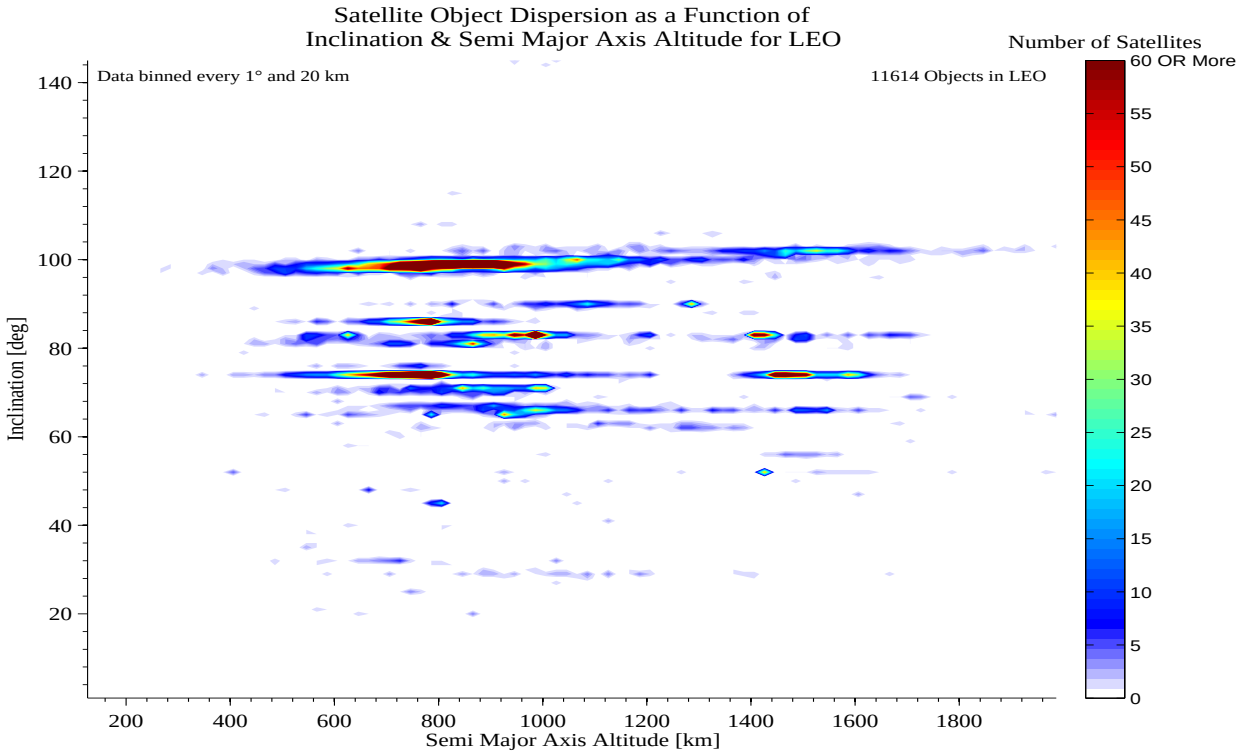

Figure 8.3: Space object dispersion as a function of semi-major axis and inclination of orbit for LEO region.

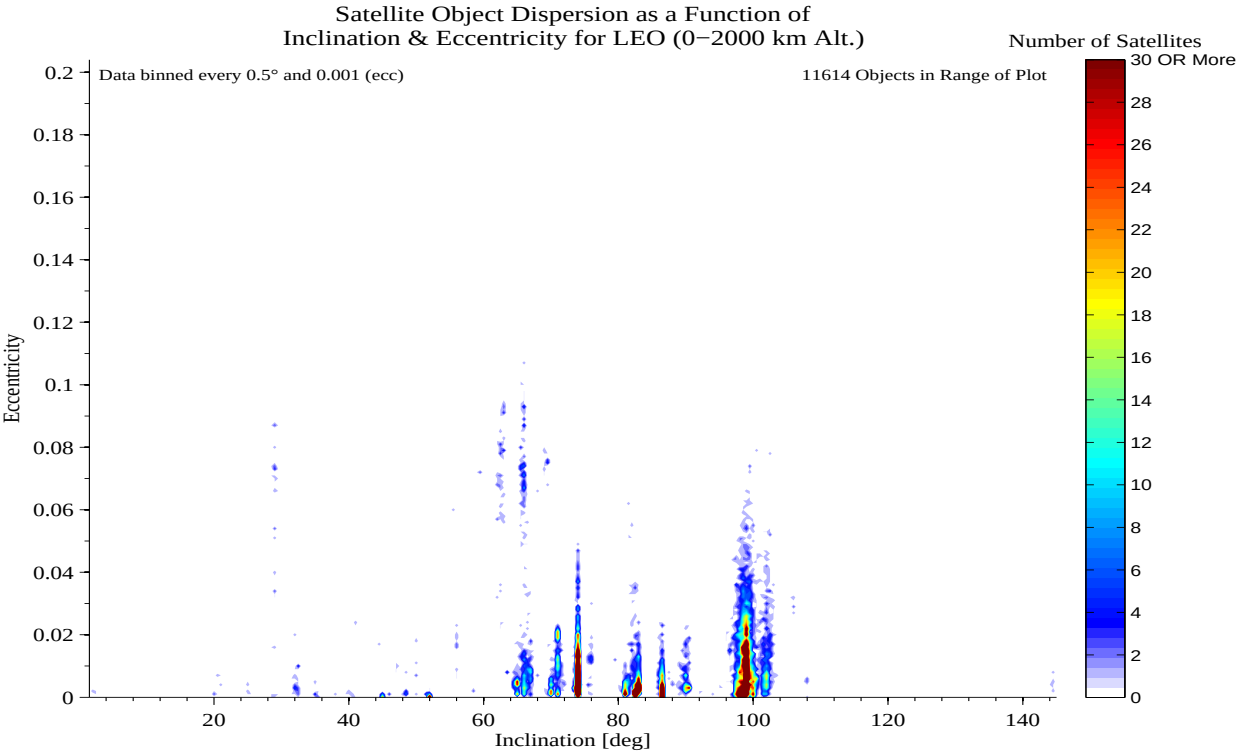

Figure 8.4: Space object dispersion as a function of semi-major axis and inclination of orbit for LEO region.

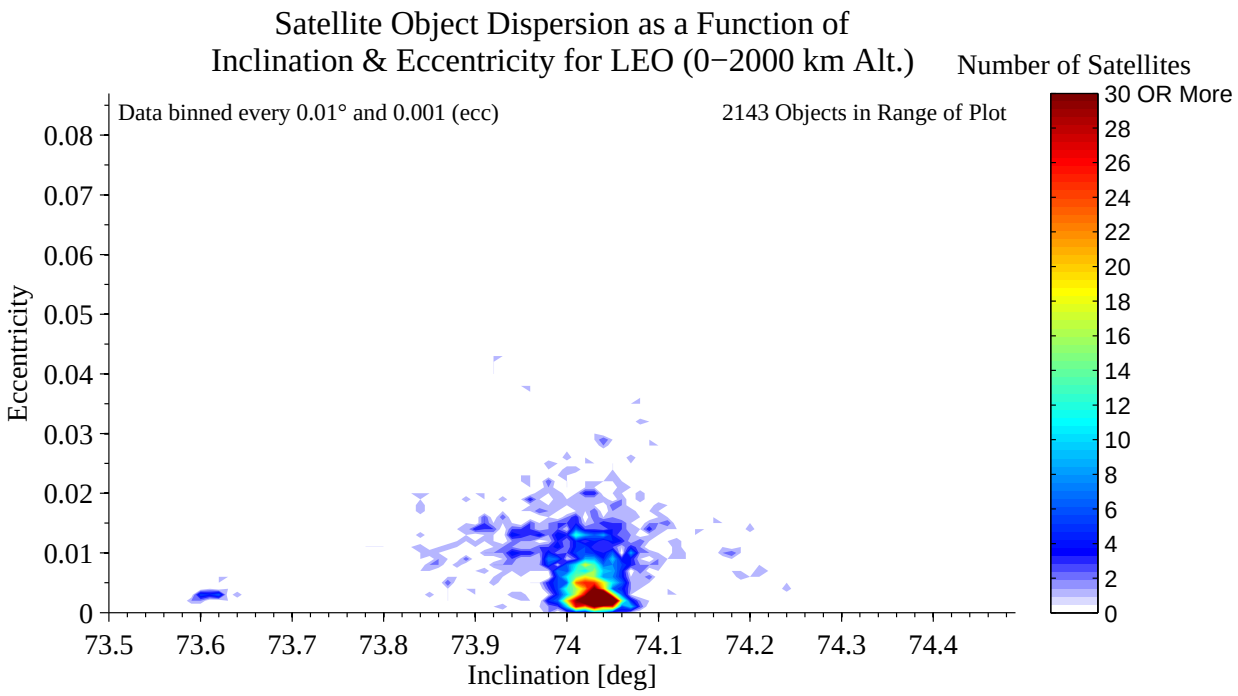

Figure 8.5: Zoomed in RSO dispersion as a function of inclination and eccentricity of orbit for LEO region.

degree inclination, 1100 km altitude orbit. Figure 8.6 shows the Carrier in this orbit, the red circle, and the LEO RSO population $\pm 1^{\circ}$ inclination from the Carrier, gray dots. From this staging point, individual inspection and debris disposal sorties will require a mean altitude change of 400 km and a mean inclination change of 0.25 degrees. Over a 5 year period, the differential precession of the Carrier ascending node will provide access to all the objects in this band that are more than 300 km below or above the Carrier. This 5 year period will act as a responsiveness requirement. Hence, the altitude of the Carrier orbit is located in the middle of two high LEO RSO density populations, one below at 500-800 km altitude, and the other above at 1400-1600 km altitude.

The Carrier-less single satellite that the carrier concept is compared to will also initially be deployed to the same orbit as the carrier concept.

8.1.1 LEO Inspection Missions

When transferring to a LEO RSO, the Inspector first executes a small plane change at the LEO RSO/Inspector line-of-nodes to accommodate small LEO RSO inclination and

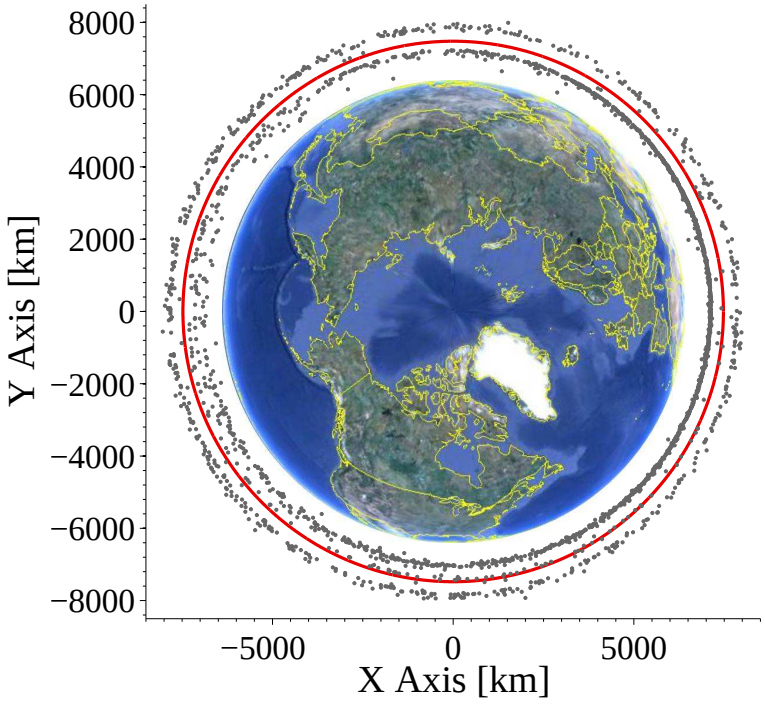

Figure 8.6: Carrier orbit orbit at 74° inclination and 1100 km altitude with LEO RSO population ±1° inclination.

ascending node differences, taking into account a small amount of differential nodal precession that will occur during the sortie. Proper phasing is achieved by adjusting the departure time up to ±12 hours. The Inspector then transfers into a co-elliptic orbit by executing two Hohmann-like transfer maneuvers at the points where the LEO RSO line-of-apsides intersects the Inspector orbit. The altitude of the co-elliptic orbit is chosen to ensure final phasing for rendezvous. This sequence of maneuvers has not been optimized.

As the Inspector approaches the LEO RSO from above or below on the co-elliptic trajectory, it executes a maneuver to transfer directly to the LEO RSO. Trajectory correction maneuvers are executed to position the Inspector in the vicinity of the LEO RSO at a range of 100 m – 1 km in front of or behind the LEO RSO where the inspection begins. Optional co-elliptic flyby inspections and circumnavigating orbit inspections are also possible.

When the inspection is complete, the Inspector executes a similar set of maneuvers to return and rendezvous with the Carrier. The single Carrier-less satellite will return to any orbit with a nodal precession that allows it to visit all nodes in 5 years, i.e. the Carrier-less

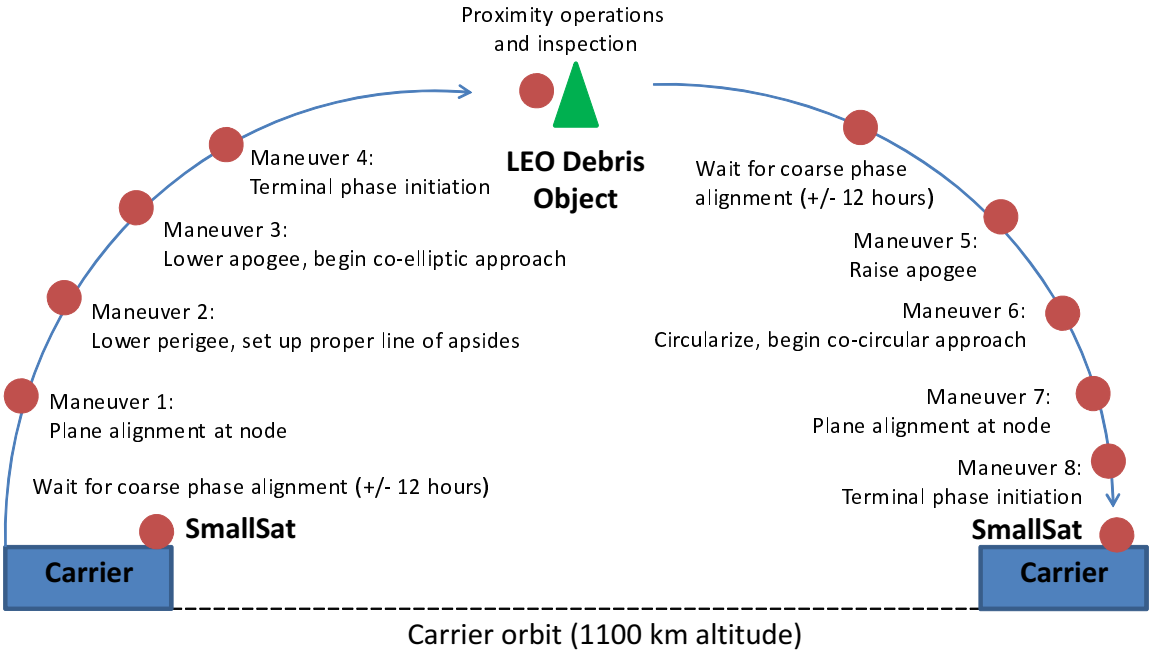

Figure 8.7: Example of Inspector maneuver sequence for LEO RSO inspection sortie.

single satellite only needs to adjust its semi-major axis and does not need to make any plane changes after the inspection. An example of an Inspector maneuver sequence for a LEO inspection sortie is shown in Figure 8.7.

8.1.2 LEO Debris Disposal Missions

For LEO RSO debris disposal sorties, the Inspector transfers to the LEO debris object in the same manner as an inspection sortie, and a set of pre-planned or autonomous maneuvers are executed to place the Inspector in a position less than 10 m from the debris object where it can attach a towing boom.

8.2 Δv Requirements for LEO Missions

To determine the total system mass for a LEO carrier concept for inspection or debris removal sorties, estimates of the delta-v requirements for individual inspection and debris disposal sorties must be determined.

The analysis presented below is ideal in the sense that it does not take into account

the Δv required for mid course corrections, and proximity operations, i.e. only the major maneuvers are considered. When total system mass estimates are determined, additional Δv is added to results of this section to account for smaller, relatively minor maneuvers.

There are other simplifying assumptions to be considered. The LEO RSO population at 74 degrees inclination lies within a ± 0.5 degree inclination band. At any given time there is also a small ascending node difference. In the analysis that follows, it is assumed that the maximum difference between the Inspector orbit plane and the LEO RSO orbit plane (commonly referred to as the wedge angle) is 1.0 degrees. Thus every inspection or debris disposal sortie is assumed to require a plane change of up to 1.0 degrees. Additionally, the eccentricities of 93% of LEO RSO population at 74 degrees inclination span a small but non-trivial range of 0.0-0.02 (see Figure 8.5). For this analysis it is assumed that all LEO RSOs are in circular orbits at varying altitudes. Since most of the eccentricities are small, this assumption is not overly restrictive.

Using these assumptions, Figure 8.8 shows the Δv required for a round trip inspection sortie as function of the LEO RSO altitude and wedge angle. The maneuvers for changing the Inspector's orbit altitude and nulling the wedge angle are made separately. All in-plane maneuvers are assumed to be optimal Hohmann transfer maneuvers. Smaller maneuvers for orbit phasing, proximity operations, and rendezvous are neglected in this data, but is considered later when total system mass estimates are determined.

While the results in Figure 8.8 are based on an Inspector sortie, they are also valid for the Carrier-less single satellite sortie. First, to meet the responsiveness requirement, the Carrier-less single satellite must return to an orbit with the same semi-major axis as the Carrier. Thus the Δv required for altitude changes is similar. Second, while the Carrier-less single satellite is not required to return to the original orbit plane via a second plane change, subsequent plane changes may be as high as 2 degrees to accommodate the entire LEO RSO population inclination band. Thus, overall, the total inspection sortie Δv is similar.

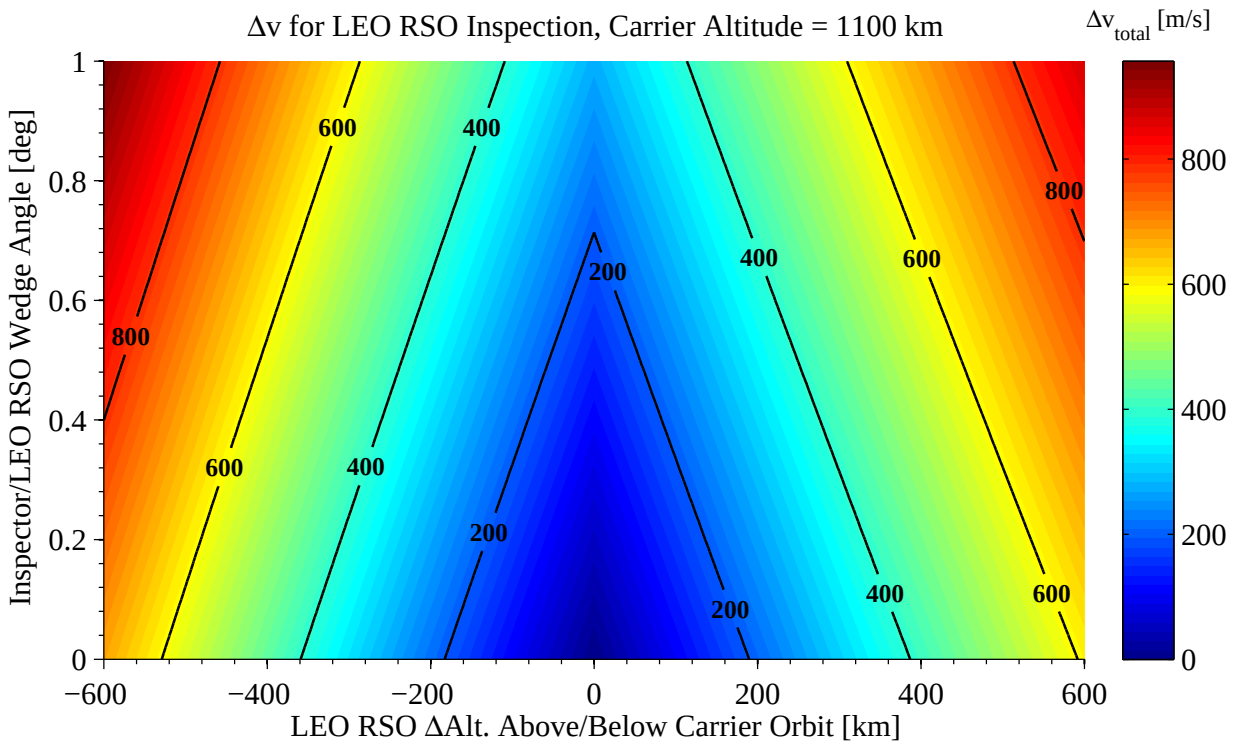

Figure 8.8: Required Inspector Δv_{total} for a LEO inspection sortie as a function of LEO RSO wedge angle and altitude.

8.3 Total System Mass Comparison

A key metric in assessing LEO inspection or LEO debris disposal missions is the initial total Carrier-less single satellite mass and the initial total carrier concept mass required to conduct a desired number of inspections, N_{ins}, or debris disposal, N_{dr} sorties. In either case, the initial mass at deployment is referred to simply as total system mass.

For multiple inspection sorties, the rocket equation as formulated in Section 7.1 along with the following assumptions: 100 kg Inspector capable mass, 12% structural mass fraction, 10% Δv for trajectory corrections, 10 m/s additional Δv for proximity operations, a 400 km mean altitude change, two 0.5 degree mean plane changes for Inspector sorties, and one 0.667 mean plane change for Carrier-less single satellite sorties. While using a mean altitude and inclination changes is reasonable for estimating the total propellant load for N sorties, it does not take into account that propellant tanks will need to sized for worst case individual sorties. However, the additional mass associated with potentially larger propellant tanks is

offset by the rather conservative 12% structural mass. The responsiveness requirement is enforced by requiring the Carrier-less single satellite to return to a an orbit with a 1100 km semi-major axis after each inspection sortie and by requiring the Inspector to return to a Carrier in a 1100 km circular orbit. An engine Isp of 220 s is assumed.

Figure 8.9 shows the required total system mass as a function of the number of required inspection sorties. The black curve shows the launch mass required for a single Carrier-less satellite to complete N inspection sorties. The colored curves show the total system mass required for a carrier concept (i.e. Inspector plus Carrier mass). The different colors show the sensitivity to Carrier capable mass.

Table 8.1 shows the mass estimation breakdown of the carrier concept compared to the single Carrier-less satellite for LEO inspection sorties. The same inputs are used in this table as in Figure 8.9. The table shows the satellites propellant, dry, and wet masses. The dry mass is the capable mass plus the required structural mass, defined by the structural mass fraction, SF. The wet mass is the dry mass plus the propellant mass. From the way the problem is set up and the analysis is performed it is not possible to perform 20 LEO inspection sorties by using a single satellite.

For multiple debris disposal sorties, the equations shown in 7.2 are used along with the following assumptions: 100 kg Inspector capable mass, 100 kg Carrier capable mass, 12% structural mass, 10% delta-v penalty for trajectory corrections, 10 m/s for proximity operations, a 400 km mean altitude change, a 400 km circular disposal orbit, two 0.5 degree mean plane changes for Inspector sorties, and one 0.667 mean plane change for Carrier-less single satellite sorties. The responsiveness requirement is enforced by requiring the Carrier-less single satellite to return to a an orbit with a 1100 km semi-major axis after each disposal sortie and by requiring the Inspector to return to a Carrier in a 1100 km circular orbit. An engine Isp of 220 s is assumed. Since the Δv for debris disposal above the nominal Carrier orbit is greater than the Δv required for debris disposal below the Carrier orbit, an average value of the two cases was used to estimate the total system mass.

Figure 8.10 shows the required total system mass as a function of the number of required

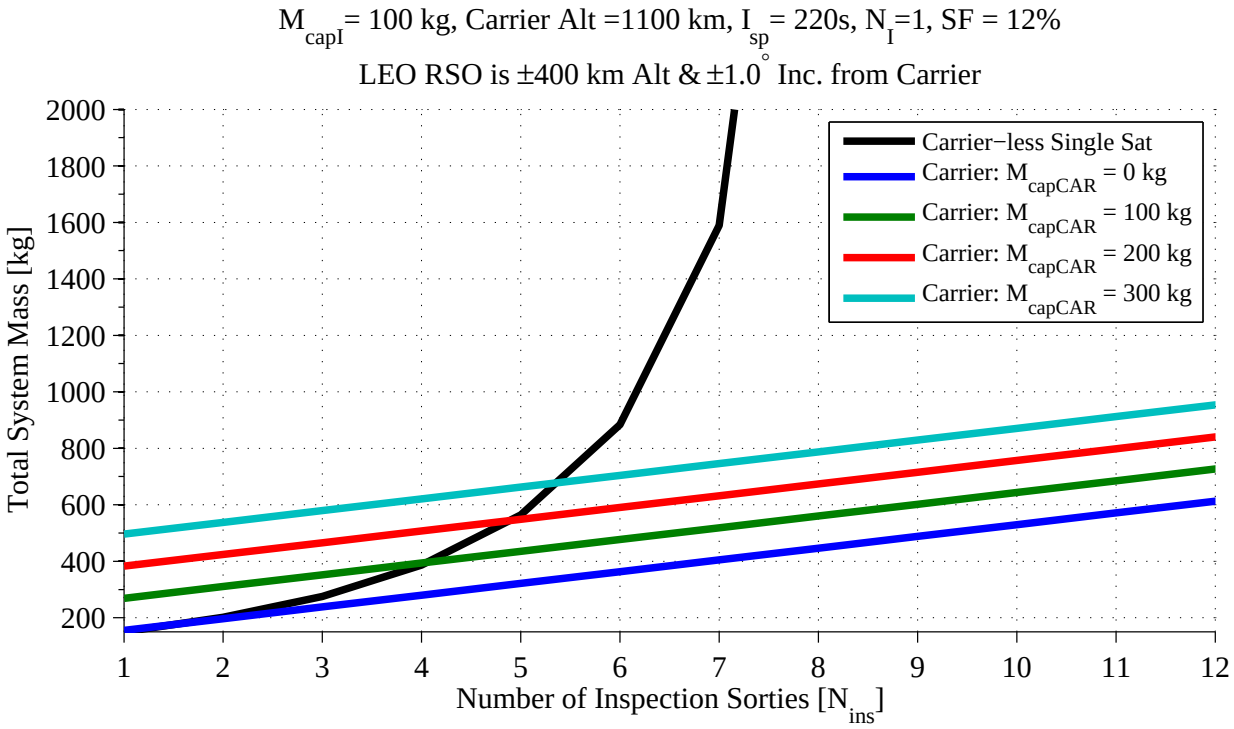

Figure 8.9: Total system mass as a function of the number of inspection sorties for a carrier concept and a Carrier-less single satellite.

Table 8.1: Mass Breakdown of LEO Inspection Sorties: Inspector Capable Mass 100 kg

		Inspector Sat: M_{capI} = 100 kg			Carrier Sat: M_{capCAR} = 100 kg			Total System Mass (kg)
		Propellant Mass (kg)	Dry Mass (kg)	Wet Mass (kg)	Propellant Mass (kg)	Dry Mass (kg)	Wet Mass (kg)	
Carrier Concept	5 Sorties	37	119	155	146	134	280	435
	8 Sorties	37	119	155	256	149	405	560
	20 Sorties	37	119	155	696	208	904	1,059
Carrier-Less Sat	5 Sorties	397	168	564				564
	8 Sorties	3,642	610	4,252				4,252
	20 Sorties	Not Possible	Not Possible	Not Possible				Not Possible

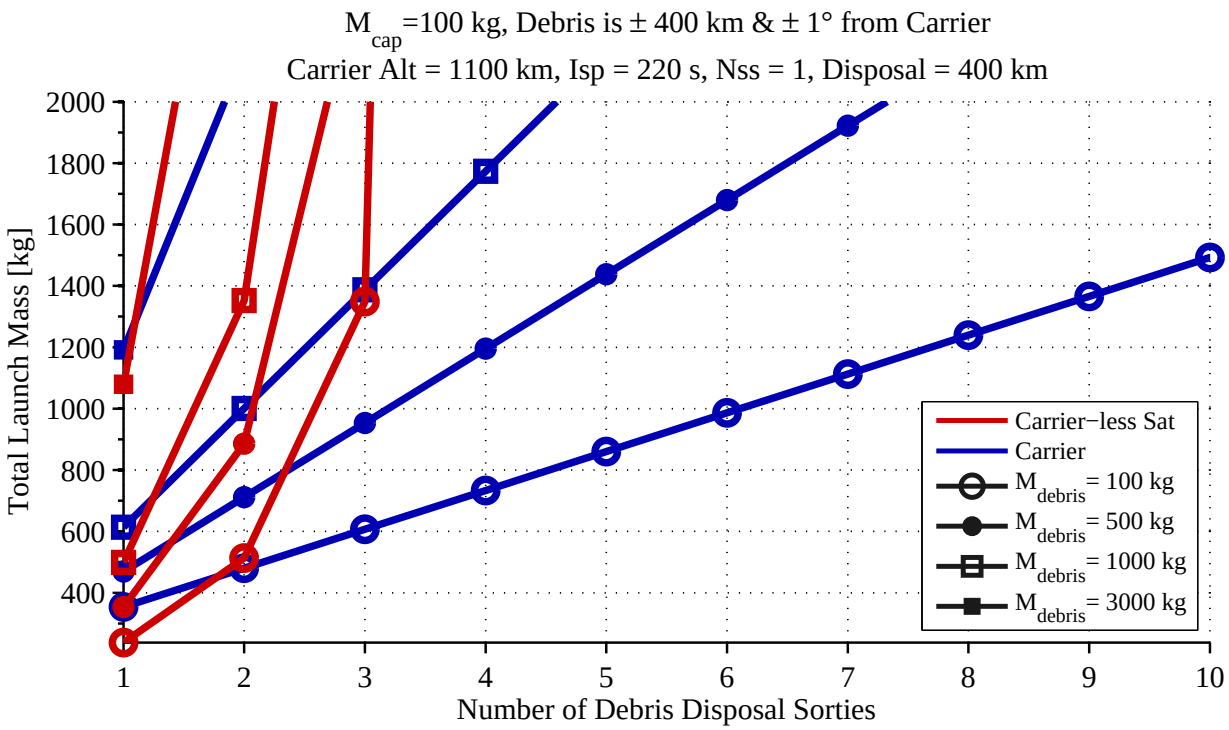

Figure 8.10: Total system mass as a function of the number of debris removal sorties for a carrier concept and a Carrier-less single satellite.

debris disposal sorties. The red curves show the launch mass required for a single Carrier-less single satellite to complete N debris disposal sorties. The blue curves show the launch mass required for a carrier concept (i.e. Inspector plus Carrier mass). The different symbols show the sensitivity to LEO debris mass being disposed.

Table 8.2 shows the mass estimation break down of the carrier concept compared to the single Carrier-less satellite. The same inputs used above and for Figure 8.10 are applied. It is not possible for the single Carrier-less satellite to perform many (more than 5) debris disposal sorties the way that the problem is set up and analyzed.

8.4 LEO Conclusions

The above results indicate an apparent advantage in using a carrier concept when more than 8 LEO inspection sorties are required or when more than only 4 LEO debris disposal sorties are required. This is in stark contrast to the GEO inspection and debris disposal results. The key difference is in the significantly larger Δv requirements for individual sorties,

Table 8.2: Mass Breakdown of LEO Debris Disposal Sorties: Inspector Capable Mass 100 kg

			Inspector Sat: M_{capI} = 100 kg			Carrier Sat: M_{capCAR} = 100 kg			Total Launch Mass (kg)
			Propellant Mass (kg)	Dry Mass (kg)	Wet Mass (kg)	Propellant Mass (kg)	Dry Mass (kg)	Wet Mass (kg)	
Debris Mass 100 kg	Carrier Concept	2 Sorties	111	129	240	111	129	240	480
		4 Sorties	111	129	240	334	159	493	733
		10 Sorties	111	129	240	1,002	250	1,252	1,492
	Carrier-Less Sat	2 Sorties	352	162	513				513
		4 Sorties	13,850	2,002	15,853				15,853
		10 Sorties	Not Possible	Not Possible	Not Possible				Not Possible
Debris Mass 500 kg	Carrier Concept	2 Sorties	213	143	356	213	143	356	711
		4 Sorties	213	143	356	639	201	840	1,196
		10 Sorties	213	143	356	1,918	375	2,293	2,648
	Carrier-Less Sat	2 Sorties	680	206	886				886
		4 Sorties	26,772	3,764	30,536				30,536
		10 Sorties	Not Possible	Not Possible	Not Possible				Not Possible
Debris Mass 1000 kg	Carrier Concept	2 Sorties	340	160	500	340	160	500	1,001
		4 Sorties	340	160	500	1,021	253	1,273	1,774
		10 Sorties	340	160	500	3,062	531	3,593	4,093
	Carrier-Less Sat	2 Sorties	1,090	262	1,352				1,352
		4 Sorties	42,924	5,967	48,891				48,891
		10 Sorties	Not Possible	Not Possible	Not Possible				Not Possible
Debris Mass 3000 kg	Carrier Concept	2 Sorties	849	229	1,078	849	229	1,078	2,157
		4 Sorties	849	229	1,078	2,547	461	3,008	4,086
		10 Sorties	849	229	1,078	7,640	1,155	8,795	9,874
	Carrier-Less Sat	2 Sorties	2,730	486	3,216				3,216
		4 Sorties	107,531	14,777	122,308				122,308
		10 Sorties	Not Possible	Not Possible	Not Possible				Not Possible

e.g. 32 m/s - 100 m/s for GEO inspection sorties, and 400 m/s - 900 m/s for LEO inspection sorties. The compounding effect of large sortie Δv on the Carrier-less single satellite via the rocket equation produces an exponential growth in total system mass versus a near linear growth for the carrier concept.

When the number of required LEO sorties is small, e.g. less than 5 or 4, the Carrier-less single satellite can be competitive and in some cases has an obvious advantage. In this regime, the benefit of using a reusable/refuelable Carrier-based Inspector is not strong enough to overcome the penalty associated with the Carrier mass. The Carrier-less single satellite wins out primarily due to the relatively low Δv required for a small number of sorties.

While these conclusions may be true for two scenarios that were considered (i.e., a Carrier-based Inspector and a single Carrier-less satellite), an alternative strategy to consider is the deployment of multiple Carrier-less single satellites, each capable of conducting multiple sorties without a Carrier or refueling. For example, the total system mass for a single Carrier-less satellite capable of conducting 4 inspection sorties is approximately 450 kg. Five of these satellites would be capably of conducting 20 inspection sorties, and the total system mass would be only 2250 kg. While this strategy does not outperform the carrier concept, it is much more competitive in terms of total system mass. A similar trend exists for debris removal missions, though the carrier concept is highly favored.

But these conclusions are not universal. If a fleet of Carrier-less single satellites can be optimized such that each satellite is capable of conducting multiple sorties, a carrier concept should be considered where each Carrier-based Inspector is capable of conducting multiple sorties before returning to the Carrier. In many cases this will reduce the total system mass of the carrier concept further because the Inspectors will not be required to return to the Carrier after each sortie.

The solution to this minimal total system mass problem will be determined only when a detailed set of mission requirements is specified. Once these requirements are known, an optimal LEO carrier concept can be designed and compared to an optimal fleet of single

Carrier-less satellites. And while there may theoretically be a mass advantage to in-space refueling, the additional mass required for a Carrier-based refueling concept – the Carrier mass, docking equipment and propellant transfer/replacement devices – must be properly assessed and traded against the additional capable mass that will be required for multiple Carrier-less single satellites.

Chapter 9

Conclusion and Future Work

The purpose of this thesis research was to determine if the unconstrained-time double rendezvous problem with a RSO from a near GEO orbit is convex and can be solved with known convex optimization techniques. A second objective was to determine the propellant and mass savings of a carrier concept with deployable Inspectors verses a single satellite for GEO RSO inspection sorties.

The thesis has shown that the unconstrained-time double rendezvous problem i.e., departing from a Carrier, rendezvousing with a GEO RSO , staying in the proximity of the RSO for a specified time, and then retuning to the Carrier, is not convex when modeled with the CW equations and unconstrained time. CVX and convex optimization techniques can not be used to find minimum propellant trajectories or control/thrust profiles.

To find minimum Δv_{total} solutions to the unconstrained-time double rendezvous problem a searching algorithm was devised using intrinsic MATLAB optimization functions. This approach was very expensive in computation time but did allow for finding minimum Δv solutions.

The minimum Δv_{total} solutions to the unconstrained-time double rendezvous problem were analyzed for a Carrier in two different near GEO orbits. The first Carrier orbit analyzed was a circular orbit ΔH above or below GEO altitude. The other Carrier orbit analyzed was an elliptical orbit with either apogee or perigee ΔH_{max} above or below GEO and the associated perigee or apogee at GEO. This was referred to as the cycloid orbit.

Comparing the minimum Δv_{total} solutions, produced by the MATLAB searching method, lower Δv_{total} can be achieved from a Carrier in a cycloid orbit as opposed to a circular orbit. When comparing cycloid to circular orbits, orbits of the same orbital energy were compared, giving the orbits the same synodic periods with GEO. Although the cycloid orbit held Δv_{total}

advantages over the circular orbit, for certain Inspector stay times at GEO, the cycloid orbit potentially had the disadvantage that it cycled in and out of the GEO protected region.

Applying the rocket equation, with the minimum Δv_{total} solutions, the required mass, for inspection sorties, of the carrier concept, i.e. the Carrier mass plus the Inspector(s) mass, was estimated. The total mass estimates of the carrier concept was then compared to a single satellite performing inspection sorties without a Carrier. The Carrier system was found to be more mass efficient only when there were a large number of inspection sorties desired. The exact number of sorties when the carrier concept was more efficient than the single Carrier-less satellite was very mission specific. The efficiency of the Carrier is determined by Δv_{total}, propulsive properties of the propellant and thrusters, and the structural mass ratio of the vehicle. Overall the carrier concept is more mass efficient when many inspection sorties are desired.

Mass estimates of the carrier concept and a single Carrier-less satellite required for debris removal missions in GEO were determined by again applying the minimum Δv_{total} solutions with the rocket equation. The carrier concept is more mass efficient after only a few, less than 10, debris removal sorties. While the mass of the carrier concept grows linearly, with more debris sorties, the single Carrier-less satellite grows exponentially and has a limit of how many missions can be accomplished. As with the inspection sorties the debris disposal sorties mass estimates depend on a number of inputs and can vary slightly.

Mass estimates for the carrier concept and single Carrier-less satellite was also performed for inspection and debris removal in LEO. Because of the higher Δv required for these sorties the Carrier becomes the more mass efficient option quicker. Also again the mass estimates of the Carrier-less single satellite grow exponentially while the carrier concept grows linear making the efficiency gap between the two grow exponentially. Again the single Carrier-less satellite is limited by a fixed number of inspection or debris removal sorties.

The work done in this thesis was a preliminary analysis for inspection and debris removal sorties in GEO using a carrier concept. Overall the Carrier is a viable option to perform these sorties. It poses a way to perform many sorties more mass efficient than a single Carrier-less

satellite. Future work on this subject includes a more in depth analysis on the Carrier in LEO. The dynamics and control also needs to be studied for attaching and removing the debris with a SmallSat in GEO and LEO. The concept of attaching to an uncooperative satellite or debris needs to be fully understood to complete the debris removal sorties. Also inspection sorties can be further researched to determine what maneuvers would need to be done while the Inspector was in proximity of the GEO/LEO RSO.

References

[1] Fortescue, P., Stark, J., and Swinerd, G. (eds), *Spacecraft Systems Engineering*, 3rd ed., Wiley, West Sussex, England, 2003.

[2] Riebeek, H., "Catalog of Earth Satellite Orbits," http://earthobservatory.nasa.gov, [cited September 2009].

[3] Butler, A., "USAF Prepares for First Sbirs GEO Launch," *Aviation Week*, April 2011.

[4] Mozurkewich, D., Armstrong, J. T., Hindsley, R. B., Jorgensen, A. M., Restaino, S. R., and Schmitt, H. R., "Toward the Ground-based Imaging of Satellites at Geosynchronous Altitude," Advanced Maui Optical and Space Surveillance Technologies Conference, September 2011.

[5] Shell, J. R., "Commercially-Hosted Payloads for Debris Monitoring and Mission Assurance in GEO," Advanced Maui Optical and Space Surveillance Technologies Conference, September 2011.

[6] Horsham, G. A., Schmidt, G. R., and Gilland, J. H., "Establishing a Robotic, LEO-to-GEO Satellite Servicing Infrastructure as an Economic Foundation for Exploration," Tech. Rep. NASA/TM-2010-216937, National Aeronautics and Space Administration, 2010.

[7] Xu, W., Liang, B., Li, B., and Xu, Y., "A Universal On-Orbit Servicing System Used in the Geostationary Orbit," *Advances in Space Research*, Vol. 48, No. 1, July 2011, pp. 95–119.

[8] Smith, D., Martin, C., Kassebom, M., Petersen, H., Shaw, A., Skidmore, B., Smith, D., Stokes, H., and Willig, A., "A Mission to Preserve the Geostationary Region," *Space Debris*, edited by W. Flury and H. Klinkrad, Vol. 34 of *Advances in Space Research*,

Comm Space Res, 2004, pp. 1214–1218, 2nd World Space Congress/34th COSPAR Scientific Assembly, Houston, TX, October 2002.

[9] NASA-STD-8719.14A, "Process for Limiting Orbital Debris," National Aeronautics and Space Administration, December 2011.

[10] Haga, R., and Saleh, J., "Epidemiology of Satellite Anomalies and Failures: A Subsystem-Centric Approach," *ACTA Astronautica*, Vol. 69, No. 7-8, September-October 2011, pp. 676–690.

[11] Clohessy, W. H. and Wiltsire, R. S., "Terminal Guidance System for Satellite Rendezvous," *Journal of the Astronautical Sciences*, Vol. 27, No. 9, September 1960, pp. 641–652.

[12] Hohmann, W., "Die Erreichbarkeit der Himmelskorper (The Attainability of Heavenly Bodies)," NASA Technical Document 19980230631, National Aeronautics and Space Administration, November 1960, Technical Translation F-44.

[13] Curtis, H., *Orbital Mechanics for Engineering Students*, 2nd ed., Butterworth-Heinemann, Burlington, MA, 2009.

[14] Lawden, D., "Orbital Transfer via Tangential Ellipses," *British Interplanetary Society Journal*, Vol. 11, 1952.

[15] Palmore, J., "An Elementary Proof of the Optimality of Hohmann Transfers," *Journal of Guidance Control and Dynamics*, Vol. 7, No. 5, 1984, pp. 629–630.

[16] Bate, R., Mueller, D., and White, J., *Fundamentals of Astrodynamics*, Dover Publications, New York, 1971.

[17] Thomson, W. T., *Introduction to Space Dynamics*, Dover Publications, New York, 1986.

[18] Battin, R. H., *An Introduction to the Mathematics and Methods of Astrodynamics*, AIAA, Reston, VA, 1987.

[19] Wertz, J. and Larson, W. (eds), *Space Mission Analysis and Design*, Springer, Torrance, CA, 1991.

[20] Chobotov, V., editor, *Orbital Mechanics*, 3rd ed., AIAA, Reston, VA, 2002.

[21] Vallado, D. A., *Fundamentals of Astrodynamics and Applications*, Microcosm Press/Springer, El Segundo, CA, 2007.

[22] Wie, B., *Space Vehicle Dynamics and Control*, AIAA, Reston, VA, 2008.

[23] Sidi, M. J., *Spacecraft Dynamics and Control: A Practical Engineering Approach*, Cambridge University Press, Cambridge, UK, 2000.

[24] Jezewski, D. and Donaldson, J., "Analytic Approach to Optimal Rendezvous Using Clohessy-Wiltshire Equations," *Journal of the Astronautical Sciences*, Vol. 27, No. 3, 1979, pp. 293–310.

[25] Broucke, R., "Solution of the Elliptic Rendezvous Problem with the Time as Independent Variable," *Journal of Guidance Control and Dynamics*, Vol. 26, No. 4, July-August 2003, pp. 615–621.

[26] Hablani, H., Tapper, M., and Dana-Bashian, D., "Guidance and Relative Navigation for Autonomous Rendezvous in a Circular Orbit," *Journal of Guidance Control and Dynamics*, Vol. 25, No. 3, May-June 2002, pp. 553–562.

[27] Woffinden, D. C., "On Orbit Satellite Inspection," Master's thesis, Massachusetts Institude of Technology, Cambridge, MA, 2004.

[28] Boyd, S., and Vandenberghe, L., *Convex Optimization*, Cambridge University Press, Cambridge, UK, 2004.

[29] Wu, Y.-H., Cao, X.-B., Xing, Y.-J., Zheng, P.-F., and Zhang, S.-J., "Relative Motion Coupled Control For Formation Flying Spacecraft Via Convex Optimization," *Aerospace Science and Technology*, Vol. 14, No. 6, September 2010, pp. 415–428.

[30] Bryson, J.,and Ho, Y., *Applied Optimal Control: Optimization, Estimation and Control*, Taylor & Francis, Levittown, PA, 1975.

[31] Robinson, S., "Application of Convex Optimization Techniques to Orbital Rendezvous," Unpublished personal notes fall 2011.

[32] Grant, M.,and Boyd, S., "CVX: Matlab Software for Disciplined Convex Programming, version 1.22," http://cvxr.com/cvx [cited February 2012].

[33] Sutton, G., *Rocket Propulsion Elements*, John Wiley & Sons, New York, 2001.

[34] Grover, D., Jacobs, S., Abbasi, V., Cree, D., Daae, M., Hay, J., He, W., Huang, X., Jun, Z., Kearney, S., Kuwahara, T., Lenzi, F., Mirahmetoglu, H., Morley, S., Otani, M., Pastena, M., Pinni, M., Schwartz, J., Shala, K., Shi, J.-F., Khoral, J. S., Steinkellner, M., Treat, D., Ulrich, S., Verheyden, P., Wang, X. Y., and Weeden, C., "Development of On-Oribit Servicing Concepts, Technology Options and Roadmap (Part I): Commercial Aspects," *Journal of the British Interplanetary Society*, Vol. 61, No. 6, June 2008, pp. 203–212.

[35] Yoshida, K., "Engineering Test Satellite VII Flight Experiments For Space Robot Dynamics and Control: Theories on Laboratory Test Beds Ten Years Ago, Now in Orbit," *International Journal of Robotics Research*, Vol. 22, No. 5, May 2003, pp. 321–335.

[36] Woffinden, D. C. and Geller, D. K., "Navigating the Road to Autonomous Orbital Rendezvous," *Journal of Spacecraft and Rockets*, Vol. 44, No. 4, July-August 2007, pp. 898–909.

[37] Dornheim, M. A., "Orbital Express to Test Full Autonomy of On-Orbit Service," *Aviation Week*, June 2006.

[38] Ulrich, S., Schwartz, J., Abbasi, V., Cree, D., Daae, M., Grover, D., Hay, J., He, W., Huang, X., Jacobs, S., Jun, Z., Kearney, S., Kuwahara, T., Lenzi, F., Mirahmetoglu, H., Morley, S., Otani, M., Pastena, M., Pinni, M., Shala, K., Shi, J.-F., Khoral, J. S.,

Steinkellner, M., Treat, D., Verheyden, P., Wang, X. Y., and Weeden, C., "Development of On-Orbit Servicing Concepts, Technology Options, and Roadmap (Part II): Technical Design," *Journal of the British Interplanetary Society*, Vol. 61, No. 6, June 2008, pp. 213–223.

[39] YuHeng, L., KaiZhong, Y., ChengSheng, S., Dan, L., Hui, G., Jun, Z., Hong, C., and Li, M., "A Preliminary Study on Dead Geostationary Satellite Removal," *Science China-Technological Sciences*, Vol. 53, No. 12, December 2010, pp. 3389–3396.

[40] "U.S. Government Orbital Debris Mitigation Standard Practices," Guideline, NASA and Department of Defense, 1997.

[41] "IADC Space Debris Mitigation Guidelines," Guideline, Inter-Agency Space Debris Coordination Committe, July 2007.

[42] "Support to the IADC Space Debris Mitigation Guidelines," Guideline, Inter-Agency Space Debris Coordination Committe, October 2004.

[43] "State of the Satellite Industry Report," Report, Futron Corporation and Satellite Industry Association, May 2012.

[44] Geller, D. K., "Course Notes from Advanced Astrodynamics," Utah State University Course MAE 6540, Fall 2010.